



HAL
open science

Computational mechanics of composite and hybrid materials: advanced multi-scale damage modeling

Dmytro Vasiukov

► **To cite this version:**

Dmytro Vasiukov. Computational mechanics of composite and hybrid materials: advanced multi-scale damage modeling. Engineering Sciences [physics]. Université Lille 1, 2024. tel-04601431

HAL Id: tel-04601431

<https://hal.science/tel-04601431v1>

Submitted on 4 Jun 2024

HAL is a multi-disciplinary open access archive for the deposit and dissemination of scientific research documents, whether they are published or not. The documents may come from teaching and research institutions in France or abroad, or from public or private research centers.

L'archive ouverte pluridisciplinaire **HAL**, est destinée au dépôt et à la diffusion de documents scientifiques de niveau recherche, publiés ou non, émanant des établissements d'enseignement et de recherche français ou étrangers, des laboratoires publics ou privés.



Distributed under a Creative Commons Attribution - NonCommercial 4.0 International License

LILLE UNIVERSITY

HABILITATION À DIRIGER DES RECHERCHES
DE L'UNIVERSITÉ DE LILLE

ÉCOLE DOCTORALE N°632 : SCIENCES DE L'INGÉNIERIE ET DES SYSTÈMES

SPÉCIALITÉ : SCIENCES POUR L'INGÉNIEUR

COMPUTATIONAL MECHANICS OF COMPOSITE AND HYBRID MATERIALS: ADVANCED MULTI-SCALE DAMAGE MODELING

BY DMYTRO VASIUKOV

DEFENDED 24 MAI 2024

JURY

PROF STÉPHANE PANIER	LTI-EA UPJV	PRÉSIDENT
PROF CHRISTIAN HOCHARD	LMA AIX-MARSEILLE UNIVERSITÉ	RAPPORTEUR
PROF DANIEL COUTELLIER	UPHF	RAPPORTEUR
PROF THIERRY CUTARD	ICA IMT MINES ALBI	RAPPORTEUR
DR JEAN-FRANÇOIS MAIRE	ONERA	EXAMINATEUR
PROF STEPAN LOMOV	KU LEUVEN	EXAMINATEUR
PROF CHUNG HAE PARK	IMT NORD EUROPE	GARANT



IMT Nord Europe
École Mines-Télécom
IMT-Université de Lille

MARCH 24, 2024

#IMTomorrow

All through my childhood, I was reading Agatha Christie.
(Thank you, Grandma!).

"I married an archaeologist because the older I grow, the more he appreciates me."

AGATHA CHRISTIE.

Before coming to France, my first book in French was "The Little Prince".

"That is very interesting," said the little prince. "Here at last is a man who has a real profession!" And he cast a look around him at the planet of the geographer. It was the most magnificent and stately planet that he had ever seen.

ANTOINE DE SAINT-EXUPERY.

I like "The Hitchhiker's Guide to the Galaxy" because it reminds me of a good time.

"Don't Panic."

"The answer to the great question...of Life, the Universe and Everything...is...forty-two."

DOUGLAS ADAMS

Acknowledgments

I would like to first thank Chung-Hae PARK for constantly supporting me in preparing for my habilitation and accepting to be my garant. I would also like to thank Stephane PANIER, who has been guiding me since I arrived in France and up to this point, and for accepting to be a part of my defense jury. I thank Patricia KRAWCZAK for her encouragement and advice in preparing for my habilitation.

My sincere gratitude goes to all the jury members, particularly to the three reviewers: Christian HOCHARD, Thierry CUTARD, and Daniel COUTELLIER, who accepted to report on my work and gave me valuable and priceless advice during my defense. I also want to thank Stepan LOMOV for his sharp-minded discussions since we first met in Stuttgart in 2015, and since then, we have had many collaborations. Last but not least, I thank Jean-Francois MAIRE, who accepted to be part of my jury and has influenced my work through all his publications long before these days.

I sincerely thank all my colleagues at Mines Douai, IMT Lille Douai, and IMT Nord Europe (since 2010) and all external collaborators. All the professors with whom I worked, discussed, or just chatted. All "maîtres de conférences" and "maîtres assistants," all colleagues from the laboratory, engineers, technicians, and assistants.

I particularly want to thank all my students and post-docs with whom I have worked during this period. Thanks to their contributions, this habilitation became possible. All students are mentioned in my CV, but I want to especially thank my very first PhD student, Yang LIU, from whom my supervisory career started.

None of this would be possible without my family. My mother, who is abroad but in my heart. My wife and my daughter, who support me daily. All my family in-law. And all my family members who are no longer here physically, but whom I remember and think about.

THANK YOU!

Contents

I	CV and list of publications	9
1	Curriculum Vitae	11
2	List of publications	23
II	Summary of research activities	29
	Introduction	31
3	Non-linear modeling of composite materials	33
3.1	Static model development	34
3.1.1	Damage phenomena in composites	34
3.1.2	Constitutive modeling of unidirectional composites	35
3.2	Extension to fatigue in composites	41
3.2.1	Principle of the proposed direct approach	43
3.2.2	Direct numerical algorithm	45
3.2.3	Industrial applications	47
3.3	Conclusion	49
4	Multi-scale modeling of textile composites	51
4.1	Introduction to textile composites	52
4.2	Textile composites modeling: literature review	52
4.2.1	Analytical modeling	53
4.2.2	Numerical modeling	54
4.2.3	Research problem statement	57
4.3	Realistic textile composites	58
4.3.1	Micro- and yarn-scale characterization	58
4.3.2	Micro- and yarn-scale modeling	60
4.3.3	Meso-structures characterization and modeling	63
4.3.4	Conformal discretization with local fiber volume fraction control	67
4.4	Textile composites with porosity	68
4.4.1	Dual-scale porosity	68
4.4.2	Characterization of the porosity at micro- and meso-scales	69

4.4.3	Numerical modeling of textile composites with voids	72
4.5	Conclusion	76
5	Numerical modeling based on FFT methods	77
5.1	Introduction	78
5.2	Homogenization problem	78
5.3	FFT-based homogenization for elastic problem	79
5.3.1	Solution of elastic problem	79
5.3.2	First attempt to modeling a damage process in FFT solvers	80
5.3.3	Research problem statement for FFT methods	81
5.3.4	Numerical artifacts in FFT solvers	82
5.3.5	Solutions to reduce numerical artifacts in FFT solvers	82
5.4	Phase-field damage modeling	84
5.5	Review of Miehe's and Wu's phase-field models	86
5.5.1	Regularization of sharp cracks	86
5.5.2	Variational approach	87
5.6	FFT-based solvers development	90
5.6.1	Miehe's phase-field damage model in FFT solver	90
5.6.2	Heterogeneous vs homogeneous formulation	91
5.6.3	Discussion on l_c sensitivity and implementation of the Wu's model	92
5.7	Conclusion	95
6	Perspectives	97
6.1	Multi-scale numerical modeling of composites	97
6.1.1	Big picture	97
6.1.2	Improvement of multi-scale observation techniques (short and mid-term)	98
6.1.3	Harmfulness and tolerance of process induced defects during LCM (mid-term)	100
6.2	Durability of composite and hybrid structures	103
6.2.1	Modeling of hybrid structures for hydrogen transport and storage (mid-and long-term)	103
6.2.2	Digital twin for composite pressure vessels for hydrogen storage and transportation (long term)	105
	Bibliography	107

Part I

CV and list of publications

1 .Curriculum Vitae

Dmytro VASIUKOV

Born 06/09/1985

MAÎTRE DE CONFÉRENCES

IMT Nord Europe, Douai Campus, 941 rue Charles Bourseul, 59508 Douai, France

Centre for Materials and Processes (CERI MP)

Tel: +33 (0)3 27 71 24 48

Email: dmytro.vasiukov@imt-nord-europe.fr

[Researchgate](#), [ORCID ID](#), [Google Scholar](#)

Qualification (N 19260276818): CNU-60-Mécanique, génie mécanique, génie civil (2019 - 2023)

Education

- **2013: PhD** from Lille University 1 Sciences et Technologies (Doctoral school: Science for Engineers (SPI), speciality: "Mécanique, génie mécanique, génie civil").
 - *Department*: Technology of Polymers et Composites & Engineering Mechanics (TPCIM) at Ecole des Mines de Douai.
 - *PhD thesis title*: "Damage modelling of fibre reinforced polymer composite materials under cyclic loadings by a simplified approach".
 - *Supervisors*: Prof. S. Panier (Mines Douai) and HDR A. Hachemi (IAM-RWTH Aachen University, Germany).
 - *Jury*: Prof. Fodil Meraghni (Président) (Arts et Métiers ParisTech Metz), Prof. Abdel Laksimi (Rapporteur) (Université de Technologie de Compiègne), Prof. Frédéric Roger (Rapporteur) (ENSTA ParisTech), HDR Abdelkader Hachemi (IAM-RWTH Aachen University, Germany), Prof. Stéphane Panier (Mines Douai, France).
- **2008: Magister degree** (equivalent to Research Master (BAC+6)), The National Technical University Kharkiv Polytechnic Institute (NTU KhPI) (Kharkiv, Ukraine), with high distinction.
 - *Department*: Dynamics and Resistance of Machines. *Specialty*: Informatics Technologies of Design.
 - *Master thesis title*: "Modeling of inductor systems for electromagnetic pulse stamping with coupled magneto-elastic behavior".
 - *Supervisor*: Prof. V.I. Lavinsky.
- **2006: Bakalavr Diploma** (equivalent to License/ BAC+3), The National Technical University Kharkiv Polytechnic Institute (NTU KhPI) (Kharkiv, Ukraine), with distinction.
 - *Department*: Dynamics and Resistance of Machines. *Specialty*: Informatics Sciences.
 - *Bachelor thesis title*: "Automated modeling of the beam structures".
 - *Supervisor*: Prof. V.I. Lavinsky.

Experience

- **Since March 2021: Associate-Professor (Maître de conférences)**, Centre for Materials and Processes (CERI MP) at IMT Nord Europe (Douai, France).
Competencies: Computational mechanics, Composite materials, Mechanics of materials, Structural mechanics.
- **September 2013 - March 2022: Research-Engineer**, Centre for Materials and Processes (CERI MP) at IMT Nord Europe (Douai, France).
Competencies: Computational mechanics, Composite materials, Mechanics of materials, Structural mechanics.
- **January 2013 - September 2013: Development Engineer**, ESI Group (Rungis, France).
Main mission: Development of constitutive models for composite materials: plasticity, damage, and fatigue damage modeling of composites.
- **August 2008 - December 2009: Research Engineer**, The National Technical University Kharkiv Polytechnic Institute (NTU KhPI) (Kharkiv, Ukraine).
Main mission: Modeling of inductor systems for electromagnetic pulse stamping with coupled magneto-elastic behavior.

Competencies

Programming:	Python, FORTRAN, C #, C++, Matlab, Maple.
Numerical methods:	Finite Elements, Fast Fourier Transformation based methods.
Modeling:	Multi-scale methods, Mechanics of Composites, Numerical homogenization, Plasticity, Damage mechanics, Fatigue, Rupture.
Software:	ABAQUS (UMAT, VUMAT), ANSYS (UMAT).
Languages:	French, English, Ukrainian and Russian (native).

Short summary of scientific contributions

Peer-reviewed international journals:	16
National and international conferences:	25
Posters:	3
Invited seminars:	6

My detailed contribution is listed in the Section '*List of publications*'.

Short summary of teaching activities

My teaching experience began in the third year of my PhD thesis with a *Dynamics of Solids: Analytical Mechanics* course that I taught the master students at the first year of the *Mechanical Engineering* specialty of Mines Douai. Since the beginning of my career as an assistant professor, I have regularly taught three main courses: *Mechanics of Composites*, *Dynamics of*

Solids, and Fracture Mechanics and Fatigue. On average, it represents from 60 to 100 equivalent TD hours (HETD) per year. For more details, please refer to the *Teaching section*.

Granted, Travel Programs, Short Stay Visits

- **2006 July: Student travel program** of Deutscher Akademischer Austausch Dienst (DAAD), (Magdeburg, Dresden, Halle-Wittenberg, Germany). Program: lecture classes, lab sessions, and visits of the laboratories.
- **2007 April - November: Leonard Euler Grant** of Deutscher Akademischer Austausch Dienst (DAAD). Joint program between The National Technical University Kharkiv Polytechnic Institute (NTU KhPI) (Kharkiv, Ukraine) and Center of Engineering Sciences, Martin-Luther-University (Halle - Wittenberg, Germany).
- **2008 Mai: Best Young Researcher Award**, delivered by the head of Kharkiv department, Ukraine.
- **2019: Project FoCUS: *Advanced numerical methods for textile composites modeling***, Short stay at KU Leuven.
- **2019-2020: Project OCTET: *Reduced order modeling for advanced nonlinear multi-scale numerical methods of composites***, Short stay at KU Leuven and UGhent, .
- **2021: Project LAPHCO 3D: *Laser welding of 3D printed hybrid composites parts: from process to mechanical and thermal performances***, Short stay at KU Leuven (Leuven and De Nayer Campuses).

Membership

- **NAFEMS** International Association for the Engineering Modeling, Analysis and Simulation Community;
- **ESCM** European Society for Composite Materials;
- **EUROMECH** European Mechanics Society member;
- **Fédération Lilloise de Mécanique** - FED 4130;
- **MECAFIB** GDR CNRS 2024 (Multiscale mechanics of Fibrous Media).
- **MIC** GDR CNRS 3671 (Mise en œuvre des composites et propriétés induites).
- **AFM** (Association Française de Mécanique)

Conference and journal session organization

- **Co-organization** of the mini-symposium *Mechanics of Textile Composite Reinforcements and Fibrous Materials* at the 11th European Solid Mechanics Conference (4-8 July 2022, Galway, Ireland). In collaboration with Stepan Lomov (KU Leuven, Belgium), Philippe Boisse (INSA Lyon, France).
- **Co-organization** with KUL of the Special Issue in Materials MDPI: *Manufacturing defects in composite materials and structures*. In collaboration with Jan Ivens and Stepan Lomov (KU Leuven, Belgium), Chung-Hae Park (IMT Nord Europe, France). [Link to the special issue](#)

- **Co-organization** of ECCM21 Special session *Manufacturing defects in composite materials and structures*, 2-7 July 2024, Nantes. In collaboration with Jan Ivens and Stepan Lomov (KU Leuven, Belgium), Chung-Hae Park (IMT Nord Europe, France).
- **Co-organization** of ESMC2025 – *Mechanics of Fibrous Materials and Textiles*, 7-11 July 2025. In collaboration with Stepan Lomov (KU Leuven, Belgium), Catalin Picu (Rensselaer Polytechnic Institute, USA).

Responsibilities related to teaching and research

- **Coordinator of the research thematic** of CERI MP (Since 2020) *Computational Mechanics and Modeling of Materials and Processes*.
- **Responsible for Teaching Units:**
 - **Numerical Design** (since 2019) - fundamental Value Units (100 h) of the *Domain Eco-Materials, Industry, and Civil Engineering*, CI2 (equivalent to the first year of the master cycle).
 - **Bio-mimicry in EcoDesign** - selective module (24 h), level CP2 (equivalent to the second year of the university program).
- **Referent of the Informatics** department for the CERI MP (since January 2020): Strategic management of the informatics equipment of the CERI MP.
- **Scientific responsible** (2015-2018) of the Work Package (*Tool development and durability testing*) in the European program H2020, JOIN'EM (*JOINing of copper to aluminium by ElectroMagnetic fields*).

Peer-reviewing for international journals

- [Composite Structures](#)
- [Composites Part A](#)
- [Composites Part B](#)
- [Computer Methods in Applied Mechanics and Engineering](#)
- [International Journal of Fatigue](#)
- [Materials](#)

Assistant professor recruitment committee

- **2023:** Comité de Sélection pour le poste MCF (CNU 60) de l'UML-Polytech-Lille.

External scientific committee member of PhD thesis

- [J1] UD DIN Israr, *Coupled damage plasticity modeling for Non Crimp Fabrics (NCFs) Fiber Reinforced Polymers (FRPs) based on Puck's theory*, University of Picardy Jules Verne, 30 November 2018.

- [J2] **HAO Pei**, *Mechanical behaviour of woven composite under multiaxial loading conditions by using modified Arcan fixture*, University of Picardy Jules Verne, 28 November 2019.
- [J3] **WINTIBA Badadjida**, *Automated procedures for the computational modeling of 3D woven composites*, Free University of Brussels, public defense 09 Dec 2019.
- [J4] **ZHAO Yinglun**, *Effect of Defects in Filament Wound Composite Products (Fibre Misalignment, Voids)*. Department of Materials Engineering, KU Leuven. .

Supervision

Master thesis supervisor

- [M1] **T. Kondouri**, M2, *Development of anisotropic constitutive model based on coupled plasticity-damage theory*, 2012. The participation rate: 70 %.
- [M2] **B. Li**, M2, *Multi-scale analysis based on nested finite element approach*, 2012. The participation rate: 70 %.
- [M3] **S.-H. Nambiyankulam Hussain**, M2, *Numerical characterization of sheared organo-sheets based on realistic interpenetration-free geometry*, in collaboration with Siemens (Leuven, Belgium), 2019. The participation rate: 50 %.
- [M4] **N. Chatit**, M1, *Modeling of the highly charged extruded polymers: formulation, characterization and mechanical modeling*, 2019. The participation rate: 100 %.
- [M5] **K. Khati**, M2, *Intelligent placement of the sensors for structural health monitoring of the equipment under pressure*, in collaboration with CETIM, 2021. The participation rate: 20 %.
- [M6] **C. Corte**, M2, *Characterization and modeling of the individual protections against shock and vibrations*, in collaboration with MAPA, 2021. The participation rate: 70 %.
- [M7] **A. Jbeli**, M2, *Crack assisted manufacturing based on the phase field model of brittle fracture (for micro/nano/bio applications)*, 2021. The participation rate: 100 %.
- [M8] **B.H. Tran**, M1, *Impact of integrated sensors and manufacturing defects on the mechanical behavior of hybrid structures: composite-metal and composite-polymer*, support work for Chair ANR project CORENSTOCK, 2021. The participation rate: 50 %.
- [M9] **O. Bouihi**, M2, *Characterization and numerical modeling of the bituminous waterproofing membranes*, in collaboration with SOPREMA, 2022. The participation rate: 50 %.
- [M10] **K.T. Kim**, M2, *Modeling non-woven composite based on recycled carbon fiber*, in collaboration with GEMTEX ENSAIT (financial support from Mechanics Federation of Lille), 2022. The participation rate: 50 %.
- [M11] **B. Dutailly**, M2, *Development of the auxetic 3D textile reinforced materials to improve low-speed impact resistance*, in collaboration with GEMTEX ENSAIT (financial support from Mechanics Federation of Lille), 2023. The participation rate: 50 %.

PhD advisor

- [D1] **Y. Liu**, *Multi-scale simulation of interlock composite damage*. Supervisors: Prof. S. Panier, 2013-2017. The participation rate: 70 %.

- [D2] **A. Wali**, *Modeling of the mechanical behaviour of the immiscible compatible polymer blends*. Supervisors: Prof. J. Soulestin and Prof. F. Roger, 2014-2017. The participation rate: 30 %.
- [D3] **J. Vasseur**, *Fiabilité prévisionnelle de la tenue en service de composants mécaniques en présence d'amas de porosités détectés et caractérisés par contrôle non destructif ultrasonore*. Supervisor: HDR. S. Chaki, 2018-2020. The participation rate: 50 %.
- [D4] **K.-K. Parvathaneni**, *Characterization and multi scale modeling of textile reinforced composite materials considering manufacturing defects*. Supervisor: Prof. C.-H. Park, 2018-2020. The participation rate: 50 %.
- [D5] **X. Ma**, *Modeling of fibre reinforced composites based on Fast Fourier Transform (FFT)*, Supervisors: Prof. C.-H. Park and Prof. S.V. Lomov, 2019-2021. The participation rate: 30 %.
- [D6] **B. Meemary**, *Design of a hot water storage element integrating food, safety, connectivity, durability and energy efficiency constraints*. Supervisor: Prof. S. Chaki, 2021-2024. The participation rate: 30 %.
- [D7] **I. Khaled**, *Modeling the mechanical behavior of equipment in service under progressive damage: towards a digital twin of a pressure vessel*. Supervisor: Prof. S. Chaki, 2022-2025. The participation rate: 30 %.
- [D8] **H. Demouveau**, *Optimisation de la fabrication des réservoirs de stockage d'H2 en composite et étude de leur comportement et de leur endommagement sous hautes pressions*. Supervisor: Prof. S. Chaki, 2022-2025. The participation rate: 30 %.
- [D9] **S. Merheb**, *Modeling of the fatigue damage of a metal pressurized hydrogen storage equipment by numerical phase field method*. Supervisor: Prof. S. Chaki, 2022-2025. The participation rate: 30 %.
- [D10] **M. Chehazi**, *Jumelage numérique pour le suivi temps réel de l'état de santé des structures composites contrôlées par émission acoustique*. Supervisor: Prof. S. Chaki and Prof. Pierre KERFRIDEN, 2023-2026. The participation rate: 30 %.

Post-Docs advisor

- [P1] **P. Cheng**, *Fatigue modeling of the composite materials for housing of the electromagnetic welding*, in the scope of the H2020 European project JOIN'EM. Supervisor: Prof. C.-H. Park, Feb 2016 - Dec 2017. The participation rate: 50 %.
- [P2] **Y. Chen**, *Multi-scale modeling of heterogeneous composite materials*, Supervisor: Prof. C.-H. Park, Jan 2018 - Oct 2018. The participation rate: 50 %.
- [P3] **C. Cruanes**, *Fatigue characterization of the textile reinforced composites with taking into account manufacturing defects*. Supervisor: Prof. C.-H. Park, Nov 2019 - Oct 2020. The participation rate: 50 %.
- [P4] **F. Abid**. *Development of a digital twin of a pressured equipment: hybridization of the physical model and machine learning*. Supervisor: Prof. S. Chaki, 2022. The participation rate: 30 %.
- [P5] **A. Ammar**. *Design optimization of the hot water tank storage: multi-physical modeling, optimal sensor placement*. Supervisor: Prof. S. Chaki, 2022-2025. Nov 2022 - Mar 2023. The participation rate: 50 %.

Academic and industrial collaborations

- **KU Leuven (Belgium)** department of Mechanical Engineering: Prof. S.V. Lomov (common PhD student X. MA and short stay mobility projects) et Prof J. Ivens (during short stay mobility projects).
- **Institut für Allgemeine Mechanik (IAM)-RWTH Aachen (Germany)**: Prof. A. Hachemi (who is my thesis supervisor).
- **Ghent University (Belgium)**, Faculty of Engineering and Architecture, Department of Materials, Textiles and Chemical Engineering Mechanics of Materials and Structures: Prof. dr. F.A. Gilabert (short stay mobility project).
- **Université Libre de Bruxelles (ULB) (Belgium)** Building, Architecture and Town Planning Dept, Structural and Material Computational Mechanics: Prof. T.J. Massart (research collaboration).
- **Siemens Industry Software NV Digital Factory Division (Belgium)**: A. Matveeva, PhD Research Engineer and K. Vanclooster, PhD Research Engineer.
- **ESI Group in France and Germany**: A. Trameçon, S. Mueller (European project MAPICC3D).
- **Owens Corning (France)**: D. Blandin, V. Lartisien (during research and innovation projects).
- **G. MAGYAR SA (France)**: F. Laurent (project ADEME LIGHT TANK).
- **CEA Saclay (DEN/DMN/SRMA) (France)**: L. Gelebart (research projects for FFT-solver development FFT AMITEX).
- **Fraunhofer-Institut für Werkzeugmaschinen und Umformtechnik IWU (Germany)**: Dr. V. Psyk (during European project H2020 JOIN'EM).
- **MINES Paris - PSL**: L. Laiarinandrasana and S. Joannes (proposal of the European project and preparation of the technical seminar of IMT), Prof. P. Kerfriden (PhD thesis finaced by Institut Carnot M.I.N.E.S).
- **CETIM**, Senlis. Participation in the activity of the LATEP - joint laboratory between IMT Nord Europe and CETIM: A. Assaf, M. Bennebach, P. Rohart (several ongoing projects, JUNAP and PhD thesis).
- **ENSAIT GEMTEX** Textile research laboratory, Roubaix: Prof. D. Soulat (research collaboration).
- **UML** - Unité de Mécanique de Lille - Joseph Boussinesq, **MMS** - Mécanique des Matériaux et des Structures, Lille: T. Kanit (research collaborations).
- **IRDL** - ENSTA Bretagne - Institut de Recherche Dupuy de Lôme, Brest: P. Le Grogneec (research collaboration).

Participation in the collaborative projects

- **European project FP7 MAPICC** (One shot Manufacturing on large scale of 3D upgraded panels and stiffeners for Lightweight thermoplastic textile composite structures),
Subvention IMT: ~ 700 k€,
Period: 2012-2015,
Responsibility: Fatigue modeling of thermoplastic composites,
Partners: Mecaplast, Volvo Trucks, Alstom, Coexpair, Tencate, PD Fiber Glass, Steiger, Latvijas Finieris, Reden, Polytechnico Milano, ENSAIT, Technische Universitaet Dresden, ESI Group, ITF and RTU.
- **Project FUI ACCUM** (Armement Caténaire Composite Universel Multitension),
Project leader: Stratiforme,
Subvention IMT: ~ 185 k€,
Period: 2014-2017,
Responsibility: Task modeling of the composite structure,
Partners: SNCF, RFF, Stratiforme and "Centre d'Essais Ferroviaire".
- **European project H2020 JOIN-EM** (JOINing of copper to aluminium by ElectroMagnetic fields),
Project leader: Fraunhofer IWU,
Subvention IMT: ~ 240 k€,
Period: 2015-2018,
Responsibility: Scientific responsible for IMT-Lille-Douai, WP-leader modeling of composite structure for pulse-welding structures.
Partners: Alkè, Belgian Welding Institute, Calyos, CeGasa, Fraunhofer IWU, Innovaltech, ICAM Lille, Phimeca, Recendt, Refco, Veritech Group, Whirlpool et EWF.
- **Project ADEME LIGHTTANK** (Allègement des véhicules routiers - Réduction émissions des GES),
Project leader: MAGYAR,
Subvention IMT: ~ 220 k€,
Period: 2017-2021,
Responsibility: Responsible for the modeling task of the reduced prototype of the composite reservoir.
Partners: G. MAGYAR SA, Université de Haut Alsace via le portage SATT CONECTUS Alsace, Université de Bourgogne, Armines,
- **Project JUNAP** (JUmeau Numérique d'un Appareil à Pression : évaluation de la tenue mécanique et maintenance prédictive),
Project leader: CETIM (Senlis),
Subvention IMT: ~ 150 k€,
Period: 2021-2023,
Responsibility: Numerical modeling of the chemical reactor, development of the algorithm for intelligent sensor placement.
Partners: CETIM, STCN, INEOS, IMT Nord Europe (CERI for Materials and Processes

and CERI Numerical Systems).

- **Project Chair ANR CORENSTOCK** (Conception orientée cycle de vie & approche systémique pour l'efficacité énergétique du stockage de systèmes de chauffage),
Project leader: M. Lagardère,
Subvention IMT: ~ 250 k€,
Period: 2021-2025,
Responsibility: Responsible for the numerical design of the reservoir made of composites, multi-scale modeling, microscopic modeling of sensors integration.
Partners: elm.leblanc, IMT Nord Europe (CERI MP, EE et SN), l'Institut Fayol de l'École des Mines de Saint-Étienne (MSE-Fayol)
- **Project ANR JCJC SHORYUKEN** (Assemblage de composite carbone hybride thermoplastique - thermodurcissable : personnalisation de structures complexes),
Project leader: A.C. Akue Asseko,
Subvention IMT: ~ 360 k€,
Period: 2021-2025,
Responsibility: Characterization (mechanical testing, optical microscopy, μ CT) of the laser welded composite assembly.
- **Project Horizon Europe ECOHYDRO** (Economic Manufacturing Process Of Recyclable Composite Materials For Durable Hydrogen Storage),
Project leader: C. H. Park,
Subvention IMT: ~ 1.1 M€,
Period: 2024-2028,
Responsibility: Multi-scale modeling of composite materials considering manufacturing defects.
Partners: Basaltex NV, KUL, Promat, AIRBUS, Canoe, Mahytec, ARKEMA, D.P. Materials Design and processing, Haesaerts, LIST, Politechnika Wroclawska, Electra, FEV, TEMSA.

Teaching

Period Mines Douai (2013-2019)

During this period, the teaching program was the old program of the Ecole des Mines de Douai (with specialization option including major and minor courses). I have taught mainly three specialties: Engineering Mechanics (IM) and Technology of Polymers and Composites (TPC) at Mines Douai; and third-year students of Institut Supérieur de Plasturgie en Alternance (3A ISPA) (Alençon, France). Here is the list of classes (sorted by year):

2012: *Dynamics of Solids: Analytical Mechanics* (in English), students: first-year master of IM specialty, 8h of courses.

2013: *Mechanics of Composites* (in English), second-year master students of IM specialty and second-year master students of TPC specialty, 20h of lectures and 8h of lab sessions.

2014:

- *Fracture Mechanics* (in English), international master program of IAM-RWTH Aachen University (Germany), 12h of lectures;
- *Mechanics of Composites* (in English, in hybrid bi-sites mode), second-year master students of IM specialty, second-year master students of TPC specialty and third-year students of ISPA, 20h of lectures, and 8h of lab sessions.

2015, 2016 and 2017:

- *Fracture Mechanics and Fatigue* (in English), second-year master students IM specialty, 20h of lectures and 8h guided tutorials (TD);
- *Mechanics of Composites* (in English, in hybrid bi-sites mode), second-year master students of IM specialty, second-year master students of TPC specialty and third-year students of ISPA, 20h of lectures and 8h of practical sessions.

2018 and 2019:

- *Dynamics of Solids: Analytical Mechanics*, first-year master students of IM specialty, 20h of lectures;
- *Fracture Mechanics and Fatigue* (in English), second-year master students of IM specialty, 20h of lectures and 8h guided tutoring (TD);
- *Mechanics of Composites* (in English, in hybrid bi-sites mode), second-year master students of IM specialty, first-year master students of TPC specialty and third-year students of ISPA, 20h of lectures and 8h of lab sessions.

To this list should be added the supervision of groups of students in the following projects every year:

- Project (PST) *Design of composite bridge (concours SAMPE France)*, for first-year master students of IM and TPC specialties, 120h per year;

- Project (PDR) *Discovery of Research* for first-year master students of IM and TPC specialties, 80h per year.

Period IMT Lille Douai and later IMT Nord Europe (2019-2023)

The major difference of this period is the organizational mode of the teaching process. All programs are divided into blocks (Units of Value, UV) that represent a 100-hour pedagogical load. I have taught two specialties at IMT Nord Europe: IMF - *Ingénierie Mécanique & de la Fabrication* and PC - *Matériaux Polymères & Composites*. I also continue to teach the students of the third year of the Institut Supérieur de Plasturgie en Alternance (3A ISPA) (Alençon, France).

Here is the list of classes (sorted by year):

2019:

- *Morphing structures for energy harvesting*, UV project for master students of the first and second year of the specialties IMF et PC, 100h of project;
- *Car prototype for shell eco-marathon*, UV project for master students of the first and second year of the specialties IMF et PC, 100h of project;
- *Fracture Mechanics and Fatigue* (UV.CONSTR), second-year master students of IMF specialty, 12h of lectures;
- *Mechanics of Composites*, students: second-year master of IMF specialty and second-year master of PC specialty, 20h of lectures and 8h of practical sessions;
- *Mechanics of Composites* (video-conference), third-year students of ISPA, 20h of lectures, and 8h of lab sessions.

2020:

- *Numerical Design*, students: second-year student of the integrated preparatory cycle (L2), in Elective Module (ME) *Introduction to materials*, 5h lectures;
- *Numerical Design*, students: second-year student of the integrated preparatory cycle (L2), in Elective Module (ME) *Bio-mimicry in EcoDesign*, 5h lectures and 10h guided project;
- *Computer-aided engineering* (UV.CNU), students: first-year master students of IMF specialty, 16h guided project;
- *Mechanics of Composites* (UV.CADIST) and *Multi-scale modeling of composites* (UV.CNUA), students: first-year master students of IMF specialty and second-year of PC specialty, 20h lectures and 8h of lab sessions;
- *Mechanics of composites: test case hydrogen* (UV.CADIST), students: second-year of PC specialty, 4h guided project;
- *Mechanics of composites*, students: third-year students of ISPA, 20h lectures and 8h of lab sessions;

- *Dynamics of solids: Analytical Mechanics* (UV.DYNAM), students: second-year master of IMF specialty, 20h lessons and 12h lab sessions;

2021 and 2022:

- *Numerical Design*, students: second-year student of the integrated preparatory cycle (L2), in Elective Module (ME) *Introduction to materials*, 5h lectures;
- *Numerical Design*, students: second-year student of the integrated preparatory cycle (L2), in Elective Module (ME) *Bio-mimicry in EcoDesign*, 5h lectures and 10h guided project;
- *Computer-aided engineering* (UV.CNU), students: first-year master students of IMF specialty, 12h of lab sessions and 16h guided project;
- *Mechanics of thin wall structures*, students: first-year master students of IMF specialty and second-year of PC specialty, 20h lectures and 8h of lab sessions;
- *Mechanics of composites*, students: third-year students of ISPA, 20h lectures and 8h of lab sessions.

2 .List of publications

Journal articles

- [A1] X. Ma, **D. Vasiukov***, M. Shakoov, S.V. Lomov, C. H. Park. *Implementation of a phase field damage model with a nonlinear evolution equation in an FFT-based solver*. Engineering Fracture Mechanics, Volume 290, 27 September 2023, 109518. [DOI](#)
- [A2] J. Vasseur, N. Leymarie*, V. Dorval, B. Dupont, **D. Vasiukov**, S. Chaki. *Simulation of ultrasonic TFM/FMC imaging for porosity clusters using multiple scattering modelling: Quantitative analyses and experimental comparisons*. NDT & E International 137, (2023). [DOI](#)
- [A3] X. Ma, Y. Chen, M. Shakoov*, **D. Vasiukov**, S.V. Lomov, C.-H. Park. *Simplified and complete phase-field fracture formulations for heterogeneous materials and their solution using a Fast Fourier Transform based numerical method*. Engineering Fracture Mechanics 279, (2023). [DOI](#)
- [A4] K. Shinde, V. Itier, J. Mennesson, **D. Vasiukov**, M. Shakoov*. *Dimensionality reduction through convolutional autoencoders for fracture patterns prediction*. Applied Mathematical Modelling 114, (2023). [DOI](#)
- [A5] C. Cruanes, K.K. Parvathaneni, **D. Vasiukov**, C.-H. Park*. *Investigation of fatigue behavior of three dimensional interlock composites by time-lapse micro-computed tomography*. Journal of Composites Science 6(1), 14, (2022). [DOI](#)
- [A6] X. Ma, M. Shakoov*, **D. Vasiukov**, S.V. Lomov, C.-H. Park. *Numerical artifacts of Fast Fourier Transform solvers for elastic problems of multi-phase materials: their causes and reduction methods*. Computational Mechanics 67, 1661-1683 (2021). [DOI](#)
- [A7] N. Naouar, **D. Vasiukov**, C.-H. Park, S.V. Lomov, P. Boisse*. *Meso-FE modelling of textile composites and X-ray tomography*. Journal of Materials Science 55, 16969-16989 (2020). [DOI](#)
- [A8] B. Wintiba, **D. Vasiukov**, S. Panier, S.V. Lomov, K.E.M. Kamel, T.J. Massart*. *Automated reconstruction and conformal discretization of 3D woven composite CT scans with local fiber volume fraction control*. Composite Structures 248, (2020), 112438. [DOI](#)
- [A9] J. Vasseur, F. Lefebvre*, **D. Vasiukov**, S. Chaki, I. Huther, M. Marzin, B. Dupont, N. Leymarie. *Methodology of fatigue life assessment on components with porosity cluster*. Theoretical and Applied Fracture Mechanics 108, (2020), 102619. [DOI](#)
- [A10] Y. Chen, **D. Vasiukov**, L. Gélébart*, C.-H. Park. *A FFT solver for variational phase-field modeling of brittle fracture*. Computer Methods in Applied Mechanics and Engineering 349, (2019):167-190. [DOI](#)
- [A11] Y. Chen, **D. Vasiukov**, L. Gélébart, C.-H. Park*. *Fast Fourier transform solver for damage modeling of composite materials*. JMST Adv. 1, (2019):49-55. [DOI](#)
- [A12] Y. Liu, I. Straumit, **D. Vasiukov***, S.V. Lomov and S. Panier. *Prediction of linear and non-linear behavior of 3D woven composite using mesoscopic voxel models reconstructed from X-ray micro-tomography*. Composite Structures 179, (2017):568-579. [DOI](#)
- [A13] A.R. Labanieh, Y. Liu, **D. Vasiukov***, D. Soulat and S Panier. *Influence of off-axis in-plane yarns on the mechanical properties of 3D composites*. Composites Part A: Applied Science and Manufacturing 98, (2017):45-57. [DOI](#)

- [A14] **D. Vasiukov***, S. Panier and A. Hachemi. *Non-linear material modeling of fiber-reinforced polymers based on coupled viscoelasticity-viscoplasticity with anisotropic continuous damage mechanics*. Composite Structures 132, (2015):527-535. [DOI](#)
- [A15] **D. Vasiukov***, S. Panier, A. Hachemi. *Direct method for life prediction of fibre reinforced polymer composites based on kinematic of damage potential*. International Journal of Fatigue 70, (2015):289-296. [DOI](#)
- [A16] **D. Vasiukov***, S. Panier, A. Hachemi. *Direct computational method for life prediction of UD fibre reinforced polymers based-on plasticity-damage simulation*. Applied Mechanics and Materials 232, (2012): 492-496. [DOI](#)

(*) - corresponding author.

International conferences with proceedings

- [CP1] I. Khaled, M. Bennebach, S. Chaki, M. Shakoor, **D.Vasiukov**, J.-L. Iwaniack, P. Rohart, S. Assaf. *Digital Twin for Predicting Progressive Damage in Operating Pressure Vessels*. Fatigue Design. 29-30 November 2023, CETIM Senlis, France.
- [CP2] **D. Vasiukov***, S.V. Lomov, X. Ma and M. Mehdikhani *In situ optical observation of the transverse crack nucleation and growth in cross-ply laminates*. ECCM20, June 26-30, 2022, Lausanne, Switzerland.
- [CP3] X. Ma, M. Shakoor, Y. Chen, **D. Vasiukov***, S.V. Lomov, C.-H. Park. *Characteristic length-insensitive phase-field damage modeling of cracks in fiber-reinforced composites with FFT solver*. ECCM20, June 26-30, 2022, Lausanne, Switzerland.
- [CP4] K. Shinde*, V. Itier, J. Mennesson, **D. Vasiukov**, M. Shakoor. *Deep learning based dimensionality reduction for fracture mechanics*. The ECCOMAS Congress 2022. June 6, 2022, Oslo, Norway.
- [CP5] J. Vasseur*, **D. Vasiukov**, S. Chaki, B. Dupont, I. Huther, M. Marzin, F. Lefebvre, N. Leymarie. *Fracture of in-service mechanical components with porosity cluster detected and characterised by ultrasonic NDT*, 12th International Conference on Multiaxial Fatigue and Fracture (ICMFF-12), 23-26 Septembre 2019, Bordeaux, France.
- [CP6] B. Wintiba, **D. Vasiukov**, S. Panier, S. Lomov, K.E.M. Kamel, T. Massart*. *Level set post-processing for automated meshing of woven composite CT scans with local fiber content control* (Keynote), 7th ECCOMAS Thematic Conference on the Mechanical Response of Composites: COMPOSITES, 18-20 September, 2019, Girona, Spain.
- [CP7] **D. Vasiukov(!)**, Y. Chen, C.-H. Park, L. Gelebart. *FFT solver for local and non-local damage in heterogeneous materials*, NAFEMS World Congress 2019, 17-20 June 2019, Quebec city, Canada.
- [CP8] Y. Chen, **D. Vasiukov***, C.-H. Park. *Influence of voids presence on mechanical properties of 3D textile composites*. 13th International Conference on Textile Composites (TEXCOMP-13). 17-19 Septembre 2018, Milan, Italy. IOP Conf. Series : Materials Science and Engineering 406 (2018) 012006.
doi :10.1088/1757-899X/406/1/012006.
- [CP9] **D. Vasiukov***, K.-K. Parvathaneni, S.V. Lomov, C.-H. Park. *Multi-Scale Modelling of 3D Textile Composites with Different Orthogonal Mesostructures Including the Influence*

of the Composite Manufacturing Process. In proceedings of European Conference for Composite Materials 18 (ECCM18), 2018, Athens, Greece.

- [CP10] I. Straumit, I. Baran, L. Gorbatikh, L. Farkas, C. Hahn, K. Ilin, J. Ivens, L. Lessard, Y. Liu, N. Nguyen, A. Matveeva, M. Mehdikhani, O. Shishkina, J. Soete, J. Takahashi, D. Vandepitte, **D. Vasiukov**, Y. Wan, E. Winterstein, M. Wevers, S.V. Lomov*. *Micro-CT-Based Analysis Of Fibre-Reinforced Composites: Applications*. In proceedings of European Conference for Composite Materials 18 (ECCM18), 2018, Athens, Greece.
- [CP11] **D. Vasiukov**, A. Trameçon and S. Mueller*. *Fatigue modeling in composite materials for industrial application*. NAFEMS. 26-27 October 2016, Hamburg, Germany.
- [CP12] **D. Vasiukov**, A. Trameçon, S. Panier and S. Mueller*. *Strategies and Numerical Implementation of Fatigue Life Models for Continuous Fiber Reinforced Polymers*. Proceedings of the American Society for Composites, 19-22 September 2016 Williamsburg, Virginia, USA.
- [CP13] Y. Liu, I. Straumit, **D. Vasiukov***, S.V. Lomov, S. Panier. *Multi-scale material model for 3D composite using Micro CT Images geometry reconstruction*. In proceedings of European Conference for Composite Materials 17 (ECCM17), 2016, Munich, Germany.
- [CP14] **D. Vasiukov**, S. Panier*, A. Hachemi. *A new approach for the life prediction of FRP composites based on kinematic hardening growth of damage*. In proceedings of Proceedings of 1st International Conference on Mechanics of Composites, June 8-12, 2014, Stony Brook University, Long Island, NY State, USA.
- [CP15] A. Hachemi*, **D. Vasiukov**, S. Panier. *Life prediction of FRP composites by a direct method*. In: Proceedings of 85th Annual Meeting of GAMM hosted by FAU, March 10-14, 2014.
- [CP16] **D. Vasiukov***, S. Panier, A. Hachemi. *Direct Computational Method for Life Prediction of UD Fibre Reinforced Polymers Based-on Plasticity Damage Simulation*. In: Proceedings of the 2011 Symposium on Control and Modeling Cyber-Physical Systems, July 7-8, 2012, Paris, France.
- [CP17] **D. Vasiukov***, S. Panier, A. Hachemi. *Direct Computational Method for Composites Based-on Coupled Plasticity and Continuous Damage Mechanics*. In: Proceedings of 2nd International Conference on Advanced Composite Materials and Technologies for Aerospace Applications June 11-13, 2012, Wrexham, UK.

(*) - presenting author

(!) - has not been presented due to technical reasons.

National conferences with proceedings

- [NP1] Y. Liu, **D. Vasiukov***, S. Panier. *A numerical approach to reconstruct mesoscopic yarn section of textile composites based upon X-ray micro-tomography*. CFM 2017-23ème Congrès Français de Mécanique, 2017, Lille, France.

(*) - presenting author

National and international conferences without proceedings

- [C1] S. Merheb*, **D. Vasiukov**, M. Shakoor, S. Chaki, D.G. Sales, P. Rohart, S. Assaf. *Modélisation de l'endommagement en fatigue d'un acier faiblement allié assisté d'hydrogène sous pression par méthode numérique de champ de phase*. FCTM-ESOPE. 26-27 Septembre 2023, Paris, France.
- [C2] I. Khaled*, M. Bennebach, S. Chaki, **D. Vasiukov**, M. Shakoor. *Modélisation du Comportement Mécanique d'un Equipement en Service sous Endommagement Progressif: Vers un Jumeau Numérique d'Appareil à Pression*. Congrès des Jeunes Chercheurs en Mécanique (MECA-J), En ligne, France .
- [C3] X. Ma, M. Shakoor, Y. Chen, **D. Vasiukov***, S.V. Lomov, C.-H. Park. *Effect of characteristic length parameter in phase-field damage modeling on fibrous composites*. 11th European Solid Mechanics Conference, 4-8 July 2022, Galway, Ireland.
- [C4] **D. Vasiukov***, S.V. Lomov, X. Ma, M. Mehdikhani. *In situ optical observation of the transverse crack nucleation and growth in cross-ply laminates*. Hybrid Fibre-reinforced composites: achieving Synergetic effects through microstructural design and advanced simulation tools. HyFiSyn school & conference. 13-16 Sept. 2021, Leuven, Belgium. (on-line)
- [C5] X. Ma*, M. Shakoor, **D. Vasiukov**, S.V. Lomov, C.-H. Park. *Numerical artifacts in FFT solver for elastic problems of multi-phase materials and their reduction with a level-set based composite voxel method*. 14th International Conference on Advanced Computational Engineering and Experimenting, ACEX, 5-9 July, 2021, Malta.
- [C6] K.-K. Parvathaneni*, **D. Vasiukov**, C.-H. Park. *Automated RVE generator of realistic voids for 3D textile composites manufactured by RTM*. FiBreMoD Conference, 11-12 Decembre 2019, Leuven, Belgium.
- [C7] **D. Vasiukov***, P. Cheng, C. Scheffler and V. Psyk. *Multi-physics modeling of composite materials for magnetic pulse welding tools*. 3rd International Conference on Mechanics of Composites (MECHCOMP3). 4-7th July 2017, Bologna, Italy.
- [C8] **D. Vasiukov***, Y. Liu, S. Panier. *Multi-scale modeling of 3D interlock composites material: manufacturing, testing and material model development*. 2nd International Conference on Mechanics of Composites (MECHCOMP2). 11-14 July 2016, Porto, Portugal.

(*) - presenting author

Posters

- [A1] I. Khaled*, M. Bennebach, S. Chaki, M. Shakoor, **D.Vasiukov**, J.-L. Iwaniack, P. Rohart, S. Assaf. *Digital Twin for Predicting Progressive Damage in Operating Pressure Vessels*. Fatigue Design 2023. CETIM Senlis, France.
- [A2] X. Ma*, K.-K. Parvathaneni, S. Lomov, **D. Vasiukov**, M. Shakoor, C.-H. Park, *Quantitative comparison between fast Fourier transform and finite element method for micromechanical modeling of composite*, FiBreMoD Conference, Leuven, Belgium, 11-12 Decembre

2019.

- [A3] **D. Vasiukov**, S. Panier*, A. Hachemi. *Multi-scale modeling of fatigue damage of continuous fiber reinforced polymer composites*. In : Proceedings of JET May 2-4, 2012, Marrakech, Maroc.
- [A4] **D. Vasiukov***, S. Panier, A. Hachemi. *Multi-scale modeling of fatigue damage of continuous fiber reinforced polymer composites*. In: Proceedings of Fatigue Design conference November 23-24, 2011, Senlis, France.

(*) - presenting author.

Invited seminars and technical meetings

- [S1] **D. Vasiukov***, S. Chaki. *Technology of materials metals/composites/hybrids for the hydrogen storage developed at IMT Nord Europe in CERI MP*. 2 June 2022 Technical industrial days - New materials and processes for de-carbonised transport.
- [S2] M. Shakoor*, S. Assaf, **D. Vasiukov***. *Démonstration : réacteur chimique - Optimisation de la performance d'un procédé en exploitant les jumeaux numériques*. Journée Technique 20 ans du LATEP : Equipements sous pression et nouvelles technologies applications industrielles Laboratoire. IMT Nord Europe, 3 Décembre 2021.
- [S3] B. Dupont*, **D. Vasiukov***. *Diagnostic de défauts à partir de mesures sans contact : détection des fissures et prévision durée de vie résiduelle (DVR) sur une structure métallique*. Journée Technique 20 ans du LATEP : Equipements sous pression et nouvelles technologies applications industrielles Laboratoire. IMT Nord Europe, 3 Décembre 2021.
- [S4] L. Laiarinandrasana*, **D. Vasiukov***, S. Joannes, Y. Chen, C.-H. Park. *Modélisation multi-échelle des propriétés mécaniques des matériaux hétérogènes en tenant compte de l'influence des porosités*, Journée Industrielle "Matériaux haute performance et écomatériaux dans les transports", Institut Mines-Télécom (IMT), Paris, 21 mai 2019.
- [S5] **D. Vasiukov***, S. Panier. *Fatigue Life Prediction of Fiber Reinforced Composite Structures*. Composites Virtual Prototyping Expert Seminar. Stuttgart, January 27-28, 2015.
- [S6] **D. Vasiukov***. *Textile composites: nonlinear material modeling and multi-scale phenomena*. 34ème Journée Technologique "Les Renforts Textiles dans les Matériaux Composites". ENSAIT, Roubaix, 2 juillet 2015.

(*) - presenting author

Industrial magazine articles

- [MAG1] A. Trameçon, **D. Vasiukov**, C.-H. Park, P. Krawczak. *Fatigue modelling of composite materials for industrial applications*. JEC Composites Magazine, 2016, 53(108), pp. 52–54.
- [MAG2] **D. Vasiukov**, Y. Liu, C.-H. Park, P. Krawczak. *3D textile-reinforced composites: From manufacturing to structural design*. JEC Composites Magazine, 2018, 55(121), pp. 67–69

Part II

Summary of research activities

General Introduction

This manuscript presents the synthesis of my research activities since my PhD thesis defense in May 2013. It contains various components of my work with collaborators (refer to Section *Research and Industrial Collaborations* of my CV) and all my students (refer to Section *Supervising* of my CV). I have organized the synthesis of all works into four chapters, with the last chapter dedicated to Perspectives.

The First Chapter describes all the activities dedicated to material model development. I have been working with heterogeneous materials such as composites (UD-ply composites, two-dimensional (2D) textiles, three-dimensional (3D) textiles). In recent decades, significant advancements have been made in material modeling. However, the commercial availability of existing material models is still quite limited, often relying on strong assumptions. Thus, in this Chapter, I have summarized my developments of the anisotropic damage model for heterogeneous materials, considering various nonlinear viscoelastic and viscoplastic effects [**Vasiukov et al., 2015b**]¹. These developments were pursued by my first PhD student, Yang LIU, and applied for the meso-scale damage modeling of 3D textile-reinforced composites [**Liu et al., 2017a**]. The anisotropic damage model has also been extended to predict the fatigue life of composites [**Vasiukov et al., 2015a**].

One of the main challenges is determining the level of accuracy we aim to achieve. The *World Wide Failure Exercise* [**Kaddour and Hinton, 2013**]² has revealed that one of the best models required tens of material parameters for identification. This fact motivated my researches grouped in the Second Chapter which shows my contributions to multi-scale modeling of composites and hybrid (composite/metal) structural materials. The primary objective of these contributions is to enhance the accuracy of numerical models that are applied for design of structures made of new composite materials. Variability during manufacturing processes should also be considered, including local variations of constituent materials, interfaces, or voids. Numerical modeling should offer an effective means to predict complex phenomena across different material scales (micro, meso, and macro) of heterogeneous materials (e.g., multiaxial composites, polymer blends, or textiles-reinforced composites). The developed approaches should be supported by advanced experimental characterization techniques (such as digital image correlation and micro-CT tomography). All aspects are extensively documented in the PhD thesis of YANG LUI (2014-2018). These research developments continued with another PhD student, K.K PARVATHANENI (2018-2021). The findings from these research endeavors were published in several journal articles [**Liu et al., 2017a**, **Labanieh et al., 2017**, **Wintiba et al., 2020**, **Naouar et al., 2020**] and presented at numerous national and international conferences [**Liu et al., 2017b**, **Straumit et al., 2018**, **Vasiukov et al., 2018, 2019**].

Descending from the macro- to meso- and from meso- to micro-scale, it became apparent that describing all observed mechanisms at these different scales would necessitate creating a numerical model with billions of degrees of freedom. Therefore, the acceleration of calculations plays a crucial role. Various techniques of High-Performance Computing can be employed, or consideration can be given to accelerating the calculation process itself. Furthermore, image-based experimental observations, particularly μ -CT, became increasingly accessible to researchers. In

¹The bold text is used for the author's citations.

²WWFE was organized to determine which material modeling provides better predictions using blind tests.

2017, I initiated the first investigations in our department into the application of Fast Fourier Transform-based solvers (FFT-solver³) for textile composites. This solver, freely available, was initially proposed by [Moulinec and Suquet, 1994]. Subsequently, this research was continued by post-doc YANG CHEN (2018-2019) and published in [Chen et al., 2019c,b], introducing the first FFT-solver for the non-local phase-field damage model. The results were so promising that we initiated a new PhD thesis in collaboration with KU Leuven (Composites group at MTM Department). This marked the commencement of the third PhD, XIAO MA (2019-2022). The outcomes were published in three journal papers [Ma et al., 2021, 2023a,b].

I have aligned the perspectives of my research activities with the main trends of "*Ecological transition*" and "*Numerical transition*" of our society, which are also two mainstreams of the Horizon Europe⁴ program. As presented in the last Chapter the works related to "*Transport of hydrogen*"⁵ are becoming of high interest in the last decade.

³From here onwards, FFT-solver will be used in the text.

⁴"*New materials*" and "*Green deal*"

⁵New calls on the construction of the hydrogen platforms in the Horizon Europe program: [Hydrogen Valleys](#)

3 .Non-linear modeling of composite materials

In this chapter, I present a summary of my research activities, which are focused on developing new models using a phenomenological approach to predict non-linear material behavior at the macro-scale. The design process of structures made of advanced composite materials necessitates a model (or criterion) that ensures robust prediction of mechanical performance. Therefore, the main motivation was to address the question: **What is the most efficient model allowing us to design a new structure made of composites?**

In this regard, the primary focus of this chapter is model development for laminated composites as anisotropic homogenized material, considering the anisotropy, the viscous behavior of the matrix (viscoelasticity and viscoplasticity), and the damage mechanisms.

The chapter is organized into three sections. The first section describes the derivation of the constitutive equations (for the implicit scheme) for a general 3D case. The second section is dedicated to extending the phenomenological model to fatigue life prediction. The latter is based on the original direct approach and, in our case, is grounded on the assumption that the composite material can reach a "stabilized damage state".

The results of this chapter have already been published in [Vasiukov et al., 2015b] and [Vasiukov et al., 2015a] at the beginning of my career. These developments were pursued by my first PhD student Lui [2017].

This chapter provides a summary of the following research activities:

- 2 Master 2 projects: **T. Kondouri** (M2, *Development of anisotropic constitutive model based on coupled plasticity-damage theory*, 2012, [M1] in my CV) and **B. Li** (M2, *Multi-scale analysis based on nested finite element approach*, 2012, [M2]).
- 2 collaborative projects: **European project FP7 MAPICC** (*One shot Manufacturing on large scale of 3D upgraded panels and stiffeners for Lightweight thermoplastic textile composite structures*, 2012-2015) and **Project FUI ACCUM** (*Armement Caténaire Composite Universel Multitension*, 2014-2017).
- 6 international conferences (see in CV [CP11], [CP12], [CP14], [CP15], [CP16] and [CP17]).
- 1 invited in one scientific seminar to Stuttgart University (see in CV [S5]).
- 2 journal papers (see in CV [A14] and [A15]).
- 1 PhD thesis advising of **Y. LUI** (see in CV [D1]).

3.1 Static model development

3.1.1 Damage phenomena in composites

The damage mechanisms are generally classified according to the material scales (see Fig. 3.1a).

1. Micro scale

- *fibre breakage* (or failure) is a crucial failure mechanism that leads to catastrophic failure of composites and occurs when the load applied to a composite material reaches a maximum strength value. Fibre breaking can take place during longitudinal tension or compression and the energy consumed by these failure processes is much larger than matrix or fibre/matrix debonding. In compression, fibre breaking usually occurs as a result of the microbuckling and the formation of *kink-band*.
- *matrix microcracking* is an intralaminar form of damage, and involve cracks or voids between fibres within a single composite layer or lamina. Matrix damage is a complex phenomenon because initiation starts at defects or at fibre/matrix interfaces.
- *diffuse damage* is associated mainly with fibre/matrix debonding. This is a fundamental mechanism in order to explain the behavior of a ply, especially under shear loading. This debonding is assumed to be homogeneous within the ply.

2. Meso scale

- *matrix transverse cracking* is caused by 3D tunnelling (through the entire ply) cracks spread from small flaws located on the matrix of the 90° layers in the direction transverse to the applied load. This cracking is usually the source of the first-ply-failure.
- *local delamination* refers to the interface's degradation initiated at the tip of the transverse microcrack. The local delamination cracks occur in a damaged interface.
- *diffuse delamination* refers to a diffuse degradation of the interface microvoids and microdecohesions which are assumed to be homogeneous within the interface.

3. Macro scale

- *delaminations* are separations between internal layers of a composite laminate caused by high through - thickness stresses. It is potentially the more critical mode of failure and causes significant structural damages. Delaminations cause large stiffness drop and reduction in load-bearing capabilities. It may occur from a few reasons, namely, (i) interlaminar stresses arising from geometric factors, (ii) material discontinuity from design features (edge or hole), and (iii) matrix cracking (structural loading).

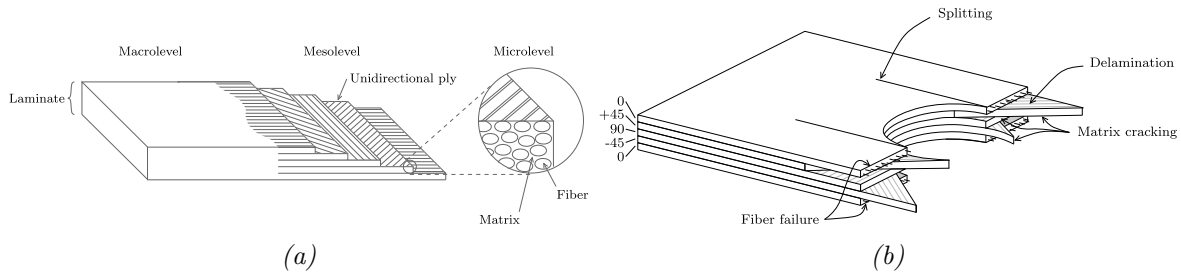


Figure 3.1: Material scales in composites in UD composites (a) and schematic representation of the failure mechanisms in the composite [van der Meer, 2012](b).

3.1.2 Constitutive modeling of unidirectional composites

There exist many material models for nonlinear constitutive behavior of composites. Here, we will focus on the modeling based on Continuous Damage Mechanics (CDM) framework; thus, it can be classified as phenomenological modeling (so-called meso-scale material modeling). This type of modeling considers a composite ply as a homogeneous material, and damage effects are considered by introducing effective properties (stiffness and compliance tensor) along with damage kinematics rules. These damage mechanisms stand for different degradation effects at the microscopic level (as shown in Sec. 3.1.1). These types of methods are widely applicable in the majority of commercial and scientific software. The main idea is to define specific energy potentials for a ply and interface, which depend on damage mechanisms [Maire and Chaboche, 1997]. The thermodynamic forces conjugated with damage could be defined as partial derivatives of the strain energy with respect to damage variables. One of the first models for composite material was developed by Ladeveze and Dantec [1992], in which the damage mechanisms were described by three scalar variables, and the accumulation of inelastic strain was considered in-plane shear response.

More recent developments involve modeling of material non-linearity using the plasticity framework [Vyas et al., 2011, Vogler et al., 2013], continuous damage mechanics (CDM) [Lubineau and Ladeveze, 2008, Hassan and Batra, 2008], or coupled plasticity with CDM [Vyas and Pinho, 2012, Chen et al., 2012, Vogler et al., 2013]. In [Maimí et al., 2007, Flatscher and Petermann, 2011], brittle damage models with strain softening behavior were developed. Many efforts have been made to define, represent, and describe the correlation between micro- and meso-damage phenomena [Ladeveze and Lubineau, 2001, 2002] using homogenization of the damaged composites. A number of material models presented in the literature, despite of their great development within meso-scale constitutive modeling for FRP composites, address a plane stress statement with reduced definition of the yield surface, damage criterion and material response itself. Moreover, non-linear effects due to viscoelasticity, viscoplasticity and/or damage mechanisms are often ignored.

These were main motivations for novel model development presented in [Vasiukov et al., 2015b]. The developed model reflects the following key-points of the constitutive material modeling of Fiber Reinforced Plastics (FRP) composites such as :

- The anisotropy of time-dependency effects which is modeled by anisotropic three-dimensional viscoelasticity theory.

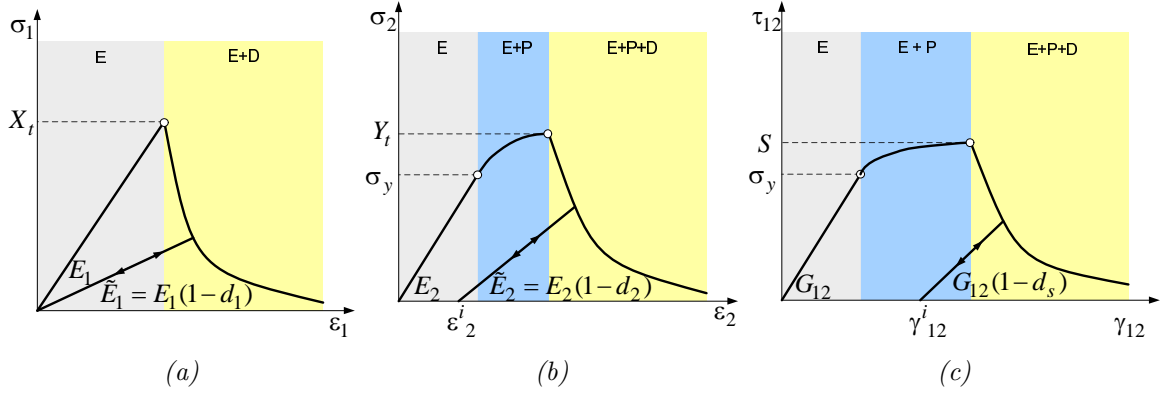


Figure 3.2: FRP composite material stress-strain behavior: a) in the fiber direction, b) in the transverse direction, c) in-plane shear.

- The anisotropy of irreversible strain accumulation, in the visco-plasticity theory with kinematic hardening. It takes in the case of matrix driven material response. It was assumed the elastic-brittle damage in the fiber direction, i.e. no inelastic strain and no time-dependency effects can be developed (Fig. 3.2a). In contrast to fiber direction, transverse and shear responses are non-linear (Figs. 3.2b, 3.2c) with anisotropy of viscoelastic, viscoplastic and damage mechanisms.
- Damage mechanisms and material degradation which are defined within continuous damage mechanics.
- Development of the constitutive model in order to take into account hydrostatic pressure sensitivity of the FRP composites which cannot be ignored.

In [Vasiukov et al., 2015b] a three dimensional non-linear model was presented. The viscoelastic strain is defined in form of the generalized standard linear solid of Kelvin-Voigt type. To begin with, the total strain rate is decomposed as follows:

$$\dot{\boldsymbol{\varepsilon}} = \dot{\boldsymbol{\varepsilon}}^e + \dot{\boldsymbol{\varepsilon}}^v + \dot{\boldsymbol{\varepsilon}}^{vp} = \dot{\boldsymbol{\varepsilon}}^{ve} + \dot{\boldsymbol{\varepsilon}}^{vp}, \quad (3.1)$$

where dot on top of the symbols denotes the time derivative, $\boldsymbol{\varepsilon}^{ve}$ and $\boldsymbol{\varepsilon}^{vp}$ stand for the viscoelastic (or reversible) and viscoplastic (or irreversible) strain tensor of the second order, respectively.

Anisotropic viscoelasticity

Viscoelastic contribution describes the time-dependent properties of the polymer matrices which were observed in creep or relaxation tests. The developed viscoelastic model will focus on the prediction of short-time creep loading cases (only 750 hours data are considered). If a longer-term description is required then the model should be extended. No temperature effects were included in the modeling. Therefore, the model can be applied for material at temperature which is less than glass transition temperature (T_g) of polymer matrix of the composite. An efficient integral form of general non-linear viscoelastic material has been proposed by Schapery

[1969] where the viscoelastic strain is defined as:

$$\boldsymbol{\varepsilon}^{ve}(t) = g_0 \mathbb{S}_0 : \boldsymbol{\sigma} + g_1 \int_0^t \mathbb{S}^{ve} (\Psi^t - \Psi^\tau) : \frac{d(g_2 \boldsymbol{\sigma})}{d\tau} d\tau, \quad (3.2)$$

where \mathbb{S}_0 and \mathbb{S}^{ve} stand for the instantaneous and transient compliance respectively, g_0 , g_1 and g_2 are the non-linear material parameters, Ψ^t represents the shifting factor induced, for instance, by temperature, ':' stands for the double-dot product. It can be shown that the general model can be reduced if g_0 , g_1 and g_2 equal to one, then Eq. 3.2 is rewritten as:

$$\boldsymbol{\varepsilon}^{ve}(t) = \mathbb{S}_0 : \boldsymbol{\sigma} + \int_0^t \mathbb{S}^{ve}(t - \tau) : \frac{d(\boldsymbol{\sigma})}{d\tau} d\tau. \quad (3.3)$$

In order to obtain numerical solutions, the transient compliance \mathbb{S}^{ve} is represented in Prony series. For the current model, the compliance tensor is defined as follows:

$$\mathbb{S} = \mathbb{S}_0 + \sum_i^n \mathbb{S}^{ve}, \quad (3.4)$$

where n is number of mechanisms in the viscoelasticity model, \mathbb{S}^{ve} is the compliance viscoelastic tensor, whose components are defined by taking into account that $E^{ve} = \sum_i^n E_i^{ve} (1 - e^{(-t/\tau_i)})$ with $\tau_i = \eta_i^e / E_i$ as the retardation times and E_i as the viscoelastic moduli. The compliance tensor \mathbb{S} is shown explicitly in the Appendix of the article of Vasiukov et al. [2015b]. For an elastic material, the following relation holds good: $\mathbb{C}_0 = \mathbb{S}_0^{-1}$, with superscript \square^{-1} denoting the inverse operation. The viscoelastic strain rate is defined as:

$$\dot{\boldsymbol{\varepsilon}}^{ve} = \sum_i^n \left(\frac{\mathbb{S}^{ve}}{\tau_i} : \dot{\boldsymbol{\sigma}} - \frac{1}{\tau_i} \boldsymbol{\varepsilon}_i^{ve} \right). \quad (3.5)$$

Using this representation, different viscoelastic materials can be modeled and the quality of approximation will depend on the number of included terms. More information can be found in Vasiukov et al. [2015b].

Viscoplasticity model

The next step is the modeling of permanent strains accumulation. It is obvious that FRPs, in contrast to metals, do not have the same micro-mechanisms that lead to permanent strain accumulation. However, meso-scale material models use the terminology which is more familiar and originally developed for the plasticity theory or the viscoplasticity to be more precisely. Permanent strains can be induced by different mechanisms at the micro-level: viscoelastic nature of the polymers, microscopic degradation, in some cases plasticity of polymer resin. Including viscoplasticity modeling allows to introduce the strain rate dependency. According to the viscoplasticity model developed by Perzyna [1966], viscoplastic strain rate is defined by:

$$\dot{\boldsymbol{\varepsilon}}^{vp} = \eta^p \langle \varphi(F) \rangle \partial_{\boldsymbol{\sigma}} F = \dot{\lambda}^{vp} \mathbf{n}_F, \quad (3.6)$$

with $\varphi(F) = (F)^n$, the plastic potential F with n as the material constant characterizing the strain rate effect. According to the strain decomposition shown in Eq. 3.1 with zero creep strain rate, the stress increment is defined as:

$$\dot{\boldsymbol{\sigma}} = \mathbb{C}^e (\dot{\boldsymbol{\varepsilon}} - \dot{\boldsymbol{\varepsilon}}^{vp}) = \mathbb{C}^e : \left(\dot{\boldsymbol{\varepsilon}} - \dot{\lambda}^{vp} \mathbf{n}_F \right) \quad (3.7)$$

The quadratic norm is chosen and written in incremental form as follows:

$$\dot{p} = \|\dot{\boldsymbol{\epsilon}}^{vp}\| = \dot{\lambda}^{vp} \sqrt{\frac{1}{2}} \|\mathbf{n}_F\|. \quad (3.8)$$

where $\|\dot{\boldsymbol{\epsilon}}^{vp}\| = \sqrt{\frac{1}{2} \dot{\boldsymbol{\epsilon}}^{vp} : \dot{\boldsymbol{\epsilon}}^{vp}}$ with normal $\mathbf{n}_F = \partial_{\boldsymbol{\sigma}} F$. In the case of the associated flow $f = F$, in order to satisfy the requirements for the material model presented above, the modified Hoffman criterion has been used as yield function in the following form:

$$f = \frac{1}{2} \boldsymbol{\xi} : \mathbb{P} : \boldsymbol{\xi} + \mathbf{q} : \boldsymbol{\xi} - \sigma_0^2, \quad (3.9)$$

where $\boldsymbol{\xi} = \boldsymbol{\sigma} - \mathbf{X}$ with $\boldsymbol{\sigma}$ as Cauchy stress tensor and \mathbf{X} as back stress tensor; \mathbb{P} and \mathbf{q} are the fourth order and second order tensors, respectively, to define the plastic potential in a generalized form, σ_0 is the material parameter. Modifications in the Hoffman criterion imply the insensitivity to the σ_{11} stress component in the fiber direction. Then plastic strain increment is obtained from:

$$\dot{\boldsymbol{\epsilon}}^{vp} = \dot{\lambda}^{vp} \partial_{\boldsymbol{\sigma}} f = \dot{\lambda}^{vp} \mathbf{n}_f, \quad (3.10)$$

with $\dot{\lambda}^{vp}$ is the Lagrange multiplier or consistency parameter, \mathbf{n}_f denotes the normal vector to yield surface. The Kuhn-Tucker conditions should be satisfied:

$$\dot{\lambda}^{vp} \geq 0, \quad f \leq 0, \quad \dot{\lambda}^{vp} f = 0. \quad (3.11)$$

Chosen plastic potential implies that:

$$\begin{aligned} \dot{\epsilon}_{11}^{vp} &= \dot{\lambda}^{vp} \partial_{\sigma_{11}} f = 0, \\ \dot{\alpha}_{11} &= \dot{\lambda}^{vp} \partial_{X_{11}} f = 0. \end{aligned}$$

The Frederick-Armstrong hardening law is chosen as a good candidate to represent experimental data. In incremental form it is written as:

$$\dot{\mathbf{X}} = \frac{2}{3} H \dot{\boldsymbol{\epsilon}}^{vp} - \gamma \mathbf{X} \dot{p}, \quad (3.12)$$

where C and γ are the material parameters whose values are obtained from the effective stress-plastic strain curve: for the more details see [Vasiukov et al. \[2015b\]](#).

Damage model

Now let us consider the damage mechanisms and their modeling approaches for FRP composites. Here, the anisotropic constitutive model for FRP is based on the CDM. We start from using the concept of effective stress $\tilde{\boldsymbol{\sigma}}$ proposed by [Kachanov \[1958\]](#). There are different ways to introduce damage effect on a material [[Lemaître and Desmorat, 2005](#)]: scalar or plural scalar, vector, second- and higher order tensor variables. Using the strain equivalence principle, the effective stress tensor is defined in a general form as:

$$\tilde{\boldsymbol{\sigma}} = \mathbb{M} : \boldsymbol{\sigma}, \quad (3.13)$$

where \mathbb{M} is the fourth-order damage effect tensor. The derivation of the effective stiffness tensor can be deduced from the existence of the Gibbs free energy potential [[Maire and Chaboche,](#)

1997], which is based on the complementary strain energy equivalence principle [Chow and Lu, 1989]. The energy of a layer is defined as:

$$\mathcal{G}^e(\tilde{\boldsymbol{\sigma}}, 0) = \mathcal{G}^e(\boldsymbol{\sigma}, \mathbf{d}) = \frac{1}{2} \boldsymbol{\sigma} : \tilde{\mathbb{S}} : \boldsymbol{\sigma}, \quad (3.14)$$

where $\tilde{\mathbb{S}} = \mathbb{M}^T : \mathbb{S}^e : \mathbb{M}$ - effective compliance tensor. In three dimensional cases the effective stiffness tensor is defined by the effective compliance tensor ($\tilde{\mathbb{C}} = \tilde{\mathbb{S}}^{-1}$). Then, according to hypothesis of the equivalence complimentary energy for damaged and undamaged material, the following relation is valid:

$$\begin{aligned} \boldsymbol{\sigma} &= \tilde{\mathbb{C}} : \boldsymbol{\varepsilon}^e, \\ \tilde{\boldsymbol{\sigma}} &= \mathbb{C}^e : \boldsymbol{\varepsilon}^e. \end{aligned} \quad (3.15)$$

Different types of \mathbb{M} tensor and their symmetrization problem have been discussed in [Voyiadjis and Park, 1997]. It is accepted following Voigt notation to write \mathbb{M} tensor as:

$$[M] = \text{diag} \left[\frac{1}{\sqrt{1-d_1}}; \frac{1}{\sqrt{1-d_2}}; \frac{1}{\sqrt{1-d_3}}; \frac{1}{\sqrt{1-d_4}}; \frac{1}{\sqrt{1-d_5}}; \frac{1}{\sqrt{1-d_6}} \right], \quad (3.16)$$

where damage variables represent following damage mechanisms: $d_1 = d_f$ - fiber damage; $d_2 = d_{m1}$ matrix damage in the second principal material direction; $d_3 = d_{m2}$ matrix damage in the third principal material direction; $d_4 = (d_2 + d_3)/2$, $d_5 = (d_1 + d_3)/2$ and $d_6 = (d_1 + d_2)/2$. The thermodynamic damage forces are derived from Eq. 3.14 by taking partial derivative of the potential with respect to damage tensor:

$$\mathbf{Y} = \partial_{\mathbf{d}} \mathcal{G}^e(\boldsymbol{\sigma}, \mathbf{d}). \quad (3.17)$$

Damage criterion and kinetics

Depending on the type of modeling, the damage potential can be defined in different ways: in strain space, stress space or thermodynamic forces space. Here, Hashin's damage model [Hashin, 1980] is used for the description of UD composites. Only three damage mechanisms are independent. For those mechanisms, the damage potential functions are defined using the invariant form as shown by Kress [2012]:

$$\begin{aligned} I_1 \geq 0 : \quad F_{d_{ft}} &= \left(\frac{I_1}{\sigma_A^+} \right)^2 + \frac{I_4}{\tau_A^2} = 1, \\ I_1 < 0 : \quad F_{d_{fc}} &= \left(\frac{I_1}{\sigma_A^-} \right)^2 = 1, \\ I_2 \geq 0 : \quad F_{d_{mt}} &= \left(\frac{I_2}{\sigma_T^+} \right)^2 + \frac{I_3}{\tau_T^2} + \frac{I_4}{\tau_A^2} = 1, \\ I_2 < 0 : \quad F_{d_{mc}} &= \left[\left(\frac{\sigma_T^-}{2\tau_T} \right)^2 - 1 \right] \frac{I_2}{\sigma_T^-} + \left(\frac{I_2}{2\tau_T} \right)^2 + \frac{I_3}{\tau_T^2} + \frac{I_4}{\tau_A^2} = 1, \end{aligned} \quad (3.18)$$

with the definitions of the stress measurements as follows: $I_1 = \sigma_1$, $I_2 = \sigma_2 + \sigma_3$, $I_3 = \tau_{23}^2 - \sigma_2 \sigma_3$ and $I_4 = \tau_{12}^2 + \tau_{13}^2$. For both orthogonal directions, we suppose that: $F_{d_{mt}} = F_{d_{m2t}} = F_{d_{m3t}}$

and $F_{d_{mc}} = F_{d_{m2c}} = F_{d_{m3c}}$. For three damage mechanisms, the evolution laws is written in an exponential form as following:

$$d_\gamma = 1 - \frac{1}{f_{d_\gamma}} e^{S_\gamma(1-f_{d_\gamma})l_e/(G_\gamma C_{ii})}, \quad \gamma = (f, m1, m2), \quad i = (1, 2, 3) \quad (3.19)$$

where C_{ii} , S_γ are the stiffness and strength components respectively, l_e the characteristic elements size and G_γ is the fracture energy for each damage mechanism. That form is widely used in the development of the material models with softening damage effects. In Eq. 3.19 can be found by the reflection of a crack band model originally introduced by Bažant and Oh [1983].

Stress increment derivation and consistent tangent stiffness

The proposed viscoelastic-viscoplastic model coupled with damage has been implemented in ABAQUS/Standard finite element software by means of the user-defined subroutine UMAT. In order to integrate the stress-strain relationship the implicit Euler backward method is used. While implementing this method, it could be assumed that: the continuum problem is represented by discrete one. The constrained-optimization problem is reduced to a numerical solution of the iterative convex mathematical optimization problem which in turn reduces to a standard problem of finding the closest distance of the point to a convex set [Simo and Hughes, 1997]. The point and convex set stand for a trial state and elastic domain respectively. Therefore, there are three basic steps of the return-mapping algorithm:

1. *Elastic trial state.* For which trial values of the local variables are calculated. If trial state satisfies the admissibility condition, then the current step is accepted as elastic and exits from the procedure. If not, proceed to the next step.
2. *Plastic correction.* The non-linear system of equations is solved considering plastic flow with enforcing Kuhn–Tucker conditions and using trial step variables. The non-linear single equation solution can be accomplished using a local Newton–Raphson method.
3. *Damage deterioration.* It is performed by calculation of the damage potential and update damage component values with subsequent recalculation of stress tensor, effective stiffness properties and tangent operator.

The implicit time-integration is required by the end of the time-increment to calculate new stress components and tangent operator. The first step is the calculation of anisotropic elasto-viscoplastic solution. Generally, the stress increment can be evaluated from single equation by using accepted flow rule and statement of the Euler backward algorithm [Neto et al., 2008]:

$$\boldsymbol{\sigma}_{n+1} = (\mathbb{I} + \Delta\lambda^{vp}\mathbb{C}^e : \mathbb{P})^{-1} : (\boldsymbol{\sigma}^{trial} - \Delta\lambda^{vp}\mathbb{C}^e : \mathbf{q}), \quad (3.20)$$

where $\boldsymbol{\sigma}^{trial}$ denotes the trial stress tensor. Then, by integrating Eq. 3.20 into the yield condition Eq. 3.9 and enforcing that ($\dot{f} = 0$), the non-linear equation is derived. An approximate solution to that equation is obtained by using Newton-Raphson method. The algorithmic stiffness tensor \mathbb{D}^{ep} is defined by:

$$\begin{aligned} \Delta \boldsymbol{\sigma}_{n+1} &= \mathbb{D}^{ep} : \Delta \boldsymbol{\varepsilon}_{n+1} \\ &= \left[\mathbb{C}_{n+1}^* - \frac{\mathbb{C}_{n+1}^* : \bar{\mathbf{n}}_F \otimes \mathbf{n}_f : \mathbb{C}_{n+1}^*}{\mathbf{n}_f : \mathbb{C}_{n+1}^* : \bar{\mathbf{n}}_F + (2/3)H\partial_{\mathbf{X}}F : \bar{\mathbf{n}}_F - \gamma\bar{\mathbf{n}}_F : \mathbf{X}} \right] : \boldsymbol{\varepsilon}_{n+1} \end{aligned} \quad (3.21)$$

with $\mathbb{C}_{n+1}^* = ((\mathbb{C}^e)^{-1} + \Delta\lambda_{n+1}^p \partial_{\bar{\boldsymbol{\sigma}}\bar{\boldsymbol{\sigma}}}^2 f)^{-1}$ as 'pseudo-elastic' stiffness matrix [Simo and Hughes, 1997], $\bar{\mathbf{n}}_F = \mathbf{n}_F + \Delta\lambda_{n+1}^p \partial_{\lambda} \mathbf{n}_F$. The time-dependency of the material response is modeled by Perzyna viscoplasticity model. In order to avoid instability of the single step integration algorithm, this model was implemented into general return-mapping method as described in [de Borst et al., 2012]. Taking into account accepted assumptions, the algorithmic stiffness relation (Eq. 3.21) is rewritten as:

$$\begin{aligned} \Delta \boldsymbol{\sigma}_{n+1} &= \mathbb{D}^{vp} : \Delta \boldsymbol{\varepsilon}_{n+1} = \\ &= \left[\mathbb{C}_{n+1}^* - \frac{\mathbb{C}_{n+1}^* : \bar{\mathbf{n}}_F \otimes \mathbf{n}_f : \mathbb{C}_{n+1}^*}{\mathbf{n}_f : \mathbb{C}_{n+1}^* : \bar{\mathbf{n}}_F + (2/3)H\partial_{\mathbf{X}}F : \bar{\mathbf{n}}_F - \gamma\bar{\mathbf{n}}_F : \mathbf{X} + \frac{1}{\eta^p \Delta t}} \right] : \Delta \boldsymbol{\varepsilon}_{n+1} \end{aligned} \quad (3.22)$$

where the last term of the denominator $\frac{1}{\eta^p \Delta t}$ describes the viscosity effect, η^p is the viscosity parameter of the material.

3.2 Extension to fatigue in composites

Damage accumulation and stabilization

The main damage mechanisms observed under fatigue loading are: matrix cracking, fibre/matrix interfacial debonding, delamination, fibre breaking and finally global fracture. The damage evolution is a non-linear function of the number of cycles and exhibits, in general, three characterizing patterns (Fig. 3.3a). At the beginning and near the end of fatigue life, damage growth is rapid, but for most of the life damage accumulation is gradual and linear [Harris, 2003]. The severity of each stage and total amount of damage depend on laminate stacking sequence, material properties and loading conditions. The similarity have been noticed during the evolution of the temperature field which is a consequence of the dissipation due to damage [Sawadogo et al., 2012].

Stage I is characterized initially by fibre/matrix debonding which occurs depending upon the strength of the interfacial bond between fibre and matrix material. Then matrix micro-cracking process is initiated. The increase of crack density leads to micro-cracks coalescence and then to damage saturation. In Fig. 3.4a is shown the evolution of the crack densities in different layers of a tube under cyclic tension/compression [Schmidt and Horst, 2010]. The matrix damage saturation is a common process in laminates and the damage state is given by the saturated matrix cracking and has been termed as *Characteristic Damage State* [Reifsnider, 1991]. It is the starting point for those processes, which control the strength, stiffness and life of a laminate. The damage state can be accurately described and predicted. A schematic representation of damage initiation and growth process is shown in Fig. 3.3b.

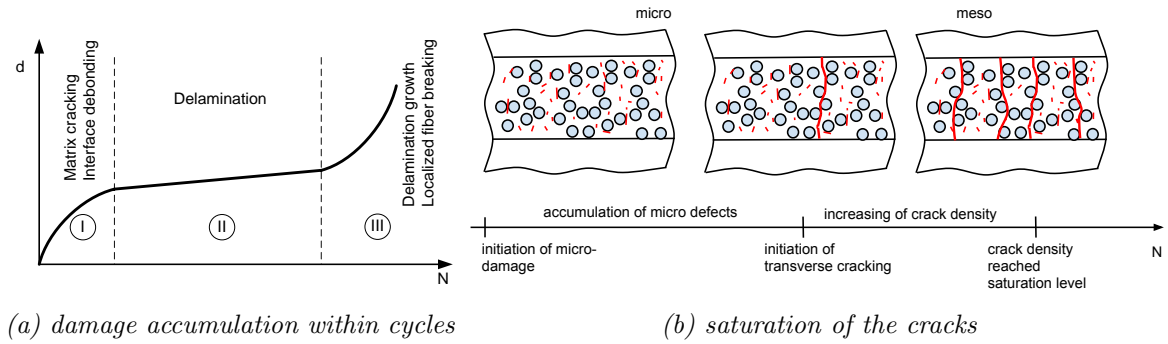


Figure 3.3: Schematic representation of fatigue damage in FRP [Vasiukov et al., 2015a].

Stage II is mostly characterized by the initiation and propagation of delamination which occurs near free edges or on the tips of transversal cracks [Reifsnider, 1991, Ladevéze and Lubineau, 2003]. During this stage, the damage can remain constant or gradually increase. It was shown that stiffness degradation is relatively higher for the lower stress levels in the case of $[\pm 45]$ composites under a loading ratio of $R = \sigma_{min}/\sigma_{max} = 0.1$ [Eliopoulos and Philippidis, 2011]. The linear dependency between normalized maximum stress and stiffness degradation is observed.

Stage III is the last stage of damage growth. All the damage modes would be developing rapidly in a fast-decreasing stiffness of the laminate. As the stress state reaches a critical value, fracture of the laminate would be initiated.

Mechanical response of FRP materials

Let us begin with the classification of material response under cyclic loading which, basically, can have four kinds of behavior [Weichert and Maier, 2000]: *elastic response*; *elastic shakedown response*, when the elasto-plastic behavior becomes purely elastic after a limited number of cycles; *plastic shakedown* (alternating plasticity), when the elasto-plastic behavior becomes stabilized after a limited number of cycles, and the total deformation over a cycle converges to zero; *ratcheting response*, also called progressive deformation or incremental collapse, where the structure shows an elastic-plastic behavior, but the total deformation over a cycle never converges to zero.

Here, we extend direct methods theory to the case of FRP for which anisotropic damage should be taken into account. Some fatigue test data have been reported by [Cain et al., 2006, Schmidt and Horst, 2010] for different laminates as shown in Fig. 3.4. During fatigue tests, a block of cycles have been recorded periodically to determine the strain-stress hysteresis loop (as reported in Cain et al. [2006]) and to evaluate the modulus (also called fatigue modulus). Representative loops for a typical $[\pm 45]$ composite specimen are shown in Fig. 3.4d for a shear loading. It can be concluded that initially non-linear response becomes linear after a certain number of cycles. By analogy with metallic materials, this phenomenon can be named as elastic shakedown. If the amplitude of the applied load is higher, the hysteresis becomes larger and gradually increases within cycles. This is associated with plastic shakedown.

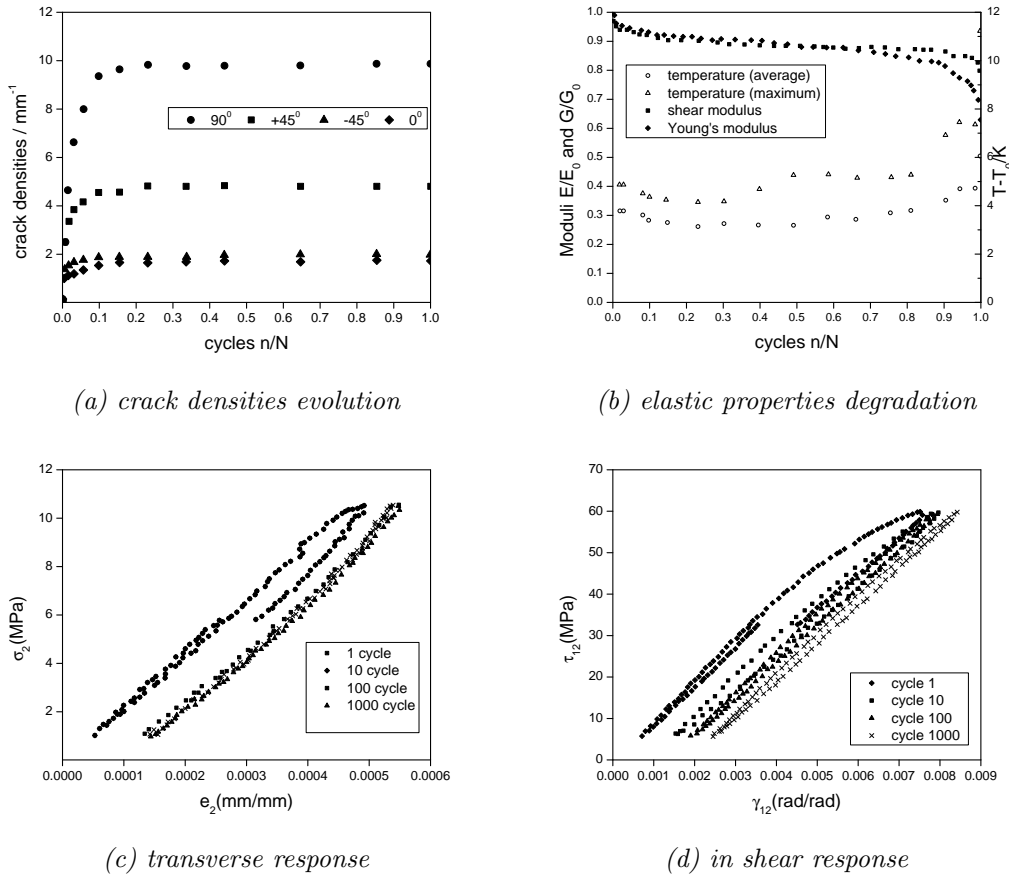


Figure 3.4: Experimental evidence of the damage stabilization process: (a) and (b) data from *Schmidt and Horst [2010]*, (c) and (d) data from *Cain et al. [2006]*.

3.2.1 Principle of the proposed direct approach

From the previous section, we can retain the following aspects of the fatigue damage:

1. damage can be divided into three main stages: (i) rapid growth, (ii) levelling-off and (iii) rapid damage accumulation;
2. under certain conditions (stacking, loading) the damage can reach an asymptotic value at the end of stage I followed by a very small variation during stage II;
3. under cyclic loading, the stress-strain behavior can be purely elastic, elastic shakedown, plastic shakedown or ratcheting.

This approach is based on the original ideas of *Zarka et al. [1990]* which were extended to the case of FRP composites in order to predict damage limit state of a structure under cyclic loading. The SDM allows to directly calculate the stabilized cycle of a structure subjected to cyclic loading from purely elastic response and solution of convex optimization problem.

Constitutive damage model

Now let us consider the damage mechanisms and their modeling approaches for FRP composites. Here, the anisotropic constitutive model for FRP is based on the CDM. We start from using

the concept of effective stress $\tilde{\boldsymbol{\sigma}}$ proposed by [Kachanov \[1958\]](#). There are different ways to introduce damage effects on a material [[Lemaître and Desmorat, 2005](#)]: scalar or plural scalar, vector, second- and higher order tensor variables. The constitutive model development is based on the model presented in [Sec. 3.1.2](#).

Considering FRP materials, we suppose that the Gibbs free energy potential is decomposed into two parts: the one is associated with damage and the other with inelastic dissipation:

$$\mathcal{G}(\boldsymbol{\sigma}, \mathbf{d}, \boldsymbol{\Gamma}) = \mathcal{G}^e(\boldsymbol{\sigma}, \mathbf{d}) + \mathcal{G}^d(\boldsymbol{\alpha}^d), \quad (3.23)$$

where superscripts e, d denote the elastic and damage terms; $\{\boldsymbol{\sigma}, \mathbf{d}, \boldsymbol{\alpha}^d\}$ are the internal second-order tensor variables denoting the stress, the damage and the kinematic damage hardening, respectively; thermodynamic associated variables: $\{\boldsymbol{\epsilon}^d, \mathbf{Y}, \mathbf{H}\}$ stand for the plastic strain, the thermodynamical forces conjugated with damage and back-stress tensor, respectively. The thermodynamic damage forces are derived from [Eq. 3.14](#) by taking partial derivative of the potential with respect to damage tensor as shown in [Eq. 3.17](#), and take into account [Eq. 3.13](#), the thermodynamic damage force tensor is defined by using energy equivalence principle [[Chow and Lu, 1992](#)]:

$$\mathbf{Y} = \boldsymbol{\sigma} : \left[\tilde{\mathbb{S}} : \mathbb{M}^{-1} : \partial_{\mathbf{d}} \mathbb{M} \right]^s : \boldsymbol{\sigma}, \quad (3.24)$$

where superscript s denotes the symmetrization.

[Al-Rub and Voyiadjis \[2003\]](#) utilized a quadratic damage surface with two types of nonlinear hardening for conventional materials. Later, [Barbero et al. \[2005\]](#) applied the quadratic surface in constitutive modeling for composite materials. Here, the modified damage surface is considered and defined as:

$$g = \sqrt{(\mathbf{Y} - \mathbf{H}) : (\mathbf{Y} - \mathbf{H})} - Y_0^f \quad (3.25)$$

where Y_0^f is the threshold value of the thermodynamic forces associated with damage. The shape of the loading surface is convenient to construct the direct algorithm. Linear damage hardening function is accepted as following:

$$\mathbf{H} = C^d \boldsymbol{\alpha}^d \quad (3.26)$$

where C^d is the kinematic damage modulus and $\boldsymbol{\alpha}^d$ which is introduced previously. In order to demonstrate the ideas of the direct analysis, we consider the case of plane stress. The damage can be described by three variables $d_1 = 1 - \frac{E_1}{E_1^0}$, $d_2 = 1 - \frac{E_2}{E_2^0}$ and $d_{12} = 1 - \frac{G_{12}}{G_{12}^0}$. Under the assumption of small perturbations, regarding [Ladeveze and Dantec \[1992\]](#), the Gibbs free energy \mathcal{G} is written as follows:

$$\mathcal{G} = \frac{1}{2} \left[\frac{\sigma_1^2}{E_1^0 (1 - d_1)} + \frac{\langle \sigma_2 \rangle_+^2}{E_2^0 (1 - d_2)} + \frac{\langle \sigma_2 \rangle_-^2}{E_2^0} \right] - \frac{\nu_{12}^0}{E_1^0} \sigma_1 \sigma_2 + \frac{\sigma_{12}^2}{G_{12}^0 (1 - d_{12})} \quad (3.27)$$

where $\langle \sigma_2 \rangle_+$ and $\langle \sigma_2 \rangle_-$ are non-zero in case the stress value is respectively positive and negative; ν_{12} is the Poisson's ratio. The material is assumed to be brittle and non-sensitive to the cyclic loading in the direction of fibers. For the developed approach, a new scalar variable is defined which represents the equivalent damage as follows:

$$d_{eq} = \sqrt{\mathbf{d} : \mathbf{d}} = \sqrt{d_2^2 + d_{12}^2} \quad (3.28)$$

Transverse meso-cracking

Many efforts were made to evaluate meso-scale cracks density functions and its influence on the degradation of material properties (stiffness or strength). Damage variables can be related to the crack density using the fracture mechanics approach as shown in [Lubineau and Ladeveze, 2008] for three-dimensional problem statement. According to two-dimensional model, the original model is reduced to following one:

$$Y_\rho = Y_{22}\partial_\rho d_{22} + Y_{12}\partial_\rho d_{12} \quad (3.29)$$

where ρ denotes the crack density. Then different types of the criteria could be applied. For instance, in Lubineau and Ladeveze [2008] the mixed-mode criterion was used. The authors have shown the relation of the fracture mechanics parameters (such as G_i^c and G_{ii}^c which stand for the critical energy release rates) and considered them using continuous mechanics. Ladeveze and Lubineau [2001] have reported that the crack density evolution can be represented by the thermodynamic forces. The importance of meso-scale damage mechanisms on the life prediction was extensively investigated for multiaxial composites [Quaresimin et al., 2014]. Therefore, in the development of the life prediction approach, these arguments have been addressed through the threshold parameter for damage mechanisms.

3.2.2 Direct numerical algorithm

Iterative procedure to evaluate stabilized states

The developed algorithm for life prediction analysis is inspired by the *ZAC* method [Zarka et al., 1990] which was developed for metallic materials and used internal variables to represent a loading surface. This method is a particular direct method and is used to evaluate the limit state. Further, the method was applied for the life prediction involving mesomechanics [Jabbado and Maitournam, 2007]. Here, *ZAC* method is extended to the case of FRP taking into account the evolution of damage loading surface. Suppose that loading can be discretized by n instants (t_1, \dots, t_n) then at the initial time-step ($t = 0$) the material does not contain inelastic strain and is defect-free. Starting from the origin, in the \mathbf{H} -space, successive projections on the convex sets $C_d(t_i)$ and centered on $\mathbf{Y}(t_i)$ allow to calculate the internal variable $\boldsymbol{\alpha}^d$ which is proportional to the damage tensor \mathbf{d} . This variable is associated with the stabilized damage which is equivalent with the damage defined previously ($d_s(t_i) = d_{eq}$), if the stabilized state condition is achieved.

In this work, the proportional cyclic loading with constant amplitude is considered. The damage is calculated from the movement of the hyper sphere on one stabilized cycle. Based on accepted assumption the distance between two centers is calculated using norm $\|\mathbf{Y}(t_i)\|$ in the \mathbf{Y} -space. The total distance then is related to the stabilized damage as:

$$d_s = \frac{2}{C_d} \sqrt{(Y_2(t_2) - Y_2(t_1))^2 + (Y_{12}(t_2) - Y_{12}(t_1))^2} \quad (3.30)$$

The algorithm is partially based on the constitutive damage model proposed by Ladeveze and Dantec [1992]. However, it is important to emphasize that the approach has no restrictions to use other types of damage modeling.

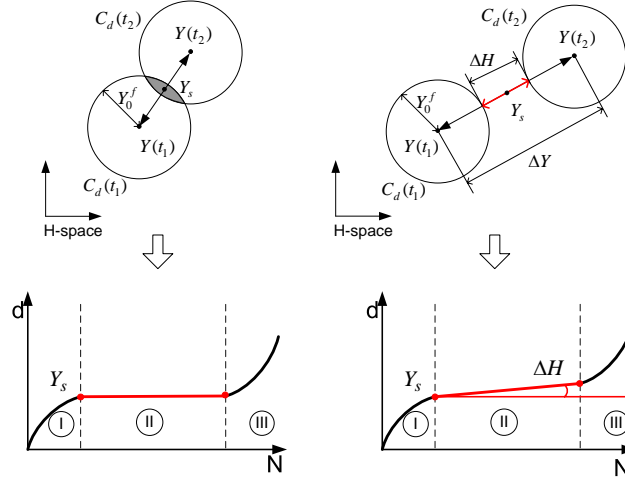


Figure 3.5: Geometrical representation of the damage surface movement.

Life prediction methodology

It is assumed that the life depends on the amount of damage at the end of the stage I and II as shown in Fig. 3.5. The proposed relationship for the life prediction is defined as:

$$N = AY_s^\alpha + B(\Delta H)^\beta = AY_s^\alpha + B(\Delta Y - 2Y_0^f)^\beta$$

where $Y_s = \max(\mathbf{Y}(t)) - \min(\mathbf{Y}(t))/2$, $\Delta Y = \|\max(\mathbf{Y}(t)) - \min(\mathbf{Y}(t))\|$ and $\Delta H = \|\max(\mathbf{H}(t)) - \min(\mathbf{H}(t))\|$, α, β and A, B are the parameters to identify from tests (see [Vasiukov et al., 2015a]). In the case of the radial loading, both values are schematically shown in Fig. 3.5. Stress ratio effect is implicitly considered in the Y_s . In the case of high-cycle fatigue, when the applied stress are low, the intersection of the convex sets C_d is non-void leading to $\Delta H = 0$. In case a stabilized cycle has non-void intersection of the convex sets $C_d(t_i)$ then damage is saturated and the life is predicted based on the amplitude of Y_s . In another case, when stabilized cycle has void intersection of the convex sets $C_d(t_i)$ and stabilized plasticity then the life is predicted based on the amplitude of Y_s and the distance (ΔH) between convex sets $C_d(t_i)$. The last case is that when a cycle is non-stabilized, a ratcheting phenomenon is observed. For the last one, the proposed approach cannot be applied.

Fatigue life prediction for cross-ply laminates

The developed methodology was applied to predict the fatigue life of $[0/90]_s$ cross-ply laminate composites, which are made of glass fiber-reinforced epoxy subjected to tensile cyclic loading with $R = 0.1$. The detailed steps for material properties identification are explained in Vasiukov et al. [2015a]. The numerical results are in good agreement with the performed experimental data, shown in Fig. 3.6. As can be seen, the model is capable of predicting the two main phases of the life up to 10^6 cycles. At lower load levels where the number of cycles exceeds 10^6 , degradation in material properties is present, though not significant. In some cases, the so-called fatigue limit can be observed. However, the use of this term for composite materials should be adopted with great caution. On the other hand, if the applied load level

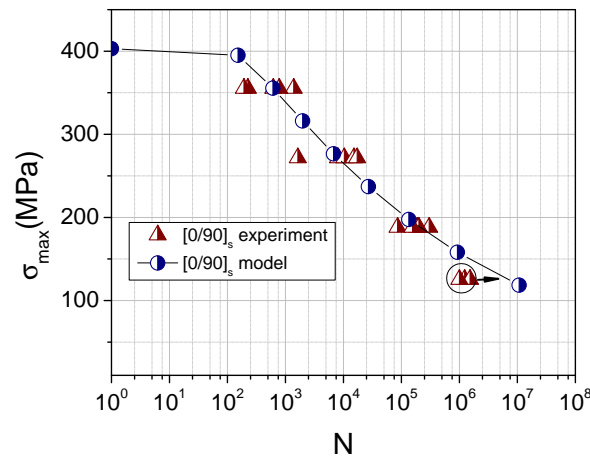


Figure 3.6: Comparison between experimental and numerical results for $[0/90]_s$ cross-ply laminate composite.

is higher than the dictated life, the presence of viscous effects and a high level of permanent strain accumulated in the material should be considered.

3.2.3 Industrial applications

The developments presented in this section have also facilitated the transfer this research results to industrial applications. Two European projects where these developments have been utilized are FP7 MAPICC3D (2012-2015) (see Fig.3.7) and H2020 JOIN'EM (2015-2018) (see Fig.3.8) (refer to *Participation in the collaborative projects* in my CV). In the first application, we have considered the very first attempt to model, using a simplified approach, the fatigue life prediction of the thermoplastic composites [Vasiukov et al., 2016, 2014]. In the second application, the fatigue life prediction method has been applied to thermoset isolating composites for a welding tool.

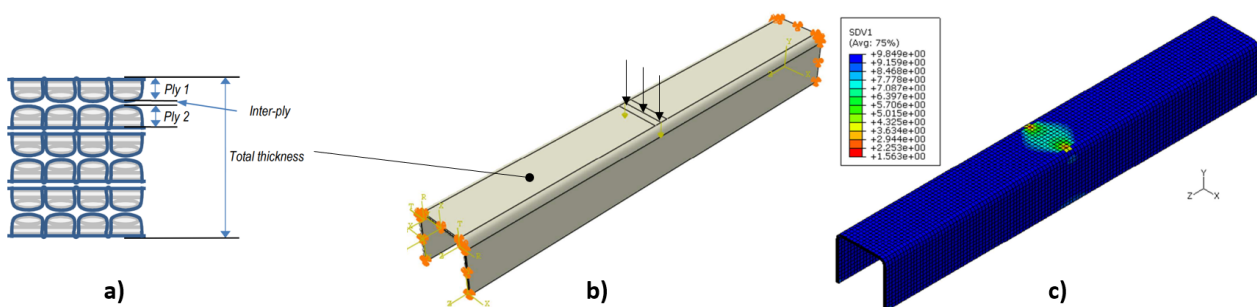


Figure 3.7: Application of fatigue life prediction for thermoplastic composites U-Shape beam subjected to bending loading: a) architecture of the composite material; b) geometry and loading conditions; and c) fatigue life prediction.

Those applications have confirmed the following observations. Model developments are intricately connected to the understanding of mechanisms observed at different material scales. These mechanisms vary depending on the following factors: (i) types of reinforcing materials

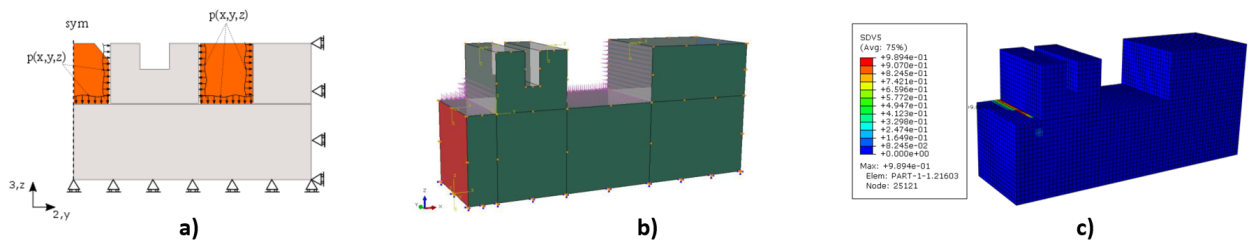


Figure 3.8: Application damage modeling of the thermoset isolating composites under impact loadings: a) schematic presentation of the electromagnetic pulse welding tool; b) geometry and loading conditions; and c) damage prediction.

(unidirectional composites with continuous fibers, textile-reinforced composites, discontinuous fibers, etc.); (ii) types of polymer materials (thermoplastics or thermosets); (iii) loadings conditions (tension, compression, multi-axial, etc.); and (iv) loading duration (impact, quasi-static, fatigue, etc.). Additionally, we should consider multi-physical phenomena (thermal, hydro, etc.) and the impact of manufacturing process parameters (manufacturing defects). All of these factors contribute to the complexity of studying and modeling composite material behaviors, involving several coupled phenomena across different scales.

3.3 Conclusion

My research activities in the field of non-linear material modeling of composite materials can be summarized into two main blocks. These results are important for the following research subjects and allowed me to construct the basis for my future research works:

- **Constitutive Modeling:** A viscoelastic–viscoplastic model coupled with anisotropic continuous damage mechanics for FRP composite material is presented. The model is derived in a general three-dimensional form for an implicit time integration scheme and has been implemented into ABAQUS/Standard via the UMAT subroutine. The following main characteristics of the material modeling for FRP composites have been implemented: (i) anisotropy of irreversible strain accumulation, modeled using viscoplasticity theory with kinematic hardening; (ii) anisotropy of damage mechanisms based on a damage model with softening; (iii) time-dependency, generally ignored in the conventional material modeling, modeled by involving both viscoplastic and viscoelastic frameworks; (iv) material properties regarded as time-dependent and strain rate dependent; (v) viscoelastic viscoplastic and damage potentials have been constructed in a generic way to take into account the hydrostatic pressure effect on material response.
- **Direct Method of Fatigue Life Prediction:** A life prediction method has been developed for FRP materials based on original ideas that involve what we call a simplified direct method. The applicability of this approach is inferred from numerous reported experiments where damage stabilization is observed after a certain number of cycles. The stabilized damage state is characterized by damage accumulated at the end of stage I (characterized by non-linear damage accumulation) and in combination with damage evolution during stage II (where damage evolution is predominantly linear). The proposed method enables the characterization of the damage state of FRP and the prediction of fatigue life based on the thermodynamic forces associated with anisotropic damage mechanisms.

Moreover, my reflection on this topic was mainly grounded in the WORLD WIDE FAILURE EXERCISE [Kaddour and Hinton, 2013], where enormous organizational work has been carried out to find out how different failure theories are performing in the prediction of the composite material failure. One of the most performed models had been identified, which is now called *Onera Damage Models*, initially proposed in [Laurin et al., 2007]. Additionally, I was also impressed by one particular reaction to this exercise from PROF. CHRISTENSEN [Christensen, 2013]. All the mentioned above have led me to research topics that I present in the next chapter.

4 .Multi-scale modeling of textile composites: process - structure - property

In this chapter, the multi-scale modeling of the behavior of textile composites is presented. In textile composites, an additional scale, so-called meso-scale, should be considered. This introduces additional difficulties in geometrical representation and transitions between the scales. All issues will be linked with the anisotropy of the materials, the prediction of the elastic properties, and the damage simulations.

This chapter is organized into three parts. In the first part, the micro-scale characterization and analysis of yarn (from microns to millimeters) are presented. This characterization is based on two (2D) or three (3D) dimensional imaging techniques. In the second part, the main focus will be placed on the meso-scale structure representation of different textiles (3D orthogonal, multi-axial, 3D interlocks). Finally, in the third part, we will discuss the dual-scale porosity defects and their impact on the mechanical properties of textiles.

The results of this chapter have already been published in [Liu et al., 2017a], [Labanieh et al., 2017], [Naouar et al., 2020], and [Wintiba et al., 2020] for FEM solvers. Partially, the meso-scale geometry will be used in the next chapter and has already been published in [Chen et al., 2019c,b, 2018] for FFT solvers. These publications became possible thanks to two following PhD theses. The first one was done by Lui [2017] on realistic yarn representation, and the second one by Parvathaneni [2020] on dual-scale porosity defects.

This chapter provides a summary of the following research activities:

- 1 Master 2 project: **S.-H. Nambiyankulam Hussain**, (M2, *Numerical characterization of sheared organo-sheets based on realistic interpenetration-free geometry*, collaboration with Siemens (Leuven, Belgium), 2019, [M3]).
- 1 Collaborative project: **European project H2020 JOIN-EM** (*JOINing of copper to aluminium by ElectroMagnetic fields*, 2015-2018).
- 6 international conferences (see in CV [CP11], [CP12], [CP14], [CP15], [CP16] and [CP17]).
- 2 Invited in one scientific seminar to Stuttgart University (see in CV [S6] and [S4]).
- 6 journal papers (see in CV [A12], [A11], [A7], [A6], [A4]).
- 2 PhD thesis advising of **Yang LUI** and **Keerthi-Krishna PARVATHANENI** (see in CV [D1] and [D4]).

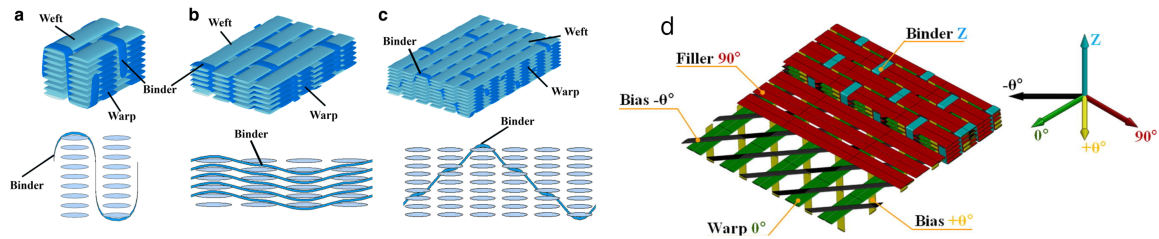


Figure 4.1: 3D textiles discussed in this Chapter: (a) orthogonal; (b) angle-to-angle interlock; (c) through-the-thickness interlocks (a-c were reprinted from [Saleh and Soutis, 2017]) and (d) multi-axis (reprinted from [Labanieh et al., 2017]).

4.1 Introduction to textile composites

In general classification of composite materials for structural applications we can distinguish the following types of composites: laminates, 2D textile reinforced and 3D textile reinforced composites [Mouritz et al., 1999, Long, 2005]. Our particular interest is placed on the modeling of textile composite materials. This type of composite materials has certain advantages compared the laminates composites, namely, improved impact damage resistance and higher through-thickness mechanical properties. On the other hand, their internal structure brings additional level of complexity into multi-scale modeling approaches. In contrast to the laminates (discussed in Chapter 3) the main difference of textile-reinforced composites (2D and 3D) lies in the definition of material scales. Conventionally, for these materials we should consider the following scales [Lomov et al., 2007]: (i) **micro-scale** (microns) to define constituent materials (generally matrix and fiber); (ii) **yarn-scale** (millimeters) to define cross-sections and material behavior of yarn; (iii) **meso-scale** (millimeters - centimeters) to define a Repetitive Unit Cell (RUC) or Representative Volume Element (RVE) of textiles; (iv) **macro-scale** (centimeters-meters) to define the behavior of a structure.

An overview of the different meso-structures that will be discussed in this Chapter is shown in Fig. 4.1.

4.2 Textile composites modeling: literature review

Modeling of textile composites should take into account a multi-scale nature of textiles, as presented previously, and might be focused on the following points:

1. **Micro-scale**: describe micro-scale constituents (shape, positions, interphase/interface etc.); define constitutive laws (linear, non-linear); prescribe boundary conditions (periodic, kinematic uniform, stress uniform, etc.).
2. **Yarn-scale**: define constitutive laws about anisotropic and phenomenological material behavior which models could be very similar to ones we use for laminates (see [Vasiukov et al., 2015b]) or multi-scale one, where the constitutive relation is a result of the homogenization from the lower material scale.
3. **Meso-scale**: describe an assembly of the yarns and their interactions; prescribe boundary

conditions, similarly as for micro-scale.

In the literature, we can observe the researches on various aspects. Some focus on lower-scale phenomena, referred to as the *localization problem*. Others are concerned with the estimation of the averaged properties of composites, a.k.a. the *homogenization problem*. There are also approaches that address all scales simultaneously, a.k.a. the *multi-scale problem* [Geers et al., 2010].

Various modeling techniques for both micro- and meso-scales share a common general classification and can be divided into two categories: **analytical** and **numerical** modeling. The following sections, 4.2.1 and 4.2.2, aim to provide a brief overview of these modeling techniques for textile composites.

4.2.1 Analytical modeling

One of the first types of analytical models is an *averaging model* that begins with the simple Rule of Mixtures (VOIGT and REUSS models). These approaches, initially developed for simplified two-phase materials, have also been applied to textile composites. One of the earliest applications was developed by Ishikawa and Chou [1982], where the authors obtained the average properties of textile composites by homogenizing several asymmetrical cross-ply laminate blocks. Similarly, Tan et al. [1999] applied this approach for the analytical modeling of 3D textiles. This type of modeling has gained attention recently, as Wang et al. [2022] extended it to nonlinear modeling of textile composites.

Another group of analytical models originates from the fundamental work presented by Eshelby [1957] and now is referenced as ESHELBY'S *inclusion problem*. This work laid the foundation for many analytical models in the micromechanics of composites. One of the very pragmatic models for engineering calculations is CHAMIS' *model* [Chamis, 1989] which is also based on Eshelby's solutions. There is still growing interest in extending these models to complex-shaped inclusions [Wu et al., 2023].

Built upon the *self-consistent solution* presented by Hill [1965], numerous extensions to nonlinear micromechanics involving plasticity and damage have been developed and can be found in [Nemat-Nasser and Hori, 2013]. By utilizing Eshelby's transformation concepts in combination with MORI-TANAKA approximations [Mori and Tanaka, 1973], the modeling of curved yarns with consideration for interactions was achieved by Huysmans et al. [1998]. This method is now widely used in textile composite modeling [Lomov et al., 2007, Wielhorski et al., 2022]. In further works ([Parvathaneni, 2020]) we will use CHAMIS' model and MORI-TANAKA estimations for more efficient scale transition.

There are also other type of analytical models such as HASHIN-SHTRIKMAN bounds (see [Hashin and Shtrikman, 1963]) and the *composite sphere assemblage* (CSA) models introduced by Hashin [1962] for very simple heterogeneous materials. These solutions have been recently revisited by Stefaniuk and Kachanov [2023].

The asymptotic homogenization theory [Bensoussan et al., 2011], initially presented in 1982 by GEORGE PAPANICOLAOU, is another method that was also be extended to 3D textile composite materials, as demonstrated by Erdata Nasution et al. [2014].

To conclude, one of the most significant advantages of such modeling is its high computational efficiency. On the other hand, the main disadvantage is that they cannot encompass all the realistic phenomena that may occur during the manufacturing of composite parts made from 3D reinforced textiles (progressive damage, processes induced artifacts, etc.).

4.2.2 Numerical modeling

In this section, numerical modeling approaches will encompass all scales (fiber, yarns, and textiles) and will be categorized as *idealistic* and *realistic* modeling techniques. All parameter-based numerical models, where the geometry is generally represented using surfaces or volumes, will be referred to as idealistic modeling. The modeling that intends to describe the real micro- and meso-structures will be defined as realistic modeling.

Micro-scale

Two types of idealistic fiber packing modes, namely *rectangular* and *hexagonal* packings, are frequently used to evaluate the effective properties of yarn. These packing modes can also be applied in multi-scale modeling (for an example, see [Wan et al., 2016]). However, it has been reported that regular packing is strong assumption when considering the real microstructure of the yarn or tow after the manufacturing of composite part (as discussed in [Mühlstädt et al., 2017]). In Fig. 4.2, specific locations are shown, typically zones where yarns contact, and where we observe a gradient of local fiber volume fraction. Similar trends were also observed for 3D textile composites [Lui, 2017], which will be discussed further.

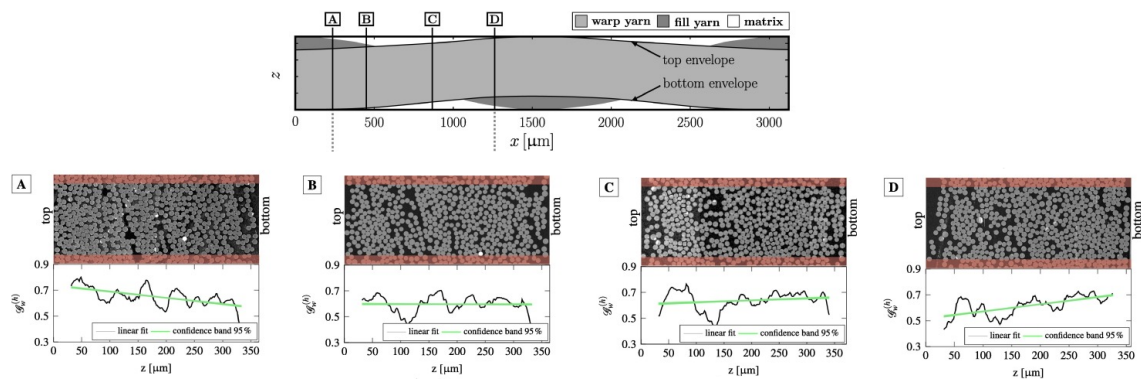


Figure 4.2: Local fiber variations for laminated textile materials as presented in Mühlstädt et al. [2017].

To take into account for this effect, several approaches have been developed to represent the distribution of fibers. Numerous algorithms exist for generating RVEs with randomly placed fibers. Initially, we will discuss only 2D models. These algorithms can be grouped into three classes based on how the fibers are generated, as outlined by Buryachenko et al. [2003]: methods based on Monte Carlo techniques, methods based on molecular dynamics (or dynamics), and methods based on close random packing (or static). We will focus on the latter two classes.

In static methods, the assembly of fibers is completed through purely mathematical computations. In contrast, in dynamic methods, generation involves the calculation of motion or resizing of particles (or fibers). Generations based on dynamic simulations can also be called

Molecular Dynamics (MD). This approach was proposed by [Lubachevsky and Stillinger \[1990\]](#) and further improved by [Ghossein and Lévesque \[2012\]](#). Further development to improve this method was carried out in [\[Lui, 2017\]](#). We have observed that dynamic-based RVE generation methods are typically very time-consuming.

As an alternative, *constructive algorithms* are becoming increasingly popular. There are several representative algorithms in this class. One of the major methods is the *Random Sequential Adsorption* (RSA)-based approach [\[Feder, 1980\]](#)¹. Where the particle (disc, sphere², cylinder³, etc.) is randomly introduced in a domain, and if it does not overlap any previous particle, they adsorb and remain fixed during the rest of the simulation. In the literature, we can find some early researches about the *advancing front method* [\[Feng et al., 2003\]](#), where particles are generated from the center and then added in a clockwise closest perimeter position, or the *inwards packing method* [\[Katalin, 2005\]](#), where the external perimeter is filled with gradual filling of the rest of the domain. These types of generators have the main purpose of preparing highly packed microstructures for further DEM simulations (see Fig. 4.3 DEM), without considering statistics about particle positions.

Some modifications to RSA methods can be found in [\[Buryachenko et al., 2003\]](#) and [\[Melro et al., 2008\]](#). Improvements in RSA methods have primarily focused on overcoming the jamming limit or improving the quality of microstructure representation. For instance, in order to achieve faster convergence to effective properties, periodic boundary conditions were employed for the RVE in [\[Melro et al., 2008\]](#). An original approach was also proposed by [Sonon et al. \[2012\]](#), where the authors used the level-set function to detect possible positions for inclusion candidates, allowing the filling region to decrease along with the adsorption process (see Fig. 4.3 LS-RSA).

To achieve not only a mechanical representation as in classical RVE but also to fulfill point pattern criteria (such as Ripley's K function and the pair distribution function), the Statistically Representative Volume Element (SRVE) concept has been introduced. One of the commonly used algorithms we found is the *Nearest Neighbor Algorithm (NNA)*, proposed by [Vaughan and McCarthy \[2010\]](#) (see Fig. 4.3 NNA). In this method, information from the statistics of the fiber locations is utilized. This method is also employed in [\[Parvathaneni, 2020\]](#) and extended to *nNNA* in order to increase the computational efficiency of the algorithm.

Finally, one of recent categories is image-based methods that generate a geometry from segmented images and consequently provide numerical discretisation. See examples in [\[Teßmann et al., 2010\]](#) for automatic fiber segmentation based on *structure tensor* (described in Sec.4.3.3). Automatic supervise learning has been also proposed by [Agyei and Sangid \[2018\]](#) to segment composites. [Baranowski et al. \[2019\]](#) have focused on the fiber orientation detection on the component level. The morphology and fiber diameter distribution have been studied by [\[Chiverton et al., 2018\]](#).

¹The earliest work in this area by Paul Hertz in September 1909, doi: 10.1007/BF01450410.

²D. W. Cooper. Random-sequential-packing simulations in three dimensions for spheres. *Physical Review A*, 38 (1):522, 1988.

³J.R. Brockenbrough, S. Suresh, and H.A. Wienecke. Deformation of metal-matrix composites with continuous fibers: geometrical effects of fiber distribution and shape. *Acta metallurgica et materialia*, 39(5):735–752, 1991.

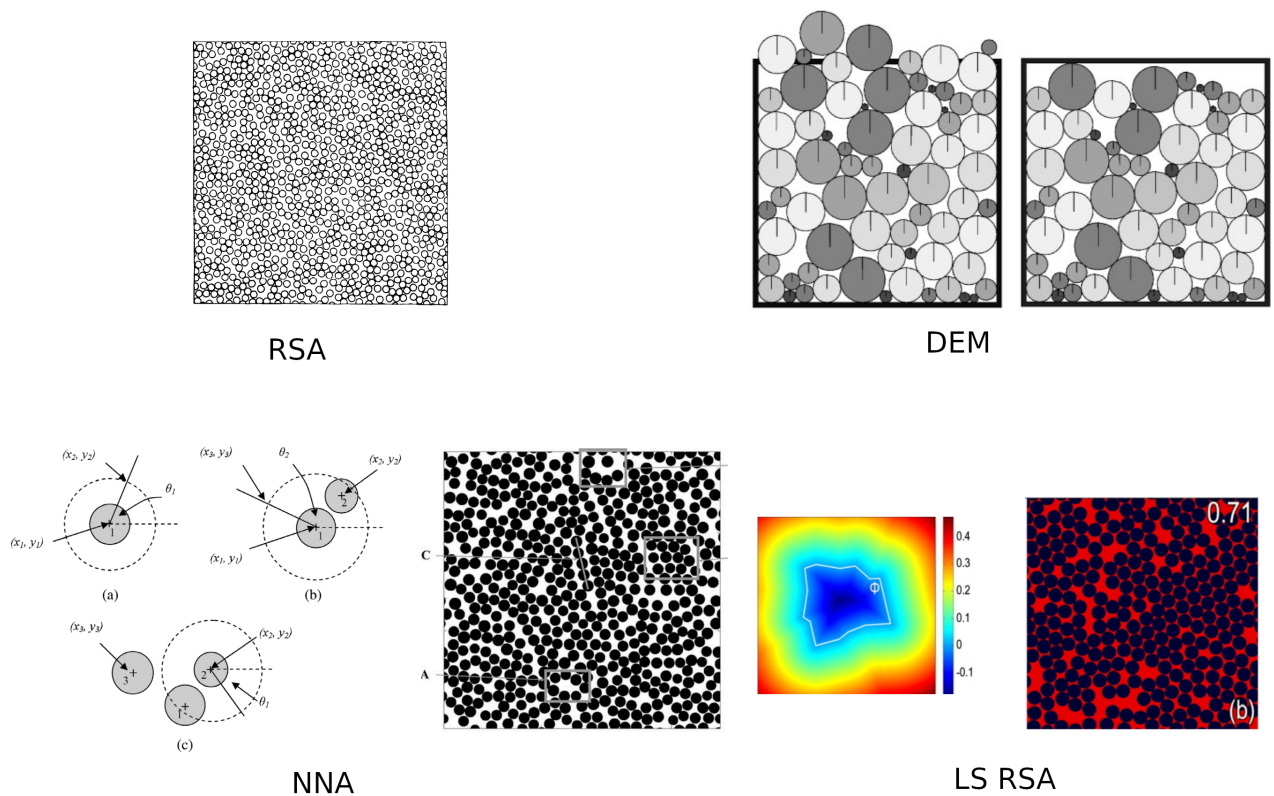


Figure 4.3: Overview of the micro-scale generators (from left top corner, clockwise): RSA - standard RSA [Feder, 1980]; DEM - Advancing front method [Feng et al., 2003] used in DEM; LS RSA - Level-set modification of the RSA [Sonon et al., 2012]; NNA -Nearest Neighbor Algorithm as presented in [Vaughan and McCarthy, 2010].

Yarn scale

Overview of modeling techniques of dry yarns is out-of-scope, however several findings could be cited here. Extended reviews can be found in [Lomov et al., 2007, Zheng et al., 2015, Wielhorski et al., 2022]. It is interesting to note, there are several approaches that treat a yarn as a homogeneous material and describe the constitutive relation using either hypo- or hyper-elastic models. On the other hand, yarns could be treated as one (hollow shells) or several discrete elements (beam, truss, hybrid). The ultimate goal of both approaches is the prediction of the more realistic cross-section of yarns during the manufacturing process, and, thus the better description of the cross-sections of yarns in a final composite part.

Meso-scale

Numerical geometries of textile RVE could be generated by using specific software such as *TexGen* [Sherburn, 2007] or *WiseTex* [Lomov et al., 2000], where textile is represented as interlacement of homogeneous yarns described by a set of geometrical parameters. This approach will be called *idealistic* geometry model. Another way is to use *MultiFill* [Durville, 2002] or a more recently developed code *Digital Fabric Mechanics Analyser* (DMFA) [Wang and Sun, 2001], where yarns are described as an assembly of discrete elements. Discrete representation of yarns allows not only better modeling of textile meso-structure but also textile manufacturing

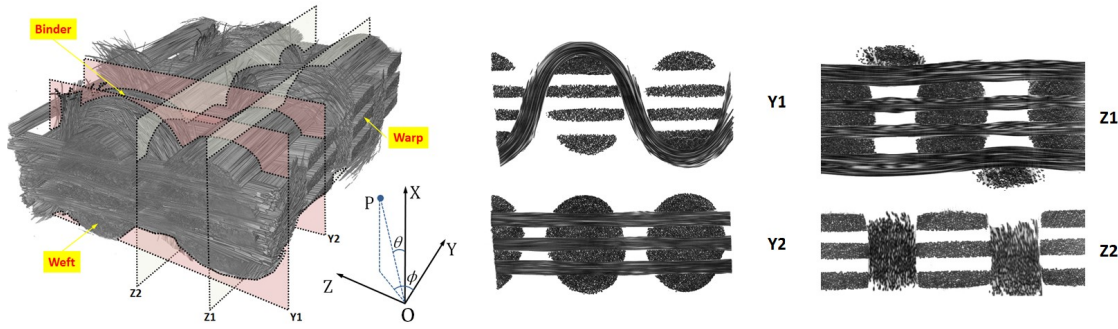


Figure 4.4: Micro CT scan of the 3D orthogonal glass fiber-reinforced textile composite: 3D reconstructed view of the volume with the hidden matrix material (left) and various cross-sections (center and right). [Liu et al., 2017a].

process simulation (for instance compaction of textile). In the literature, we can also find several in-house developed plug-ins for commercial software (ABAQUS, LS-DYNA, MSC Patran etc.) that also can model textile manufacturing process.

Remark: discrete representation of textiles is based on- a very limited number of virtual elements due to computational limits (a real yarn can contain thousands fibers).

Image-Based numerical models, in which the geometry is either directly reconstructed from images or derived from previously constructed idealized models by adjusting surfaces to accurately represent geometry variations observed in reality, will be referred to as *realistic* geometry modeling.

According to Wielhorski et al. [2022], the most common technique for 3D textiles is segmentation based on structural tensor analysis [Straumit et al., 2015] of images in conjunction with *k-means* and *multivariate Gaussian Mixture*. Liu et al. [2017a] was able to generate a voxel model for the realistic representation of 3D orthogonal composites. A step further in this development was the generation of smooth interfaces with controlled fiber volume fraction at each cross-section, as proposed in [Wintiba et al., 2020]. To achieve this, we combined the previously presented method by Sonon et al. [2012], which was extended to 3D composites [Wintiba et al., 2017], with the realistic textile geometry of Liu et al. [2017a].

Remark: All automatic methods will be very sensitive to certain anomalies, including noise and artifacts from micro-CT, low contrast, and various defects in material phases (such as broken fibers, broken bundles and yarn twist, as well as voids). Questions related to scales and resolutions will arise when observing highly specific phenomena.

4.2.3 Research problem statement

The formulation of research problem could be shown as a conclusion to this short overview. A representative sample of the 3D orthogonal textile composite, as it is shown in Fig.4.4, will help us.

Multi-scale modeling of textile composites

1. **Micro-scale.** An RVE should be able to reproduce data observed from real microstructure such as non-homogeneity in fiber distribution (gradient, clustering, etc.). Eventually manufacturing defects should be considered for (voids, cracks, broken fibers).
2. **Yarn-scale.** Yarns (weft, warp, and/or binder) have variation in shape of cross-sections and middle line of yarns can deviate significantly from the theoretical one (also called the "idealistic" structure). Variable cross-sections of yarns will also induce modified local fiber volume fractions of yarn. Moreover, some manufacturing defects should be considered (broken fiber bundles, intra-yarn porosity etc.).
3. **Meso-scale.** Assembly of all yarns and identification of the interactions between them will be discussed. Similar to the micro-scale, inter-yarn porosity should be included into the modeling.

4.3 Realistic textile composites

4.3.1 Micro- and yarn-scale characterization

The understanding of the macro-scale behavior of structures made of composites relies on the observations from lower material scale. In this Section, an experimental methodology will be briefly described. For both PhD thesis works, [Lui, 2017] and [Parvathaneni, 2020], image-based techniques were applied at micro-scale: 2D high-quality Scanning Electron Microscopy (SEM) for reference measurements and micro-computed tomography (micro-CT) for 3D information of the internal microstructure. This allowed us to collect all (or almost all) information to reconstruct a representative numerical model. Particularly, for the textile composites, this information includes: geometrical features of fibers (shape), nearest distances between fibers, fiber volume fractions (global, intra-yarn, and local), eventual process defects (voids, broken fibers, and fiber misalignment).

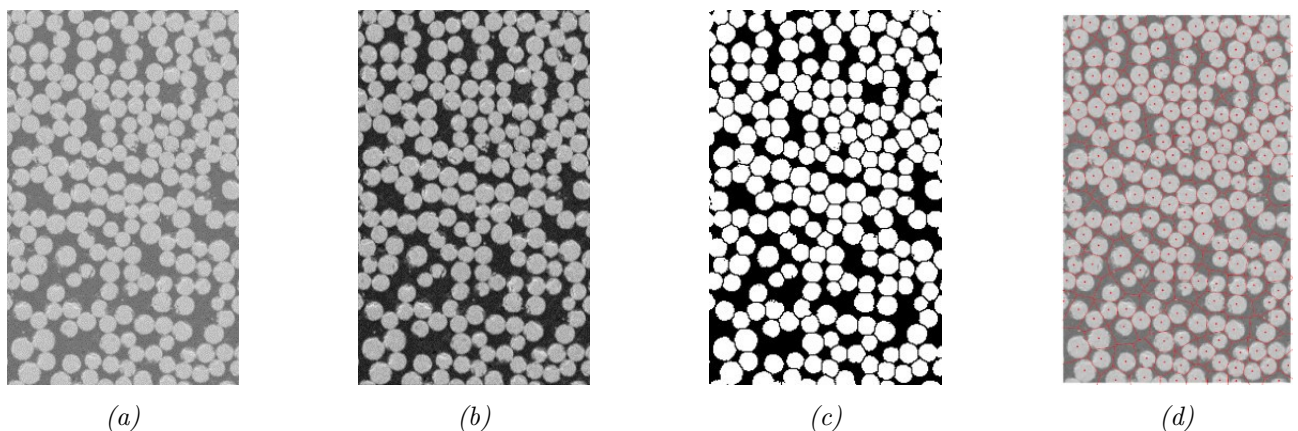


Figure 4.5: Algorithm to identify the fiber centers demonstrated on a single micrograph: (a) SEM image with resolution 0.96 microns, (b) result of low pass FFT filter, (c) watershed to remove the fiber interconnectivity, and (d) evaluated fiber centers and Voronoi tessellation.

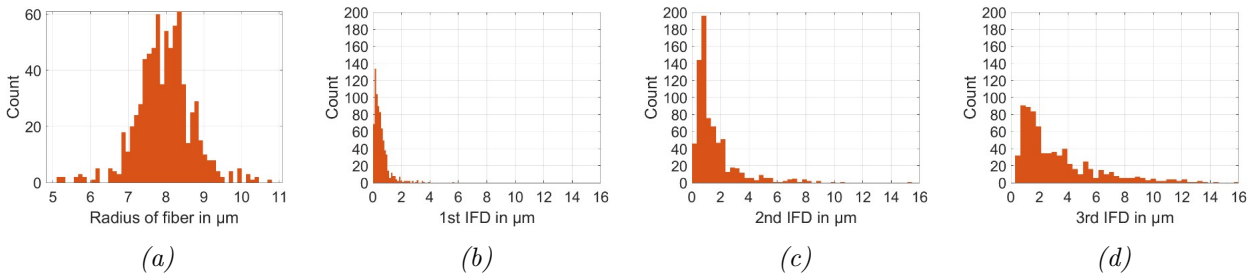


Figure 4.6: Distribution of the fiber radius (a) and inter-fiber distances: (b) 1st, (c) 2nd, and (d) 3rd nearest neighbor.

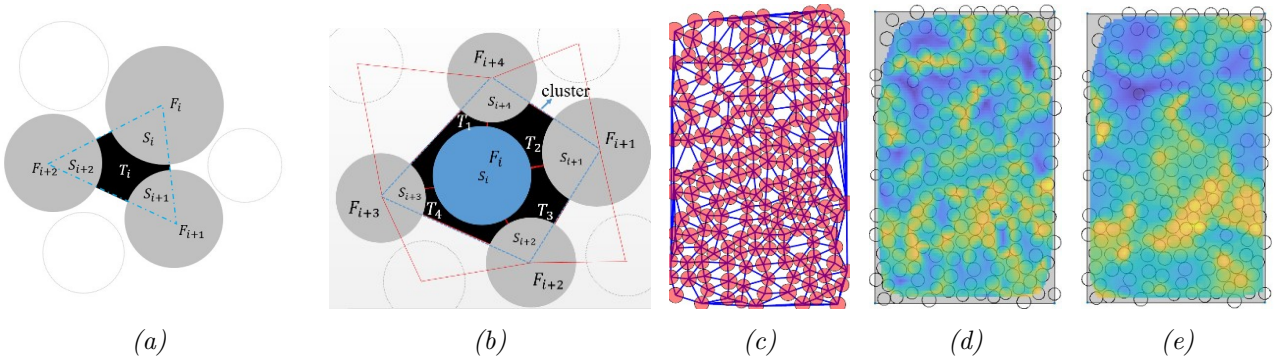


Figure 4.7: Demonstration of two measures, namely, (a) fiber density and (b) fiber packing, (c) implemented using Voronoi tessellation method to characterize fiber distribution, (d) results of fiber density and (e) fiber packing measurements.

The methodology that was applied in all following microscope observations was initially developed and validated by [Lui \[2017\]](#) and an example is presented in Fig.4.5. We applied the following steps to treat the image: (i) *Low pass FFT filtering*: to filter out all noise and high-frequency data; (ii) *Watershed*: to remove the fiber interconnectivity; (iii) *Voronoi tessellation*: to find inscribed circles. We also note that this information in general is valid for perfectly circular fibers. If we have inclined fibers we replace the last step with the *Particle analysis* (e.g. plug-in in ImageJ).

Finally, the obtained data is presented in Fig.4.6 as histograms (fiber center and inter-fiber distances). In our case, we observe that 1st, 2nd and 3rd could be very informative for our study. If we observe that 1st inter-fiber distances have low value then fibers are very close at least to one fiber. Additionally, if the 2nd and 3rd inter-fiber distances follow the same trend, thus, the region is highly-packed. Local fiber volume fraction of the textile composites in our study is in the range $V_f = (0.65 - 0.8)$ (for a glass fiber wrap-interlock composite with a total volume fraction $V_f = 0.42$). All this information is essential for our numerical modeling of the RVE.

[Parvathaneni \[2020\]](#) has introduced two additional measures of micro-scale as shown in Fig. 4.7: the first one is called **fiber density** (area of the polymer matrix constrained between the three closest fibers, see Fig. 4.7a) and the second one is called **fiber packing** (area of the polymer matrix constrained between the four closest fibers, see Fig. 4.7b). Both measurements use constructed Voronoi tessellation of a microstructure and allow to analyze the spatial position

of fibers. Although both indicators look almost the same (ratios of the area occupied by fiber and matrix) the **fiber packing** is more general and includes information on all closest neighbors of a selected fiber. These two measures will be used in the generation of numerical arrangements of fibers and matrix with manufacturing defects (Sec. 4.4).

4.3.2 Micro- and yarn-scale modeling

This section presents the numerical algorithm that have been adopted to generate representative microstructure. Two algorithms were developed: (i) *Molecular Dynamics* (MD) algorithm and their modifications (developed in [Lui, 2017]); (ii) *Nearest Neighbor Algorithm* (NNA) and their modifications (developed in [Parvathaneni, 2020]).

Molecular dynamic algorithm for fiber placement

The first method based on Molecular Dynamics modeling, initially developed by Lubachevsky and Stillinger [1990] and modified in Ghossein and Lévesque [2012], was selected for the PhD thesis work [Lui, 2017] to meet the following specific needs in the case of textile composites:

1. a scattered fiber size (which is a trivial task for any generator of microstructure);
2. a high intra-yarn fiber volume fraction ($V_{Yf} \geq 0.75$) with a controlled gap between two fibers;
3. random packing inside an irregular region, which can be approximately outlined by polygon (this generally addressed in discrete elements kind of generators);
4. user-defined fiber packing gradients.

The main steps of the conventional algorithm are shown in Fig.4.8a starting with random assignment of the position and velocities. The algorithm sequentially proceeds with the growth of the diameter of the particles and treatment of the collisions until reaching the target fiber volume fraction. The main contribution to the MD algorithm (see [Lui, 2017] and [Liu et al., 2017b]) was the enlargement to gradient fiber volume fraction case (see Fig.4.8h). These developments were motivated by the observed cross-sections of the 3D-orthogonal interlock composites manufactured by vacuum infusion molding process (observations were discussed in Sec.4.3.1).

The modifications of the algorithm include two key implementations (briefly shown in Figs.4.8e-4.8f):

1. *Mapping procedure* that allowed to present any convex cross-section of the yarn as a set of polygons (see Fig.4.8e); it needs to assign a variable fiber volume fraction.
2. *Flexible edge* case (see Fig.4.8f), that allowed a particle to cross the edge with controlled parameters.

Nearest Neighbor Algorithm for fiber placement

The second major implementation and extension of *Nearest Neighbor Algorithm* [Vaughan and McCarthy, 2010] were done by Parvathaneni [2020]. One of the main motivations for this work was to control the fiber distributions and generate Statistically Representative Volume Element (SRVE).

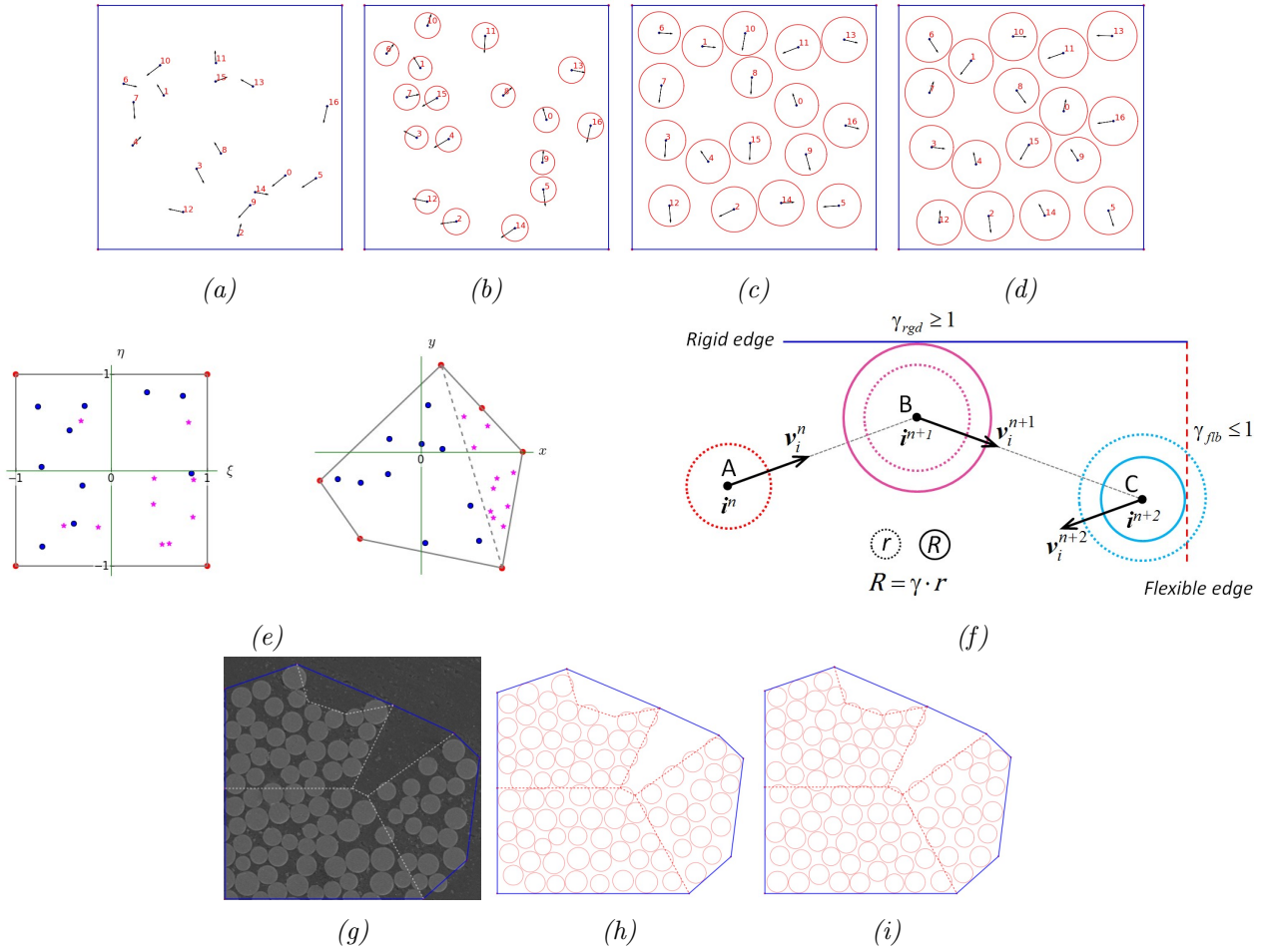


Figure 4.8: Summary of the implemented MD algorithm [Lui, 2017]. (a-d) initiation (random seeds and velocities assignment) and growth based on conventional approach. Two main contributions: (e) mapping technique and (f) flexible edges; and (g-i) an example of gradient fibers over cross-section of a yarn of the 3D-orthogonal textile reinforced composite, demonstration of the idea of rigid edges (blue lines) and flexible edges (dash lines).

Parvathaneni [2020] has started from the development of conventional Nearest Neighbor Algorithm. The algorithm has further been improved by introducing variable choice of the number of the new neighboring fibers to place (instead of one-by-one in the original algorithm). Thus, we used simultaneously the statistics for the 1st, 2nd and 3rd inter-fiber distances (see example in Fig.4.6). Each inter-fiber distance follows the distribution function that in its turn can be a purely mathematical model or measured from experiments (see Sec.4.3.1).

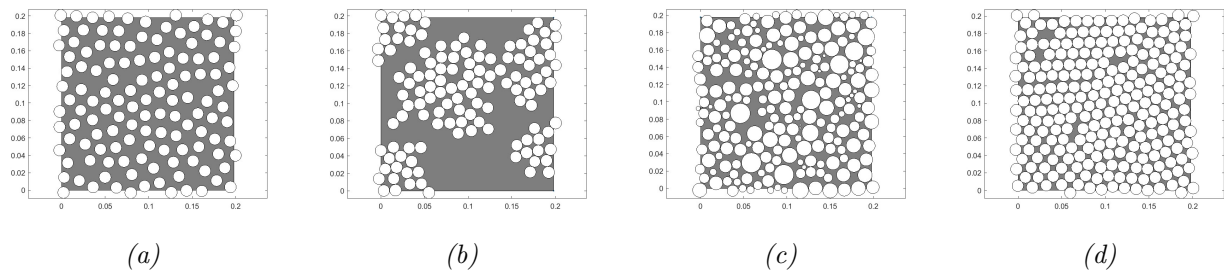


Figure 4.9: Examples of different 2D microstructures generated by modified NNA: (a) homogeneous distribution of the fibers with constant diameter and target $V_f = 0.4$; (b) clustering formation of the fibers with constant diameter and target $V_f = 0.4$; (c) random distribution of fibers with variable diameter and target $V_f = 0.7$; (d) homogeneous distribution of fibers with constant diameter and target $V_f = 0.8$.

The developed algorithm is a flexible and efficient tool to generate a variety of micro-structures (see Fig. 4.9). We can generate a homogeneous fiber distribution or clustering fiber distribution with a constant volume fraction and fiber diameters (Fig. 4.9a,b). We can also generate fibers with a variable diameter (Fig. 4.9c) which can generate the maximum fiber volume fraction. At the same time with this algorithm we can achieve the fiber volume fraction of 0.8, if the radius is constant.

Once we choose the positions of fibers, we should conduct the verification of the representativeness of the microstructure. Generally one can use different means, and the most often in the literature we can find:

1. Direct comparison of the generated probabilities of the inter-fiber distances (1st, 2nd or 3rd) measured from images.
2. Second-order intensity $K(h)$ (Ripley K -function)⁴ and radial distribution function $G(h)$ (or pair correlation function).
3. Covariance function⁵ which was used to analyse the microstructure of UD-composite⁶.

The analysis of the generated microstructures using Ripley's K -function and the modified Ripley L -function, along with a comparison with a completely randomly generated microstructure

⁴Ripley, B. D. (1977). Modeling Spatial Patterns. Journal of the Royal Statistical Society. Series B (Methodological), 39, 172-212.

⁵Matheron, G. (1971) The Theory of Regionalized Variables and Its Applications. Les Cahiers du Centre de Morphologie Mathématique in Fontainebleu, Paris.

⁶Pierre-Alexis Poulet. Effet de la variabilité microstructurale sur le comportement d'un composite UD verre/PA11 : de la caractérisation expérimentale à la modélisation multi-échelle. Matériaux. Université Paris sciences et lettres, 2017.

using a Poisson distribution, is shown in Fig. 4.10. The initial K -function is zero, indicating that the point is located at a distance less than two radii of a fiber plus the inter-fiber distance between these two fibers.

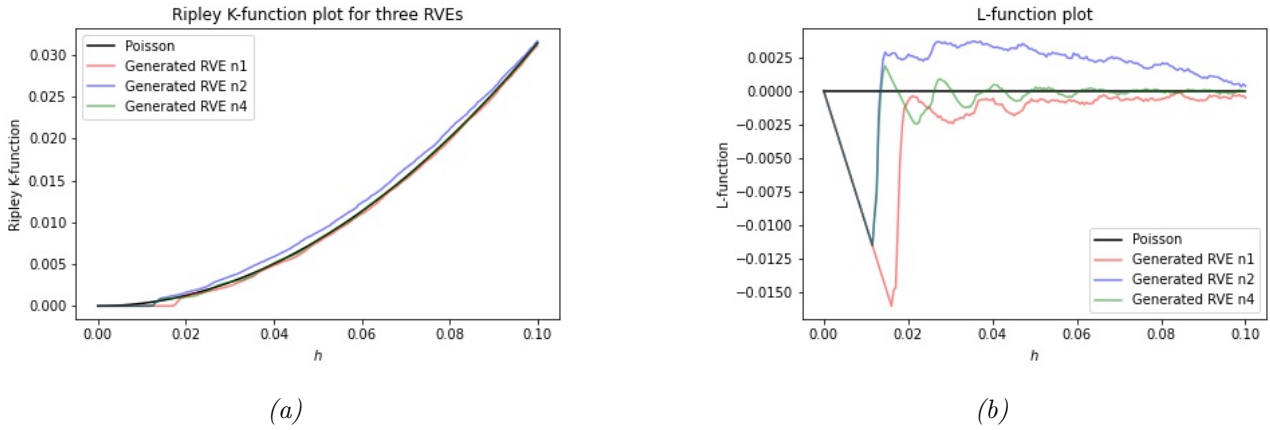


Figure 4.10: Ripley $K(h)$ function (a) and modified Ripley $L(h)$ (b) for three generated RVEs as shown in Fig.4.9a,b and d.

This algorithms will be also used in the following sections to study the impact of defects on the mechanical performance of textile composites.

4.3.3 Meso-structures characterization and modeling

This section describes the methods that were used for the meso-scale characterization and modeling of textile composites. We begin with the image acquisition method and analysis of the meso-structure. This will be followed by a detailed presentation of image segmentation based on the structural tensor, along with some numerical results (referred to as *voxel-based modeling*). Finally, we will present an original methodology for the automated reconstruction and conformal discretization of textile-reinforced composites (referred to as *conformal modeling*).

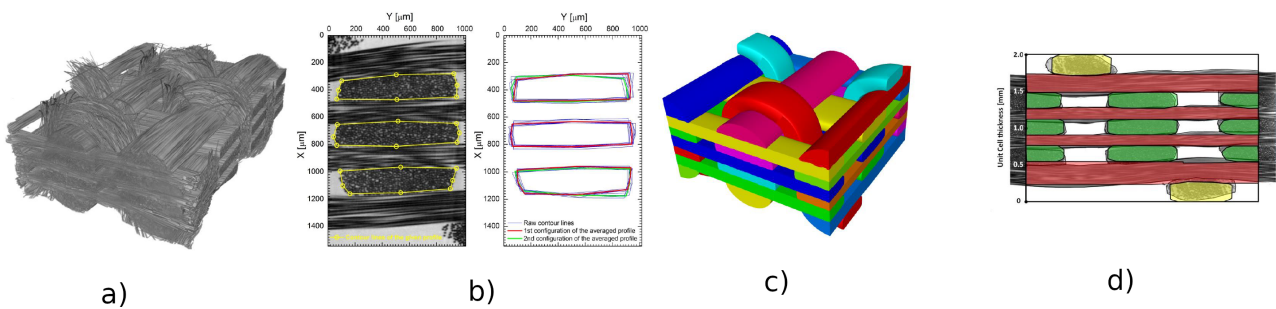


Figure 4.11: The main steps for the direct observation of the realistic meso-structure of 3D orthogonal textiles are as follows: (a) micro-CT scans; (b) retrieval of yarn cross-sections; (c) adjustment of cross-sections to an idealistic model according to measurements; and (d) comparison of idealistic adjusted modeling with the real meso-structure of the textile [Lui, 2017].

Direct measurement from images

Yarn cross-section analysis is based on micro-CT scans [Lui, 2017]. Fig. 4.11 shows the steps in which direct measurements can be used to reconstruct a more realistic meso-structure. The

warp yarns were analyzed for every slice of the micro-CT data, and the averaged contours are closer to rectangles (see Fig. 4.11b). It was observed that there were up to 10% changes in the area of the cross-sections. Two typical configurations (contours plotted by red and green thick lines in Figure 4.11d) were identified where the binding effect could be clearly seen for weft yarns due to the presence of a binder. As the binder fluctuates from top to bottom, the contour presents a certain symmetry with respect to the vertical mid-plane of the warps.

This is a very pragmatic and straightforward way to analyze meso-structure and might yield satisfactory results. However, as we can see in Fig. 4.11d, errors in the approximation of the geometry are inevitable. Moreover, the adjustment from idealistic geometry will be highly dependent on the software that is used and its limitations, namely, flexibility in trajectory definition, resolutions, and cross-section definitions.

Structural tensor segmentation

X-ray micro-tomography is defined as a 3D non-destructive technique that enables the characterization of material microstructure with high spatial resolution at the micron level. X-ray beam plays a role as a penetrating probe so that, by monitoring the light intensity variation before and after passing through the object, the constitutive phases and internal features can be distinguished by the different absorptivity of the material, which depends on the number (density) and type of atoms along the beam path. This technique is most appropriate to study textile composites at meso-scale, mainly because it offers the best balance between the resolution quality and size of the repetitive unit cell for the textile composites that could be from millimeters to centimeters. In our studies we have adopted the structure tensor-based method as proposed by Straumit et al. [2015]. This method was adopted for 3D-textile with binder yarns and 3D-textile with voids.

Firstly, the structure tensor is computed at each voxel within a user-chosen neighboring zone. The structure tensor of a 3D gray-level image I is defined as:

$$S = \int_W s dV, \quad \text{with} \quad s = \begin{bmatrix} \frac{\partial I}{\partial x} \cdot \frac{\partial I}{\partial x} & \frac{\partial I}{\partial x} \cdot \frac{\partial I}{\partial y} & \frac{\partial I}{\partial x} \cdot \frac{\partial I}{\partial z} \\ \frac{\partial I}{\partial y} \cdot \frac{\partial I}{\partial x} & \frac{\partial I}{\partial y} \cdot \frac{\partial I}{\partial y} & \frac{\partial I}{\partial y} \cdot \frac{\partial I}{\partial z} \\ \frac{\partial I}{\partial z} \cdot \frac{\partial I}{\partial x} & \frac{\partial I}{\partial z} \cdot \frac{\partial I}{\partial y} & \frac{\partial I}{\partial z} \cdot \frac{\partial I}{\partial z} \end{bmatrix} \quad (4.1)$$

where W stands for the neighboring window around each voxel. All partial derivation with respect to x, y, z is performed by 5-point derivative kernel filter $D = [1, -8, 0, 8, 1]^T$. The integral is completed by a convolution filter with a uniform kernel whose size is equal to the window size W .

With constructed structure tensor S we can have access to the following features of the meso-structure of the composite materials:

1. **Orientation vector** (N) is expressed by the eigenvectors of the structure tensor ($\lambda_1 < \lambda_2 < \lambda_3$) corresponding to the smallest eigenvalue. This allows directly to identify the characteristic angle (ϕ), which is the angle between Y -axis and vector N , to segment two types of yarns (weft or warp in the case of the 3D interlocks).

2. **Average gray-value (AVG)** is calculated as integral of gray-level over the W :

$$\text{AVG} = \int_W I dV \quad (4.2)$$

3. **Anisotropy degree (β)** which is simply calculated from eigenvalues as follows:

$$\beta = 1 - \frac{\lambda_1}{\lambda_3} \quad (4.3)$$

All those features (AVG, β , ϕ) are involved in *supervising segmentation* at the meso-scale to distinguish weft, warp and binder yarns, and matrix. It is worth mentioning that training samples (which contains only a "good" example of the constituent materials) were selected manually and provided to the algorithm. The supervised segmentation was selected because classical segmentation via two-parameter *k-means* clustering algorithm, as well as via threshold method, faces the dilemma of either mis-classification of material phases or impossibility for subdivision of raw yarn cluster.

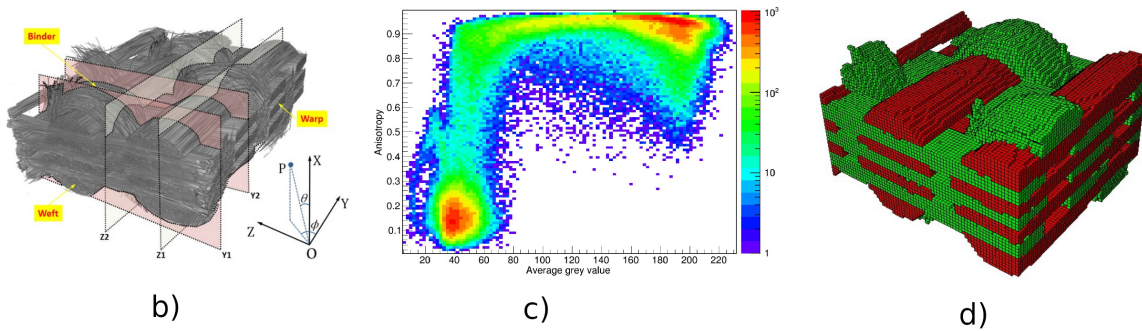


Figure 4.12: Numerical model of 3D orthogonal textile composite (matrix material is hidden) (reprinted from [Liu et al., 2017a]).

The structural tensor segmentation was effectively applied for 3D orthogonal textile reinforced composites by Lui [2017] and 3D warp-interlocks by Parvathaneni [2020]. Fig. 4.12b shows a histogram of the *anisotropy* (β) and *average gray-value* (AVG). It shows that all voxels are classified mainly into two groups. The first one has high anisotropy and AVG measurements. This group with a high probability will be classified as impregnated yarns. The second group contains voxels with low β and AVG, and will be classified as matrix material. The local fiber orientation calculated from β feature is shown in Fig.4.13b. We can see how the orientation vector follows the middle line of the yarn.

The third important feature is the characteristic angle ϕ which is shown in Fig.4.13a where we can see two main populations of the voxels. The first one has $\phi = 0$ which classifies this population as voxels belonging to warp yarns. Accordingly, the second population represents voxels that belong to weft yarns. It should be specified that some amount of the voxels can be misclassified if one is based only on ϕ feature. The main reason for that is the projection of the orientation vector N of the binder yarn can be equal to zero when the binder passes a middle plane of the composite. Thus, these voxels can be classified as the matrix. This issue was observed in 3D orthogonal composites but not in the case of warp-interlock composites

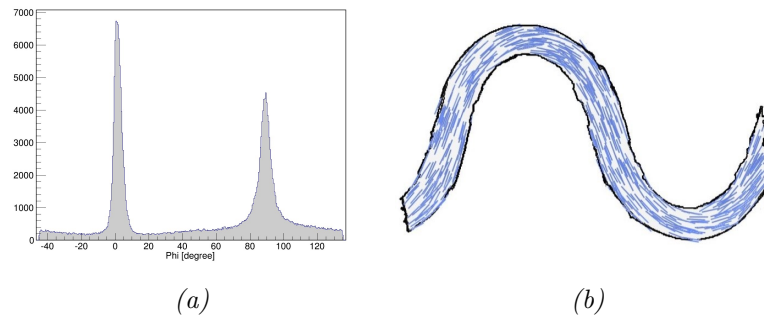


Figure 4.13: Realistic segmentation techniques: (a) classification of the ϕ feature of the voxels and (b) local fiber orientation detection for the binder.

since the orientation angle N never has a projection on xy -plane which equals zero for this materials.

[Liu et al. \[2017a\]](#) has compared spline-based generation methods, as it is implemented in Tex-Gen software (FEM voxel model is shown in Fig.4.14) with realistic generated meso-structure. A significant deviation was observed in the resulting geometries of two cross-sections. When weft-yarns (shown in red color in Fig. 4.11d) are located at the top or bottom of the composite near the binder yarn, the spline-based model tends to overestimate the cross-section. This phenomenon has also an impact on the local fiber volume fraction and will be investigated in detail in the following section.

Non-linear material modeling of realistic textile composites

To highlight an impact of the realistic meso-structure on the damage initiation and propagation, several simulations were conducted [[Liu et al., 2017a](#)]. Two typical configurations were reconstructed for both real and idealized modeling strategies. The influence of the modeled geometry on predicting the progressive damage behavior was then investigated by simulating uniaxial loading along warp yarns. In these simulations, we considered the yarn as an anisotropic damageable material, the matrix as an isotropic damageable material and the perfect interfaces between yarn-matrix and yarn-yarn. The estimation of elastic and strength properties were done according to CHAMIS' ⁷ and ROSEN's ⁸ models respectively.

Continuous damage mechanics modeling was used to model progressive damage propagation, similar to what was presented in Chapter 3. Initially, this material model was applied to continuous fiber composites [[Vasiukov et al., 2015b](#)]. It was based on the HASHIN 3D damage criterion with a *smearred crack regularization* approach. Some results are presented in Fig. 4.14. These results were grouped by the type of yarns; warp yarns and binders were presented in the same group because they had the same projection of orientation on the plane of the textile. Weft yarns were treated separately. We observe that the localization and intensity of damage are accumulated in the material vary significantly when generating realistic geometry. This effect is evident in the histograms of damage mechanisms (Fig. 4.14).

⁷[[Chamis, 1989](#)] C.C. Chamis. Mechanics of composite materials: past, present, and future. J Compos Technol Res ASTM, 11: 3-14, 1989.

⁸[[Rosen, 1965](#)]: B. W. Rosen. Mechanics of composite strengthening. 1965.

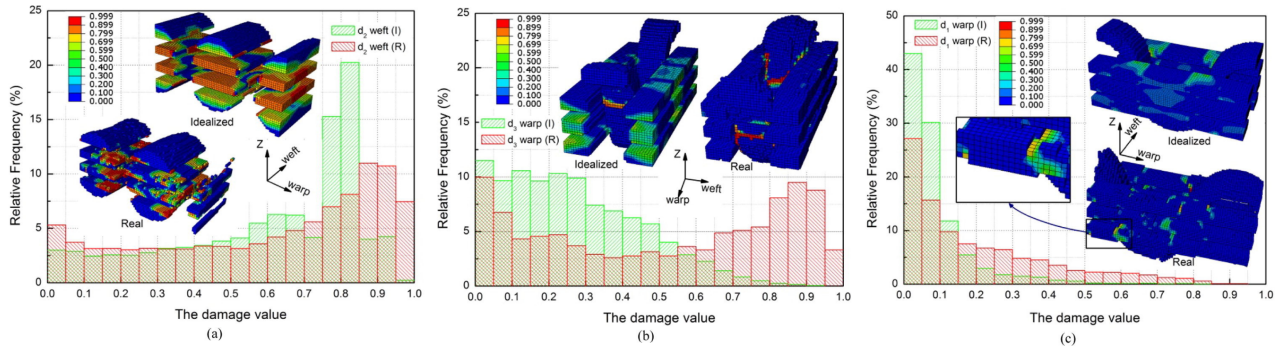


Figure 4.14: Comparison of the damage accumulation in the idealistic and realistic model.

4.3.4 Conformal discretization with local fiber volume fraction control

The voxel-based model can be obtained from 3D images treatment and one of the main advantages is the ability to generate a relatively quick numerical model for numerical homogenization of the realistic meso-structure. However, the impact of the interface discretization on the damage evolution might be significant. In other words, the reliability of voxel geometry can be questionable for damage simulations due to spurious stress concentration at the jagged shape of interfaces. This was in detail discussed by [Doitrand et al., 2015].

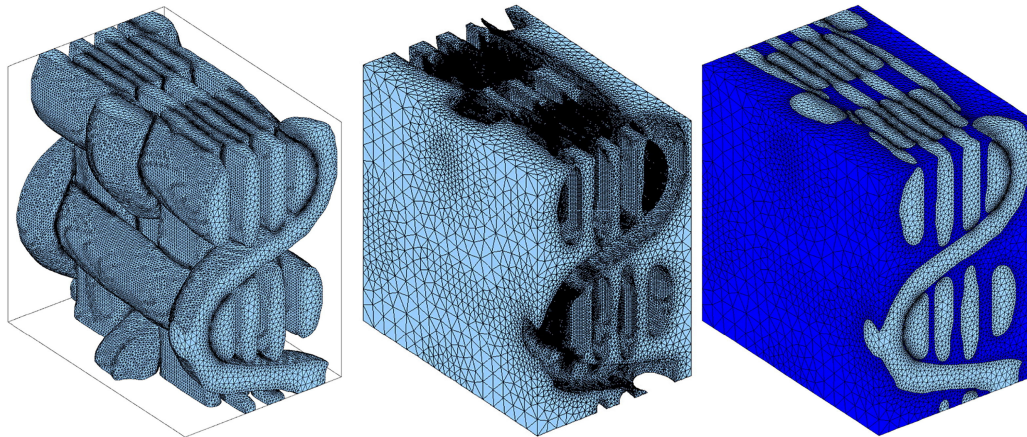


Figure 4.15: Final results of the conformal mesh of the 3D orthogonal textile reinforced composite as shown in previous section (figure reprinted from [Wintiba et al., 2020]).

The combination of the following three achievements ensures the originality of [Wintiba et al., 2020]:

1. **Image-based** segmentation, we construct a numerical model as realistic as possible that contains all defects of the manufacturing. In this case there were modifications in the cross-sections of yarns.
2. **Physical-based** method to ensure the number of fibers in the yarns. Before constructing the conformal mesh we ensure the exact number of fiber that have been initially presented in each yarn is kept constant after all treatments.
3. **Conformal** representation of the meso-structure of the composites.

The developed procedure is divided into the following steps: (i) extraction of the individual yarns; (ii) smoothing of the yarn surfaces; (iii) extraction of the geometrical features (central line and cross-sections) (iv) level-set post-processing with controlled fiber volume fraction. The necessity of having the individual yarns in the model is dictated by the fact that the *alphaShape* built-in MATLAB function which is in the core of the developed procedure. This function creates a bounding area or volume that envelops a set of 2-D or 3-D points in order to fit around the points and create a non-convex region. This function performs differently when the treated volumes are in contact with each other. In turn, this yields another challenge when the fiber volume fraction is imposed and the interpenetration is suppressed. To solve this, a local algorithm has been proposed to iteratively apply "yarn smoothing", "distance calculation", "interpenetration suppression" and "yarn offset" steps. The titles of these steps speak for themselves thus technical description will be omitted here (see [Wintiba et al., 2020] for details).

4.4 Textile composites with porosity

Previously, the modeling process was focused on the realistic meso-structure of textile materials without considering voids⁹. It is known that voids are almost inevitable defects in composite materials; aerospace applications would impose a maximum allowable 2% void volume fraction. In other applications, this limit is less strict; however, the void volume fraction is one of the measure for the quality of the manufacturing of composite parts. This also implies that the reduction of manufacturing defects will automatically increase the final cost of a part. To evaluate the impact of voids on the final mechanical properties of composites, a controlled process was used to generate induced voids. This was a major subject of the work presented by PARVATHANENI in his thesis [Parvathaneni, 2020].

4.4.1 Dual-scale porosity

The porosity defects in the Liquid Composite Molding (LCM) manufacturing process have been investigated over the last few decades [Mehdikhani et al., 2019]. However, there were still some gaps in understanding the impact on the mechanical performance of final part, especially in the case of textile-reinforced composites. To address this, the Resin Transfer Molding (RTM) manufacturing process has been selected [Parvathaneni, 2020]. Control of the RTM process allows us to generate two types of porosity separately, when classified based on the material scales of textile composites: (i) *intra-yarn voids* (also known as micro-scale porosity) and (ii) *inter-yarn voids* (also known as meso-scale porosity).

The voids in prepreg laminates are predominantly elongated in the fiber direction and are always in contact with the adjacent fibers. In textile composites manufactured by the RTM, voids have near-spherical shapes in the matrix-rich zone and elongated cylindrical shapes inside the fiber yarns [Sisodia et al., 2016]. Moreover, in prepreg laminates, voids can be concentrated between plies or in the middle of a ply (inter- and intra-laminar) which depends on the process parameters (P, T). In the case of textile composites, voids can be located between yarns or

⁹We are not distinguishing porosity and voids, both terms will be used in the text but with specified material scale in which we observe this defects.

inside a yarn (inter- and intra-yarn) which strongly depends on the resin flow velocity (see simplified illustration when the resin flow is transverse to the yarns, Fig. 4.16).

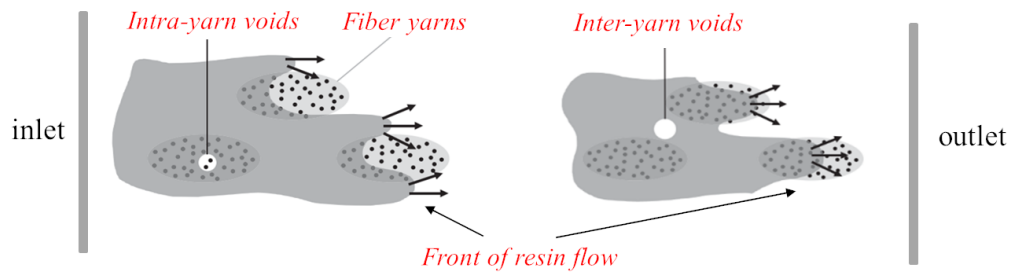


Figure 4.16: Illustration of the dual-scale porosity mechanisms during RTM process (adapted from [Chen et al., 2015]).

Parvathaneni [2020] has established an experimental setup to manufacture composite plates with controlled porosity defects, focusing on either intra-yarn or inter-yarn voids. RTM process was utilized to produce composite plates measuring 190 mm x 290 mm x 2.3 mm. Glass fiber warp-interlock fabrics were employed for this study. These fabrics were positioned in a prepared mold, leaving a gap greater than two centimeters in the injection edge to ensure rectilinear flow. A press applied a pressure of 20 bar to the mold, compressing the fabrics with an accuracy of 0.1mm in terms of mold cavity height. This process ensured the prevention of race tracking inside the mold. Subsequently, epoxy was prepared in a beaker by mixing resin and hardener in proportions of 100:28 and stirring until homogeneous. The mixture was then degassed.

Finally, the controlled defects have been achieved as presented in Fig.4.17.

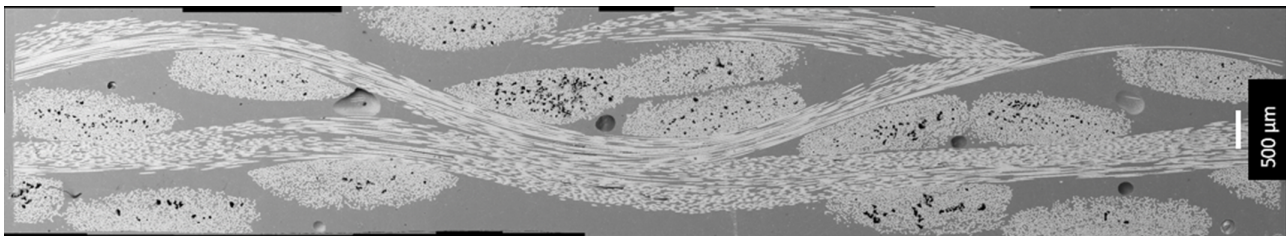


Figure 4.17: The SEM observation of warp-interlocks studied in [Parvathaneni, 2020].

4.4.2 Characterization of the porosity at micro- and meso-scales

All manufactured plates were characterized according to conventional tests^{10 11 12} for fiber and void volume content evaluations. For the more detailed analysis we used images taken by SEM and micro-CT scans (following the same procedure as presented previously Section 4.3.1). We applied threshold-based segmentation on the micrographs from upstream and downstream in warp and weft directions to obtain statistical data on voids. In the literature, the following

¹⁰ASTM International: Standard Test Methods for Constituent Content of Composite Materials.

¹¹ASTM D3171 American Society for Testing of Materials (ASTM): Standard test methods for void content of reinforced plastics, Designation D 2734-09.

¹²Kellyand, A., Zweben, C.: Comprehensive Composite Materials-Test Methods, Nondestructive Evaluation, and Smart Materials, Elsevier Science Ltd. 5, (2000)

descriptors of porosity could be found: area/volume fraction, effective radius, aspect ratio, and spatial distribution.

Descriptors of voids

Volume fraction is the most common void characteristic and is frequently adopted in the literature to quantify the effect of voids on the mechanical properties. However, there is enough work to support that the total void volume fraction is not a single parameter to account for the behavior of composites with voids. It should be noted that volume fraction is the only standardized descriptor of the quality of the composite part for the moment in the real practice.

The second descriptor is *Size*. It can be related to the cross-sectional area (A) of the volume in the case of 2D image characterization or the volume (V) of the void in the case of 3D imaging. If we introduce an equivalent void radius in both cases, we obtain the following equations: $r_{eq} = (\pi/A)^{1/2}$ and $r_{eq} = (3V/4\pi)^{1/3}$ for 2D and 3D respectively. This parameter is very simple and can be applied directly; however, it may lead to ambiguous conclusions. As was shown in [Tretiak, 2019], the equivalent radius should also be related to the area of the void to reflect the observed measurement of the effects on the interlaminar shear strength of unidirectional continuous fiber composites.

The third descriptor is *Shape*, which is one of the indicators used to describe the morphology of a void. The simplest one is aspect ratio ($A_r = \frac{d_{max}}{d_{min}}$). A small A_r means the void shape is closer to a spheroid, while a large A_r signifies that the void is elliptical. Depending on A_r , the following morphological terms are used to describe the void shapes: flattened coin-shaped, cylindrical-shaped, cigar-shaped, rod-like shaped, elliptical cylinders, and large-long shapes [Drach et al., 2013]. The shape is measured from image data, from either its micro-CT or SEM.

Last but not least is *Distribution*, which gives us the information about the spatial localization of voids. It directly influences the local state of stress and finally affects the material's mechanical response, influencing linear homogenized properties but also becoming critical to understanding the composite's performance in strength. It is a documented fact that the spatial distribution of voids is sensitive to the type of the manufacturing process and its parameters, as well as the architecture of the textile [Nikishkov et al., 2013].

Characterization of intra-yarn voids

The results from the measurements of the entire yarn are presented in Fig. 4.18. Fig. 4.18a shows a warp yarn cross-section of the 3D twill layer-to-layer interlock. This study was conducted to find the correlation between the occurrence of voids and the local packing fraction of the yarn. We observe that it is not possible to exactly predict the location of voids since it does not only depend on the fiber packing only. However, there is a likelihood of its occurrence. Moreover, the voids are only observed in the region having fiber packing in the range of (0.35 – 0.65).

To study geometrical statistics of intra-yarn voids, we used the *pixel counting method* to determine the void volume fraction in a yarn. Of practical interest to us are the following

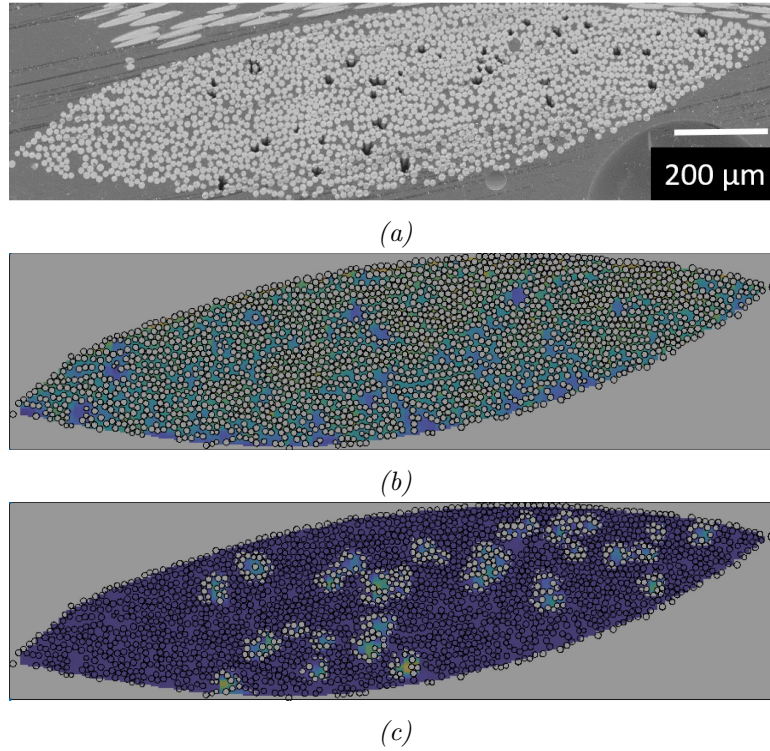


Figure 4.18: Analysis of the entire yarn: (a) initial SEM image, (b) calculated fiber packing (as explained earlier in Fig. 4.7) and (c) voids location.

void characteristics such as area (A ; or V in the case of 3D), radius which can be an equivalent measure as well, and aspect ratio (A_r as mentioned above). These were calculated by segmentation of the yarn by using the image processing tool FIJI [26,169]. These are the main steps for the procedure: (i) selection of the yarn profile; (ii) thresholding (manually selected gray-scale value); (iii) analysis using the "Particle analysis" plug-in in FIJI. Additionally, a noise removal procedure was applied to the image. In this study, the noise was related to the unwanted information in an image such as isolated or clustered pixels after the application of the threshold. To remove such noise, a numerical filter was applied to the calculated data during the post-processing so that the least value with high repetition could be removed from the data before making the final data set.

The ultimate goal of this treatment is to understand the link between the location of the voids and the parameters of the manufacturing. It was noted at this stage that the relatively high velocity of resin in the plate close to the inlet results in a dominant resin flow in the channel, thus increasing the occurrence of the intra-yarn void. Conversely, near the outlet, the velocity of the resin is lower and the capillarity of the yarns is significant enough to fill the yarns before the resin fills the inter-yarn channel. Thus, the low resin velocity in the downstream results in a small amount of intra-yarn voids.

One of the major contributions reported in [Parvathaneni, 2020] is the analysis and correlation of spatial distribution of fibers (as mentioned above using classically n -point statistics) and spatial distribution of voids. This has been done for both micro- and mesoscale porosities with homogeneous, random, and cluster distributions. All observations were performed based on available or developed techniques in image treatment.

Characterization of inter-yarn porosity

In the case of the inter-yarn porosity for the considered materials, one of the best choices is to use micro-CT image data. The process of image segmentation is described below.

Here only general findings will be mentioned revealing voids volume distribution and the aspect ratio. The statistical analysis was carried out using *regionprops3* an inbuilt MATLAB function. For this, a binarized 3D image containing only inter-yarn voids and matrix was reconstructed from the labeled text file generated by VoxTex [Straumit et al., 2015]. The total number and maximal volume of inter-yarn voids in the region close to the inlet are lower than near the outlet. However, the minimum void size has very similar values. The average aspect ratio of the inter-yarn voids near the inlet is 14% smaller than the average aspect ratio of the inter-yarn voids near the outlet. Based on the observations we can state that the inter-yarn voids have near-spherical shapes and are more elongated near the outlet.

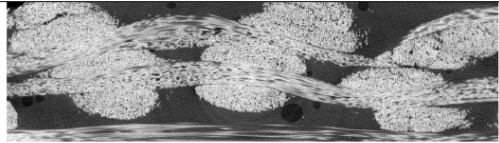
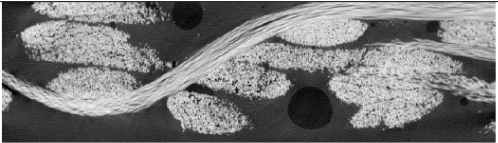
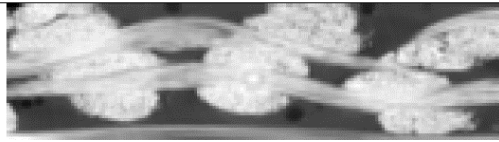
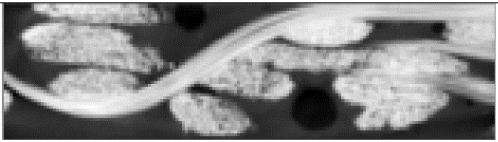

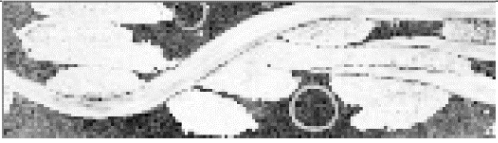


Position	Upstream	Downstream
Raw image		
Density		
Anisotropy		
Voxel model		

Figure 4.19: The steps to extract inter-yarn voids [Parvathaneni, 2020].

4.4.3 Numerical modeling of textile composites with voids

Within this scope the following developments were done Lui [2017] and [Parvathaneni, 2020] : (i) fiber generator base on Molecular Dynamics (MD) algorithm and based on Nearest Neighbor Algorithm (NNA); (ii) voids generator at the micro-scale and meso-scale; (iii) image-based reconstruction of the meso-scale repetitive unit cell at meso-scale.

Generation of the porosity at the micro-scale

As introduced previously intra-yarn voids can have a complex shape and the present literature algorithms do not generate systematically microstructures with voids. Hence two types of algorithms have been developed; one is the generation of the spherical voids based on NNA and the other one generates voids with a complex shape based on the local fiber packing.

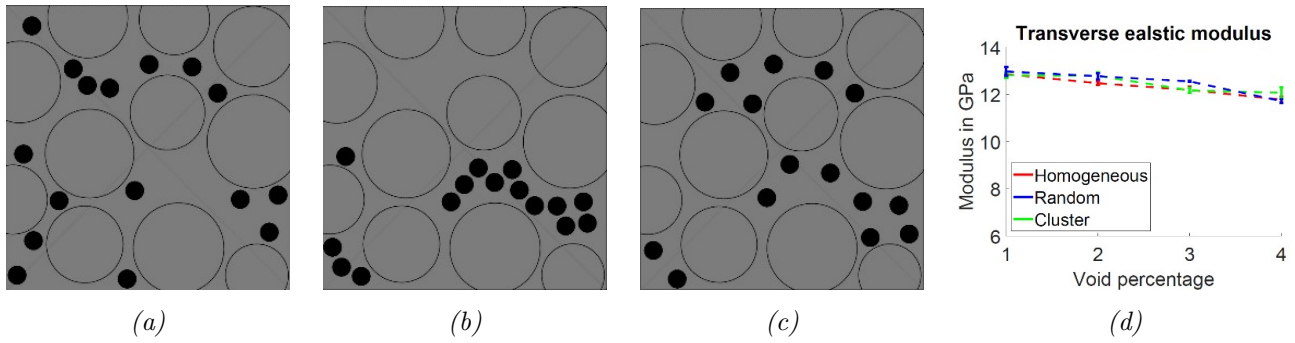


Figure 4.20: Demonstration of the void generator algorithm with random (a), cluster (b), and homogeneous (c) position with fixed cylindrical fibers (note these are cross-sections of the 3D models). In (d) results of the FEM homogenization show the impact of the void position on the mechanical performance of the composite.

Micro-scale porosity of spherical shape. Positions of the spherical voids are generated using a similar algorithm as fiber placement algorithm including some modifications such that the spheres cannot overlap on spherical voids and cylindrical fibers. Hence this algorithm is called the Double Near Neighbor Algorithm (DNNA). The void generation is based on three kinds of spatial distributions (i.e. homogeneous, random, and clusters). The position of the first void is selected randomly in the domain. This position is accepted only if the void does not overlap with the other fibers. The void volume fraction (V_V) in the RVE is calculated after positioning each void. If the V_V is greater than or equal to the V_V^{target} , the loop will be terminated and all the void information will be saved in a data file. This data will later be used in the generation of a microstructure for FEM simulations. An example of different spatial distributions of the spherical voids is presented in Fig. 4.20.

Micro-scale porosity of realistic shape. This algorithm is based on the measurements of the local fiber packing presented in the previous sections. The generation of the RVE with realistic voids is done in three steps (see Fig.4.21a): (i) initiation in the zone of specified packing fraction; (ii) propagation to the neighboring fiber cluster; (iii) termination once $V_v = V_v^{target}$.

For this algorithm, we have assumed that voids are formed in the local regions of the yarns with specified packing. During the initiation, the void is positioned concerning the local fiber packing only representing a fraction of the total void content. The voids keep growing to neighbor material with the highest packing. The void propagation is terminated if either of two conditions are met: the global void volume fraction has reached the limiting void volume fraction or the void area fraction has reached the limit area fraction selected from the calculated statistical data.

There are two possible voids which can be generated : (i) Fiber Rich zone Voids (FRV) and (ii) Matrix Rich zone Voids (MRV). At any given V_v , an RVE with voids FRV has ineffective stress transfer and results in lower elastic properties than RVE with MRV (see Fig.4.21). The matrix voids are bigger and have a high aspect ratio resulting in the orthotropic behavior of the microstructure. At maximum void content of 4.5%, MRV results in 30% of elastic properties, and FRV causes a 45% reduction of elastic properties.

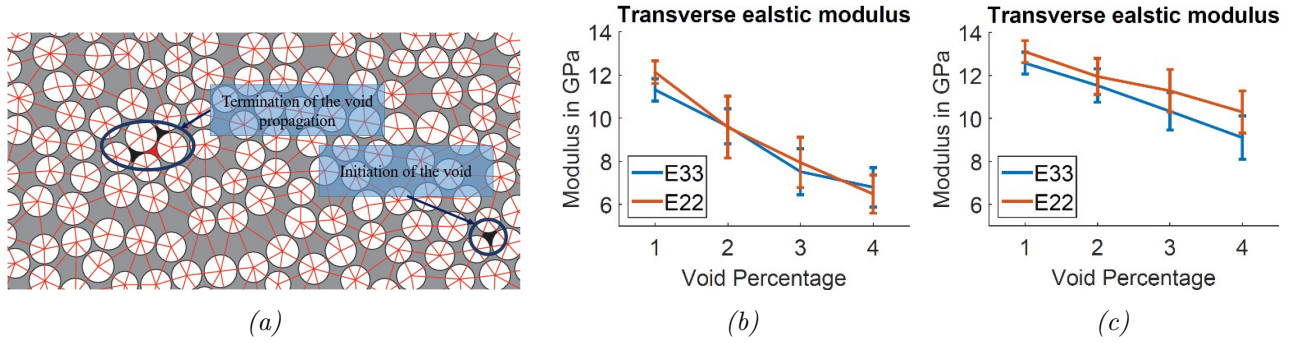


Figure 4.21: Demonstration of the realistic void algorithm (a). Results of the FEM homogenization of RVE with MRV (b) and FRV (c).

Generation of inter-yarn voids

In order to understand the inter-yarn voids influence we have also proposed an algorithm to generate artificial inter-yarn voids by post-processing the segmented image from VoxTex in MATLAB. Once the ‘.inp’ file with the matrix, warp, and weft yarns is generated it is feed to the void generation algorithm developed in MATLAB. The algorithm facilitates the generation of meso-structure with two different type of inter-yarn voids: randomly distributed voxels and spherical voids (see Fig.4.22). In the literature, we can find references that have addressed such void defects [Shigang et al., 2015].

Parvathaneni [2020] has implemented similar algorithms with randomly distributed voxel voids to compare them with spherical voids (see Fig. 4.22a), despite the fact that such random one-voxel voids have not been observed in micro-CT images. Therefore, microstructures with spherical-shaped inter-yarn voids were also analyzed. For simplicity, all the voids in this study have the same effective radius. Thus, the number of voids decreases proportionally to the reduction in the total void volume fraction, ensuring that the volume of each void remains constant. The microstructures containing spherical voids are presented in Fig. 4.22b.

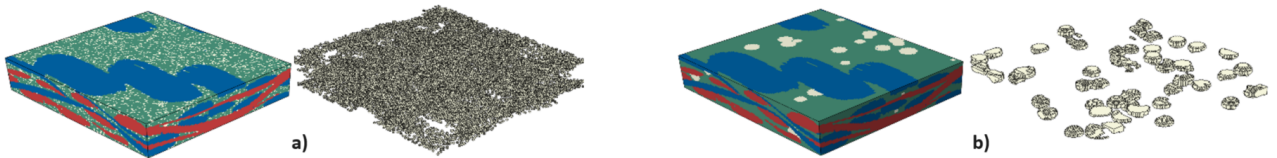


Figure 4.22: The steps to extract inter-yarn voids [Parvathaneni, 2020].

The FE-homogenization at meso-scale with random one-voxel voids has a high dispersion of the properties. Hence, an average of 5 simulations was presented for E_{22} , and E_{33} with their dispersion see in Fig. 4.22a. The overall observation implies that the elastic properties of the textile composites are more sensitive to intra-yarn voids than to inter-yarn voids. For test case 1, the inter-yarn void volume fraction of 0.18 equivalent to 0.05 total void volume fraction resulted in the 4.3 % reduction of 5.6 % E_{22} (warp direction). However, the intra-yarn voids in the warp resulted in the 7.5% reduction of E_{22} and in the weft resulted in the 7.2 % reduction of E_{22} . Shear moduli are more sensitive to inter-yarn voids than to the intra-yarn voids. The 0.05 total void volume fraction for the case of inter-yarn void only, resulted in about 10 % percent reduction in G_{13} and G_{23} respectively. The intra-yarn voids lead to an average reduction of 6 %.

Hence, we can conclude that the effect of the intra-yarn void play a crucial role in determining the in-plane tensile properties. Conversely, the out-of-plane tensile modulus and shear modulus are highly influenced by inter-yarn voids.

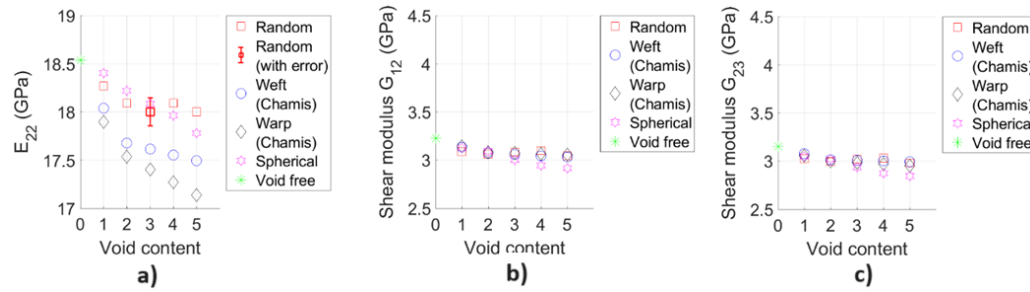


Figure 4.23: Influence of the voids at both micro-and meso-scales for transversal and shear properties [Parvathaneni, 2020].

4.5 Conclusion

In this chapter, research has focused on modeling textile-reinforced composites with the main objective of providing a realistic description at different material scales. Works related to textile-reinforced composites have made several main contributions:

- **Dynamic generator of yarn cross-sections:** The main originality was developed during Yang LUI's PhD thesis [Lui, 2017], where he presented a generator capable of reproducing observed features from real microstructures, such as non-homogeneity in fiber distribution (gradient, clustering, etc.) within a yarn.
- **Statistical RVE at micro-scale:** A robust and efficient nNNA algorithm was developed by Parvathaneni [2020]. This algorithm was proposed based on statistical data of real microstructures, capable of generating RVE with very high fiber volume fractions. Traditionally, algorithms in the literature have focused only on the fibers, but in the proposed algorithm, manufacturing defects such as voids have been considered. Additionally, a statistical representation of the voids' locations has been considered in the generation of the SRVE.
- **Image-based reconstruction of meso-scale RVE:** 3D orthogonal composites have three type of yarns which represent a challenge in the automatic segmentation of such yarns. Original work has been presented in [Liu et al., 2017a] where the realistic numerical model of textile reinforced composites including weft, warp, and binders were considered. The variations in the shape of cross-sections, as well as the middle line of yarns deviating significantly from the theoretical one, have been presented. Variable cross-sections of yarns will also induce modified local fiber volume fractions within the yarn. Moreover, non-linear damage modeling has been applied for realistic image-based RVE using earlier developed constitutive modeling [Vasiukov et al., 2015b]. The impact of the realistic meso-structure on the quantity and quality of the damage mechanisms was quantified.
- **Conformal Mesh of Textile Meso-Scale RVE:** We propose an automated method for smoothing voxel-based geometries and discretizing them conformally for CT-scan data of 3D woven composites. Our approach utilizes a level set post-processing technique to control yarn volume fraction and cross-sectional fiber fraction throughout the RVE. We study damage initiation and location using Puck failure indices between voxel-based and smoothed meshes. Results demonstrate that geometry and fiber distribution significantly impact damage prediction. Smoothed geometries yield more consistent results than voxel-based ones, which exhibit spread damage initiation due to jagged yarn edges. Damage initiation associated with the matrix failure index occurs in higher cross-sectional fiber fraction zones under transverse tensile loading. The originality in this section lies in the generation of the RVE for textile composites with controlled fiber volume fraction, thus ensuring a realistic mapping of the strength properties of the yarns.
- **Inter-yarn voids generator:** Numerical algorithms have been developed to generate random voxel voids and spherical voids at the meso-scale, enabling parametric modeling to simulate the influence of such defects. These numerical models have revealed counter-intuitive results: with constant total void content, intra-yarn voids have a higher influence.

5 .Numerical modeling based on FFT methods

This chapter presents a summary of my research on the numerical homogenization of heterogeneous materials. More specifically, we are going to consider only FFT-based methods. By definition, FFT solvers are quick and well-suited for image-based structures. We want to investigate their performance and accuracy when dealing with textile-reinforced composites. We will discuss quantitatively the errors in the prediction of elastic and damage behaviors at micro- and meso-scales.

This chapter is organized into three parts. In the first part, we discuss the numerical homogenization problem statement for the elastic properties prediction and possible numerical artifacts. In the second part, we introduce the FFT solver with a simplified formulation for the non-local damage problem in heterogeneous materials. In the third part, the complete formulation of the damage model is based on phase-field theory, and cohesive law formulation is presented.

The results of this chapter have already been published in several papers. [Chen et al. \[2019b\]](#) presented original work on a simplified non-local damage formulation based on the phase-field model. In [\[Chen et al., 2018, 2019c\]](#), the FFT solver has been applied to textile composites. We pursued a quantitative analysis of the elastic field calculation for heterogeneous materials and investigated possible causes of errors in [\[Ma et al., 2019, 2021\]](#). In [\[Ma et al., 2023a\]](#), the complete formulation was compared to the previously published simplified formulation of the non-local damage based on the phase-field model for heterogeneous materials. Finally, [Ma et al. \[2023b\]](#) introduced the Newton–Krylov algorithm for efficient solving and improving of the convergence rate of the introduced damage models.

This chapter provides a summary of the following research activities:

- Short-stay visiting : **Project FoCUS**: *Advanced numerical methods for textile composites modeling*, KU Leuven, 2019. **Project OCTET**: *Reduced order modeling for advanced nonlinear multi-scale numerical methods of composites*, KU Leuven and UGhent, 2019-2020.
- **3** international conferences (see in CV [\[C3\]](#), [\[CP3\]](#), [\[C5\]](#)).
- **5** journal papers (see in CV [\[A9\]](#), [\[A10\]](#), [\[A5\]](#), [\[A2\]](#),[\[A1\]](#)).
- **1** PhD thesis advising: **X. Ma** (see in CV [\[D5\]](#)).
- **1** PostDoc supervising: **Y. Chen** (see in CV [\[P2\]](#))

5.1 Introduction

As we delve deeper into the investigations of advanced composite materials, including textile-reinforced materials, the need for an efficient numerical model becomes more pronounced. Simultaneously, this model should closely represent the micro- and meso-structure of the material to align with reality. However, achieving these goals can sometimes be contradictory and not easily attainable.

During the design stage of textile composites, the exact mechanical behavior and effective material properties often remain uncertain. Experimental tests tend to be costly and, at times, unfeasible for acquiring all necessary properties. As a result, considerable effort is made in developing mathematical tools to assess composite performance. Analytical models can yield quick and efficient results; however, these rough approximations exhibit limitations when studying intricate behaviors and morphologies. Hence, numerical approaches like Finite Element Methods (FEM) are introduced to simulate realistic and complex models.

For FEM techniques, the conformal mesh is the most widely used, enabling the discretization of an actual model shape. However, in cases involving intricate structures, such as textile composites, interpenetration zones and non-physical distance between yarns the conformal mesh is not suitable. While algorithms exist to establish complete conformal meshes for these structures, their computational cost is substantial. Consequently, the voxel-based mesh presents an intriguing alternative to the conformal mesh. This approach avoids the need for advanced algorithms and allows for direct model creation from images.

Conventional finite element method (FEM) solvers can be cumbersome for 3D simulations and may require efficient parallel implementation [Nguyen et al., 2017] and/or automatic mesh adaptation [Zhou and Zhuang, 2018] to extend computational limits. This will be even more important when dealing with heterogeneous materials with a complex microstructure. As an alternative, numerical homogenisation can be performed by Fast Fourier Transform (FFT) solvers. FFT-based method has gained popularity owing to its intrinsic parallelization capabilities. It was initially proposed by [Moulinec and Suquet, 1994, 1995] as a voxel-based methodology that does not need stiffness matrix assembling, unlike conventional FEM solvers.

5.2 Homogenization problem

The starting point is the definition of conventional homogenization problem for heterogeneous materials as shown in Fig 5.1. This problem is formulated in the following set of equations:

$$\boldsymbol{\sigma}(\mathbf{x}) = \mathbb{C}(\mathbf{x}) : \boldsymbol{\varepsilon}(\mathbf{x}) \quad \forall \mathbf{x} \in V \quad (5.1a)$$

$$\nabla \cdot \boldsymbol{\sigma}(\mathbf{x}) = \mathbf{0}, \quad (5.1b)$$

$$\boldsymbol{\varepsilon}(\mathbf{x}) = \boldsymbol{\varepsilon}^*(\mathbf{x}) + \langle \boldsymbol{\varepsilon} \rangle \quad \text{or} \quad \mathbf{u}(\mathbf{x}) = \mathbf{u}^*(\mathbf{x}) + \langle \boldsymbol{\varepsilon} \rangle \cdot \mathbf{x}, \quad (5.1c)$$

$$\boldsymbol{\varepsilon}(\mathbf{x}) = \frac{1}{2}(\nabla \mathbf{u}(\mathbf{x}) + (\nabla \mathbf{u}(\mathbf{x}))^T), \quad (5.1d)$$

$$\langle \boldsymbol{\varepsilon} \rangle = \mathbf{E} \quad \text{and} \quad \boldsymbol{\varepsilon}(\mathbf{x}) \quad \text{periodic in } V, \quad (5.1e)$$

where V is the volume of our RVE with perfectly bonded materials phases, \square^* represents the fluctuation term, $\langle \square \rangle$ stands for the averaging operator, \mathbf{E} is the averaged strain tensor. With

the local stiffness fourth-order tensor \mathbb{C} and reference stiffness material \mathbb{C}_0 , the Eq. 5.1a can be rewritten as follows:

$$\boldsymbol{\sigma}(\mathbf{x}) = \mathbb{C}_0(\mathbf{x}) : \boldsymbol{\varepsilon}(\mathbf{x}) + \boldsymbol{\tau}(\mathbf{x}) \quad (5.2)$$

where $\boldsymbol{\tau}(\mathbf{x}) = (\mathbb{C}(\mathbf{x}) - \mathbb{C}_0) : \boldsymbol{\varepsilon}(\mathbf{x})$ is the polarization stress tensor.

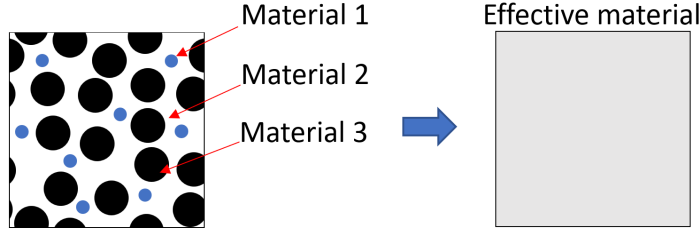


Figure 5.1: Illustration of the conventional homogenization: three phases materials (left) and homogenized (or effective) material (right).

Finally, Eq. 5.1a and Eq. 5.2 are equivalent to the periodic Lippmann-Schwinger equation [Moulinec and Suquet, 1994]:

$$\boldsymbol{\varepsilon}(\mathbf{x}) = -\boldsymbol{\Gamma}_0(\mathbf{x}) * \boldsymbol{\tau}(\mathbf{x}) + \langle \boldsymbol{\varepsilon} \rangle, \quad \forall \mathbf{x} \in V \quad (5.3)$$

with $\boldsymbol{\Gamma}_0$ as the fourth-order tensor which is called also Green operator and ”*” is the convolution product.

5.3 FFT-based homogenization for elastic problem

5.3.1 Solution of elastic problem

One of the major advantages of the FFT-based method is the high computational performance. As described previously, local strain tensor is calculated by a convolution product with a fourth-rank Continuous Green Operator (CGO, $\boldsymbol{\Gamma}_0$ in Eq. 5.3) and a polarization term ($\boldsymbol{\tau}$ in Eq. 5.2). This convolution product is transformed into a simple multiplication in Fourier space while solving Eq. 5.3 is not an easy task in real space because the numerical computation of a convolution product is complicated. Furthermore, the term $\boldsymbol{\Gamma}_0$ is easier to calculate in Fourier space. Thus, Eq. 5.3 in Fourier space simply becomes

$$\widehat{\boldsymbol{\varepsilon}}(\boldsymbol{\xi}) = -\widehat{\boldsymbol{\Gamma}}_0(\boldsymbol{\xi}) : \widehat{\boldsymbol{\tau}}(\boldsymbol{\xi}), \quad \forall \boldsymbol{\xi} \neq 0, \quad \widehat{\boldsymbol{\varepsilon}}(0) = \langle \boldsymbol{\varepsilon} \rangle, \quad (5.4)$$

where the convolution can be transformed into a simple double contraction (denoted as ”:”). In Eq. 5.4 $\widehat{\boldsymbol{\varepsilon}}$, $\widehat{\boldsymbol{\Gamma}}_0$ and $\widehat{\boldsymbol{\tau}}$ are the Fourier transforms of $\boldsymbol{\varepsilon}$, $\boldsymbol{\Gamma}$ and $\boldsymbol{\tau}$ respectively. The vector of frequency, denoted by $\boldsymbol{\xi}$, varies in Fourier space.

Because the polarization stress term $\boldsymbol{\tau}(\mathbf{x})$ in Eq. (5.2) is nonlinear, an iterative algorithm is necessary. The principle of the algorithm is to use an iterative fixed-point scheme (*basic scheme* proposed by Moulinec and Suquet [1994]) to solve Eq. (5.2) and Eq. (5.1b):

Initialization:

$$\begin{aligned} (a_0) \quad & \boldsymbol{\varepsilon}^0(\mathbf{x}) = \langle \boldsymbol{\varepsilon} \rangle, \quad \forall \mathbf{x} \in V \\ (b_0) \quad & \boldsymbol{\sigma}^0(\mathbf{x}) = \mathbb{C}(\mathbf{x}) : \boldsymbol{\varepsilon}^0(\mathbf{x}) \end{aligned}$$

Iteration ($i + 1$): $\boldsymbol{\varepsilon}^i$ and $\boldsymbol{\sigma}^i$ are known

$$\begin{aligned} (a) \quad & \boldsymbol{\tau}^i = \boldsymbol{\sigma}^i - \mathbb{C}_0 : \boldsymbol{\varepsilon}^i(\mathbf{x}) \\ (b) \quad & \widehat{\boldsymbol{\tau}}^i = F(\boldsymbol{\tau}^i) \\ (c) \quad & \widehat{\boldsymbol{\varepsilon}}^{i+1}(\boldsymbol{\xi}) = -\widehat{\Gamma}_0(\boldsymbol{\xi}) : \widehat{\boldsymbol{\tau}}^i(\boldsymbol{\xi}), \quad \forall \boldsymbol{\xi} \neq 0, \quad \widehat{\boldsymbol{\varepsilon}}(0) = \langle \boldsymbol{\varepsilon} \rangle \\ (d) \quad & \boldsymbol{\varepsilon}^{i+1} = F^{-1}(\widehat{\boldsymbol{\varepsilon}}^{i+1}) \\ (e) \quad & \boldsymbol{\sigma}^{i+1}(\mathbf{x}) = \mathbb{C}(\mathbf{x}) : \boldsymbol{\varepsilon}^{i+1}(\mathbf{x}) \\ (f) \quad & \text{Convergence test: } \frac{(\|\text{div}(\boldsymbol{\sigma}^{i+1})\|^2)^{1/2}}{\|\boldsymbol{\sigma}^{i+1}\|} \leq e \end{aligned} \tag{5.5}$$

Here $\|\cdot\|$ is the L^2 norm. The iterative algorithm (5.5) stops when the convergence condition is satisfied ($e = 1 \times 10^{-12}$ in our calculations).

The multiplication of the polarization term and the CGO are local operations that can be easily parallelized [Chen et al., 2019a]. Even if the FFT operation itself is not local, efficient parallel implementations such as FFTW [FFT] are available. As a result, large-scale simulations based on full-resolution images can be performed using the FFT-based method. Since its introduction, FFT-based method has been improved and used to study a wide range of physical phenomena in heterogeneous materials [Leclerc et al., 2016, Wang et al., 2018]. Its high performance in comparison with FEMs have been clearly demonstrated by Eisenlohr et al. [2013], Lucarini et al. [2022] and Ma et al. [2021]. However, despite the high computational performance, the FFT-methods have several drawbacks (Sec. 5.3.4) that will require the caution in their applications to realistic materials (Sec. 5.3.5).

5.3.2 First attempt to modeling a damage process in FFT solvers

Inspired by the successful application of FFT-based solvers for some study cases, as presented previously, we aimed to extend applications for more complex multi-scale simulations of *realistic* textile composites [Chen et al., 2019c, 2018]. Moreover, this should consider manufacturing defects such as fiber misalignment and voids. The material behavior should also consider the progressive degradation of the materials using damage modeling.

These numerical tests were performed on the 3D orthogonal textiles (as shown on Fig. 5.2) that we have used in the multi-scale modeling within the FEM framework (see Sec. 4.4). The geometry consists of two anisotropic phases (warp and weft yarns) and several isotropic phases (matrix, voids and margins). The margins were introduced to study the boundary effects and attenuate the strong periodicity conditions imposed by the FFT method. The anisotropic phases (weft and warp yarns) have transverse isotropic behavior and their local material orientation has been identified using structure tensor segmentation with anisotropy as

presented in Sec. 4.3.3. As for the damage model, we have introduced an anisotropic damage model into the solver, similar to what was presented in Sec. 3.1.2. This is a classical local continuous damage model with smeared crack regularization [Bažant and Oh, 1983].

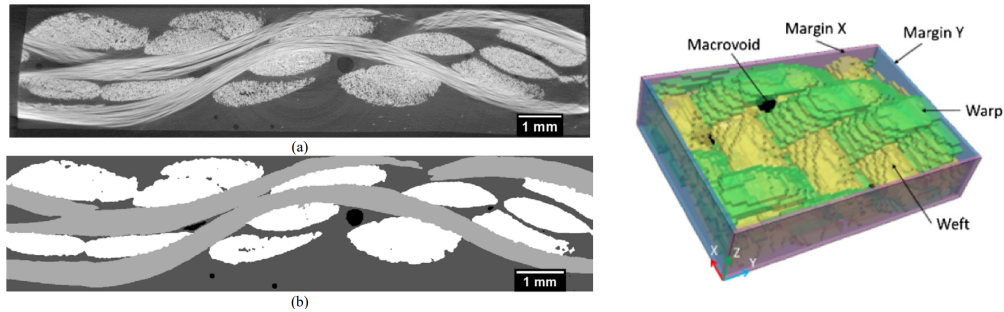


Figure 5.2: Description of the realistic voxel-based model: the first row (a) scanned image and (b) segmented image; the second row is represented voxel model for FFT-based solver. [Chen et al., 2019c]

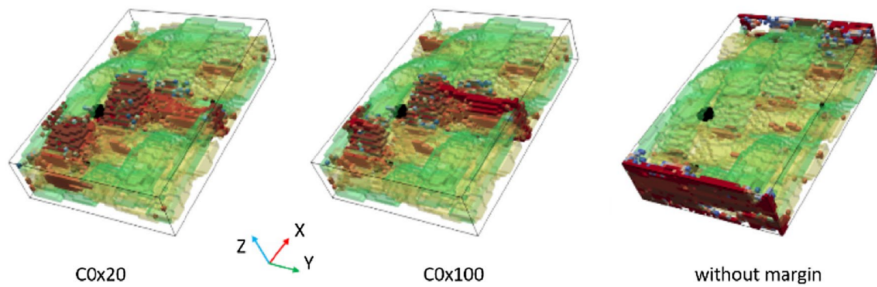


Figure 5.3: Brief results of damage field in the matrix and yarns with different contrast of the "margin" materials selections. [Chen et al., 2019c]

5.3.3 Research problem statement for FFT methods

The results of these works have opened a broad field for further investigations. Several main aspects have been formulated and listed in the next Box. 5.3.3.

Numerical modeling based on FFT methods

This implementations have raised the following groups of questions linked to:

1. **FFT-based solver.** Are the numerical artifacts that are rising from FFT method itself appropriate for extension to realistic materials?

- "Realistic" materials, in general, never respect the **periodicity** of the microstructure, whereas FFT-methods by definition are periodic. Thus, the question rises: whether we can find a remedy for this kind of microstructure? As suggested by Chen et al. [2018, 2019c], we can introduce to the model some fictive material (or as we called "margin" material).
- The issue is well-known that FFT-based models are very sensitive to the **contrast** of the phases. The more material phases, the more interface should be treated. In this case, we have several anisotropic phases (warp and weft yarns), a few isotropic phases (matrix and voids), and some fictive materials on the border of the RVE.
- How important are the **numerical artifacts** that are inherently present in the FFT

methods?

2. **Damage modeling.** Is the chosen model appropriate for textile-reinforced composites with defects?
 - Local models should be probably replaced by **non-local formulations**.
 - "Realistic" materials typically have a high volume fraction of the reinforcement phase, resulting in fibers or yarns being in close contact or proximity to each other. In the case of a non-local formulation, how does the characteristic length parameter influence damage initiation and impact crack propagation?

5.3.4 Numerical artifacts in FFT solvers

There are three main issues with this fixed-point scheme, which many researchers have attempted to overcome in the last two decades. According to [Ma et al. \[2021\]](#) the classification of the numerical artifacts is presented as follows :

1. Infinite mechanical contrast between phases ($\mathbb{C}_0/\mathbb{C}(\boldsymbol{x})$);
2. Sensitivity to the choice of reference material (\mathbb{C}_0);
3. Spurious numerical oscillations due to heterogeneity in mechanical fields:
 - No satisfaction of Shannon's theorem for heterogeneous fields (no cut-off frequency for heterogeneous fields);
 - Gibbs phenomenon of spectral methods;
 - Non-smooth "zig-zag" interfaces (voxel-type discretisation);
 - Hourglass effect (similar to reduced integration formulation in FEM).

The first issue is well reported in the literature and several solutions have already been proposed: the *accelerated scheme* [[Eyre and Milton, 1999](#)], the *augmented Lagrangian scheme* [[Michel et al., 2000](#)] and the *polarization-based scheme* [[Monchiet and Bonnet, 2012](#)]. The second issue was addressed by [Brisard and Dormieux \[2010\]](#) and [Zeman et al. \[2010\]](#) simultaneously proposing the use of *conjugate gradient solvers*. An extension to the non-linear case for conjugate gradient solvers has been proposed by [Gélébart and Mondon-Cancel \[2013\]](#). This solution appears to improve both the sensitivity to the phases contrast and the choice of reference material.

[Ma et al. \[2021\]](#) have addressed the issue of the spurious numerical oscillations, with quantitative analysis of each cause and proposed several solutions to reduce the impact for heterogeneous materials.

5.3.5 Solutions to reduce numerical artifacts in FFT solvers

Over a decade, many researchers have worked to reduce these artifacts. The following three strategies were adopted in [[Ma et al., 2021](#), [Ma, 2022](#)]:

1. Computation of the Discrete Green Operator (DGO) based on Finite Difference (FD) discretization.
This kind of approach was first proposed by [Müller \[1996\]](#) and followed by [Dreyer et al.](#)

[1999] and Brown et al. [2002] where a centered FD was considered. Backward and forward FD schemes were adopted by Willot and Pellegrini [2008]. Many papers were published in the last few years in this research direction such as Willot et al. [2014], Berbenni et al. [2014], Lebensohn and Needleman [2016], Djaka et al. [2017], Vidyasagar et al. [2017]. Among the different schemes, there is the DGO calculated based on the centered FD scheme on a rotated grid, called *rotated scheme* Willot [2015], which is one of the most interesting schemes. This scheme was implemented in the open-source software AMITEX-FFTP AMI developed by Lionel Gélébart et al.

2. Discretization scheme based on linear hexahedral element.

It was proposed Schneider et al. [2017] adapted to both the basic scheme and conjugate gradient solvers. This scheme was presented in two versions, one with reduced integration and the other with full integration, similarly to FEM. It was analytically demonstrated that the scheme with reduced integration is equivalent to the *rotated scheme* proposed in [Willot, 2015].

3. Smoothing of the interfaces.

As illustrated in Fig. 5.4, the numerical oscillations are still present even with the rotated scheme due to non-smooth interface. As a solution *composite voxels* [Kabel et al., 2015, Charière et al., 2020] and *neighbor voxels average* [Ma et al., 2019] were investigated.

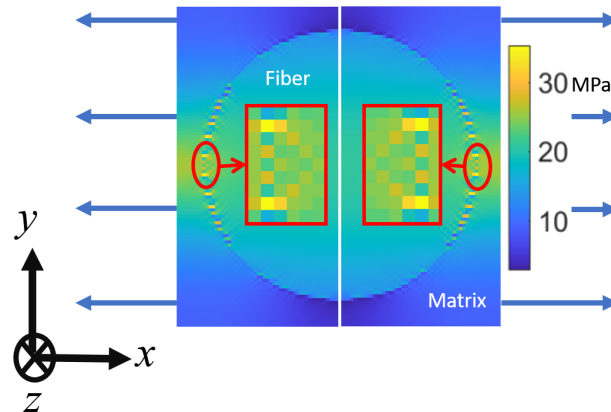


Figure 5.4: Illustration of spurious numerical oscillations (check-board patterns) of local stress field (σ_{xx}) present in FFT with rotated scheme proposed by Willot [2015] (left half part) and FEM (right half part) under tension in x -direction with the contrast between the fiber and matrix Young's moduli set to $E_f/E_m = 22$.

The highlights of the main results are shown in Fig. 5.5. A comparison of different Discrete Green Operators formulations (Moulinec-Suquet (M-S), Willot-Schneider (W-S), Schneider full integration (SF)) and FEM solutions with reduced (FEMR) and full integration (FEMF) is shown in Fig. 5.5a and Fig. 5.5b for normal and tangential interface strains respectively. The error measure ($MD = |D_j^{FFT} - D_j^{FEMR}|$) values were selected to show the absolute difference between FFT results and FEM results with the reduced formulation. This measure shows that increasing sampling frequencies does not affect the results. Some similarities with the DGO formulation have been confirmed in the literature.

Remark: Nevertheless, some open questions still remain for further investigations. Why are the

fluctuations independent of sampling frequencies, and why does M-S show fewer fluctuations than the other formulations?

The second set of results is shown in Fig. 5.5c and Fig. 5.5d to compare the strain field with smoothing techniques on the interface using the Willot-Schneider (W-S) DGO. The comparison was done for two techniques: the composite voxel technique (TCV), as shown in [Kabel et al., 2015], and the improved level-set method (OCV) proposed in [Ma, 2022]. Similarly, we only look at the normal strain and tangential strain components. Both techniques have also been compared to the FE solution with a conformal mesh. Both techniques show very similar results, and the improved OCV is performing slightly better. One of the great advantages is that OCV can be easily adapted for any kind of heterogeneous materials without knowing the distribution of the material phases in advance.

Finally, a comparison of the improved smoothing technique (OCV), averaging techniques (AVE), and conformal mesh FE simulations is shown in Fig. 5.5e. In certain cases, averaging techniques (AVE) can outperform the OCV. However, in the case of generic heterogeneous material, OCV is still one of the most effective methods to smooth the interfaces and significantly reduce numerical fluctuations due to the "zig-zag" interface shape.

5.4 Phase-field method to model non-local damage

The modeling of crack propagation using the classical continuous mechanics approach can suffer from loss of ellipticity of the governing differential equations after reaching the maximum strength of a material due to material instability [de Borst and Verhoosel, 2017]. Strain-softening behavior is manifested by localization of strain into discontinuity and ultimately lack of objectivity and poor convergence of the numerical solution. As a result, the problem converges to a solution without energy dissipation in the crack process zone, which is localized in a zero-width band. Numerical solutions exhibit mesh dependency, giving physically meaningless results that also depend on mesh alignment. To address this issue, many methods have been proposed, such as gradient-enhanced damage models [Peerlings et al., 2002] and phase-field models [Francfort and Marigo, 1998]. Even if they start from different points, both models have a common point, namely, the inclusion of similar gradient terms into the governing equations: damage gradient for the first one and spatial derivatives into the energy functional for the second one [de Borst and Verhoosel, 2016]. The latter ones have gained popularity in recent decades [Miehe et al., 2010b,a, Wu, 2017].

Phase-field models utilize a damage variable (d) to describe the failure state, where sharp cracks are regularized as diffusive crack bands by a function of d [Bourdin et al., 2000, 2008] (see Fig. 5.6(a)(b)). The damage variable d is a continuous parameter that varies in the range $[0, 1]$ and describes the degradation state of the material. The value of 0 represents an intact state and the value of 1 represents a fully degraded state. On the one hand, the evolution of the phase-field variable itself completely describes the initiation and propagation of cracks in the material. On the other hand, phase-field models are closely related to the variational approach of brittle fracture as was shown by Francfort and Marigo [1998], which enables a simultaneous approximation of the displacement field and the cracks by minimizing the total potential energy of the solid. Miehe et al. [2010b] have proved that the regularization length of

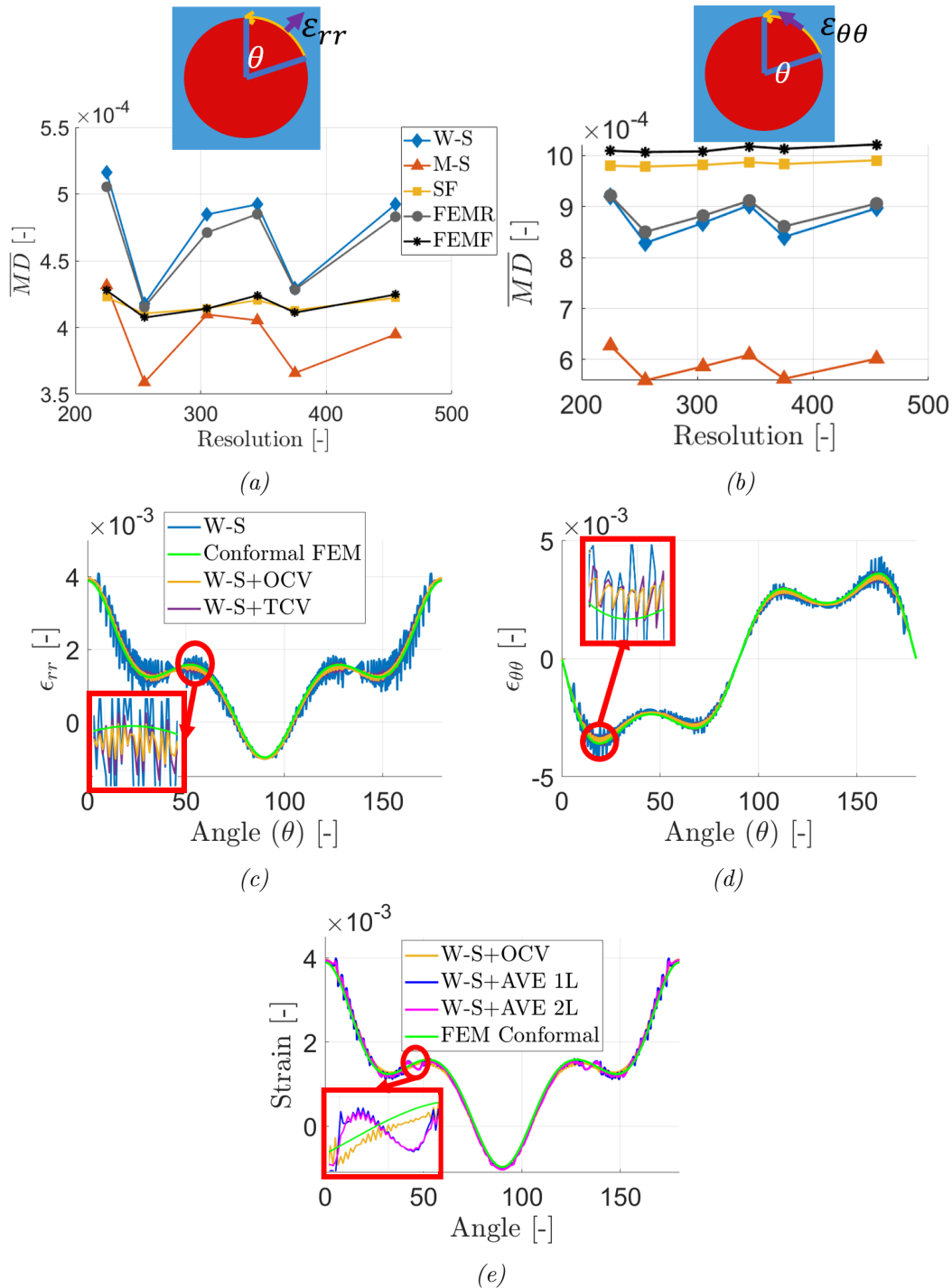


Figure 5.5: Conventional example of the single fiber Unit Cell (UC) under uniaxial traction (see [Ma et al., 2021]).

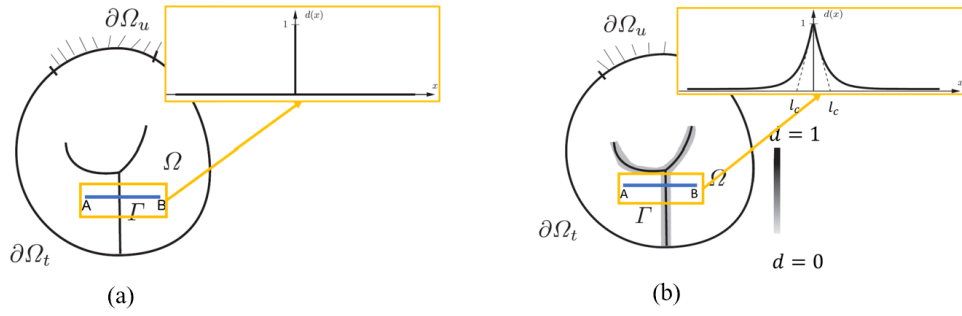


Figure 5.6: A solid body Ω with the crack set Γ : (a) conventional sharp cracks and (b) diffuse crack bands in phase-field.

the phase-field model should be at least twice the element size of the fractured zone. Thus, it requires a minimum ratio between the minimum regularization length and mesh size to ensure mesh independence. Therefore, for complex microstructures, phase-field methods necessitate a sufficiently refined mesh for better predictions. On the other hand, FFT is more conducive to massive parallelization. As a result, combining phase-field models with the FFT method for fracture problems can be advantageous. A pioneering work in this area was published by [Chen et al. \[2019b\]](#) and was successively continued by [Ma et al. \[2023a,b\]](#).

5.5 Review of Miehe's and Wu's phase-field models

In this section two phase-field models will be briefly introduced. The first model was initially proposed by [Miehe et al. \[2010b\]](#), and the second one by [Wu \[2017\]](#). For all subsequent demonstrations, the subscripts \square^M and \square^W will denote Miehe's and Wu's models, respectively.

5.5.1 Regularization of sharp cracks

The starting point of the phase-field method is to smear the sharp crack using a diffusive crack band. The smear function can vary for different phase-field models. Those used in Miehe's Eq. 5.6a and Wu's models Eq. 5.6b are described below:

$$d^M = \exp\left(\frac{-|x|}{l_c}\right), \quad (5.6a)$$

$$d^W = 1 - \sin\left(\frac{|x|}{l_c}\right). \quad (5.6b)$$

With Eq. (5.6), it is straightforward to calculate the diffusive crack surface (B) and its density (γ), where their generic forms can be expressed as follows,

$$B = \int_{-\infty}^{+\infty} \gamma dV, \quad (5.7a)$$

$$\gamma = \frac{1}{c_0} [\alpha(d) + l_c (\nabla d)^2], \quad (5.7b)$$

$$\alpha(d) = \xi d + (1 - \xi)d^2, \quad (5.7c)$$

where ξ and c_0 are the parameters that vary depending on the specific phase-field model being used. A generic expression of the geometric crack function $\alpha(d)$ was proposed by Wu [2017]. In phase-field models with $\alpha(d) = d^2$ and $\xi = 0$ the classical quadratic geometric crack function is recovered [Miehe et al., 2010b] resulting in a localization of infinite bandwidth support. In contrast, Wu's model [Wu, 2017] uses the geometric crack function $\alpha(d) = 2d - d^2$ with $\xi = 2$, which leads to a sinusoidal distribution of the crack phase-field with a finite support πl_c . The summary of different functions and values of the parameters for Miehe's and Wu's models are listed in Tab. 5.1 and the damage profiles of both models are illustrated in Fig. 5.7.

Model name	ξ	$\alpha(d)$	c_0	$d(x)$
Miehe Miehe et al. [2010b,a]	0	d^2	2	$\exp\left(-\frac{ x }{l_c}\right)$
Wu Wu [2017], Wu and Nguyen [2018]	2	$2d - d^2$	π	$1 - \sin\left(\frac{ x }{l_c}\right)$

Table 5.1: The parameters of different phase-field models.

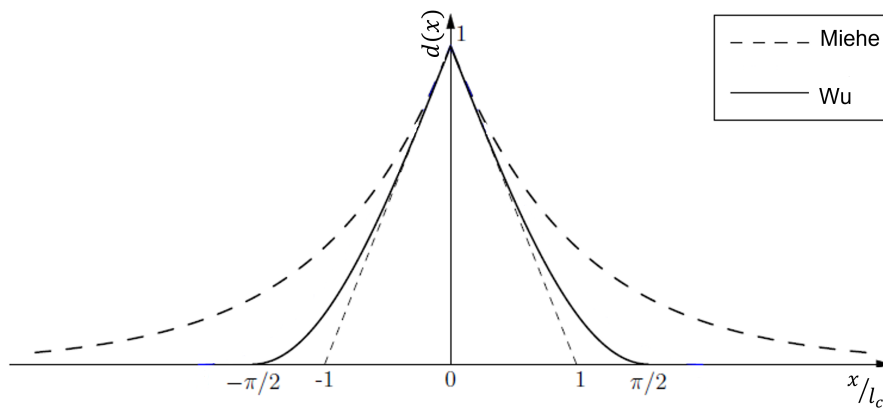


Figure 5.7: The damage profile of different diffusive crack functions Wu et al. [2020].

5.5.2 Variational approach

The diffusive crack surface (Eq. (5.7)) can then be incorporated into the variational approach of brittle fracture modeling, which is based on Griffith's energy principle [Griffith, 1920] for a cracked body. In this energetic approach, the damage evolution and crack propagation are a competition between the bulk energy stored in the body and the energy dissipation from the opening of the crack surface. From this point of view, in quasi-static loading, the total energy Π can be expressed as:

$$\Pi := \Phi_s + \Phi_d - P, \quad (5.8)$$

where Φ_s represents the strain energy stored in the cracked body, Φ_d represents the energy dissipated by opening the crack surface, and P represents the work of external loading.

In the phase-field method, the dissipated energy Φ_d can be approximated as the energy required to open the diffusive crack band, as described in Eq. (5.7). As a result, Φ_d can be converted from a surface integral to a volume integral. Meanwhile, an energetic degradation function, denoted as $g(d)$, is used to compute the value Φ_s . We consider a domain $\Omega \subset R^n$ ($n =$

1, 2, 3) that contains a crack set Γ with $\Gamma \subset R^{n-1}$ and is subject to volumetric loading by the body force \mathbf{f}^* , the displacement \mathbf{u}^* on the boundary $\partial\Omega_u$, and the surface force \mathbf{t}^* on the complementary boundary $\partial\Omega_t$. The symbol \square^* indicates the prescribed terms. In summary, a detailed formulation of the components in Eq. 5.8 is provided below:

$$\Phi_s = \int_{\Omega} \varphi(\boldsymbol{\varepsilon}, \Gamma) dV = \int_{\Omega} g(d) \varphi_0(\boldsymbol{\varepsilon}(\mathbf{u})) dV, \quad (5.9a)$$

$$\Phi_d = \int_{\Gamma} G_c dS \approx \int_B G_c \gamma(d, \nabla d) dV, \quad (5.9b)$$

$$P = \int_{\Omega} \mathbf{f}^* \cdot \mathbf{u} dV + \int_{\partial\Omega_t} \mathbf{t}^* \cdot \mathbf{u} dS + \int_{\partial\Omega_u} (\boldsymbol{\sigma} \cdot \mathbf{n}) \cdot \mathbf{u}^* dS. \quad (5.9c)$$

In Eq. 5.9a, φ denotes the elastic strain energy density stored in the cracked body, while $\boldsymbol{\varepsilon}$ and φ_0 represent the strain tensor and initial strain energy, respectively. In Eq. 5.9b, G_c stands for the critical energy release rate. Typically, the diffused crack domain B is much smaller than the considered domain Ω with $B \subset \Omega$. In Eq. 5.9c, the symbols $\boldsymbol{\sigma}$ and \mathbf{n} correspond to the Cauchy-stress tensor and the normal vector outside the boundary, respectively. Additionally, the symbols $\int dV$ and $\int dS$ represent the volume and surface integration, respectively.

The strain and phase-fields $(\boldsymbol{\varepsilon}, d)$ can then be determined by minimizing the total energy under the constraint of irreversibility, which is stated as $\dot{d} \geq 0$, and under the boundary conditions: $\mathbf{u}(\mathbf{x}) = \mathbf{u}^*$ at $\partial\Omega_u$, and $\boldsymbol{\sigma} \cdot \mathbf{n} = \mathbf{t}^*$ at $\partial\Omega_t$ with \mathbf{n} the outward unit normal vector to the external boundary $\partial\Omega$ ($\partial\Omega = \partial\Omega_u \cup \partial\Omega_t$). Eq.(5.8) can be written in a variational form:

$$\delta\Pi(\mathbf{u}, d) = \int_{\Omega} \boldsymbol{\sigma} : \delta\boldsymbol{\varepsilon} dV + \int_B \frac{\partial\varphi}{\partial d} \delta d dV + \int_B G_c \left(\frac{\partial\gamma}{\partial d} \delta d + \frac{\partial\gamma}{\partial \nabla d} (\nabla d) \cdot \delta(\nabla d) \right) dV - \int_{\partial\Omega_t} \mathbf{t}^* \cdot \delta\mathbf{u} dS, \quad (5.10)$$

where $\boldsymbol{\sigma} = \frac{\partial\varphi}{\partial\boldsymbol{\varepsilon}}$ denotes the Cauchy stress, and $\delta u = 0$ for $\forall x \in \partial\Omega_u$. Eq. (5.10) can generally be split into two components: $\delta\Pi(\mathbf{u}, d)^{P1}$ and $\delta\Pi(\mathbf{u}, d)^{P2}$, which represent the mechanical and phase-field parts, respectively. This enables a separate solution for the mechanical and damage fields, and a coupling scheme would then be employed to link these two fields. This section only focuses on the phase-field part $\delta\Pi(\mathbf{u}, d)^{P2}$, which can be expressed as:

$$\delta\Pi(\mathbf{u}, d)^{P2} = \int_B g'(d) \varphi_0 \delta d dV + \int_B \frac{G_c}{c_0 l_c} \alpha'(d) \delta d dV + \int_B \frac{2G_c l_c}{c_0} \nabla d \cdot \nabla(\delta d) dV, \quad (5.11)$$

where \square' means the first derivative. Eq. (5.11) allows us to easily derive the governing equation for the damage field in phase-field models in the following form:

$$g'(d) \mathcal{H} + \frac{G_c}{c_0 l_c} \alpha'(d) - \nabla \cdot \left(\frac{2G_c l_c}{c_0} \nabla d \right) = 0. \quad (5.12)$$

Further details can be found in [Ma, 2022]. Eq. (5.12) represents the generic form of the governing equation for the phase-field. The regularization parameters, α and c_0 , are already known for each phase-field model and are shown in Tab. 5.1. Therefore, the next step is to determine \mathcal{H} and $g(d)$ for each phase-field method.

Energetic degradation functions

The energetic degradation function, $g(d)$, varies for different phase-field models. For Miehe's phase-field model, a quadratic energetic degradation function is used, as shown in Eq. (5.13)(a).

In contrast, Wu's model with a linear softening law, which is used in this work, employs a more complex degradation function as described in Eq. (5.13)(b).

$$g(d)^M = (1 - d)^2, \quad (5.13a)$$

$$g(d)^W = \frac{(1 - d)^2}{(1 - d)^2 + a_1 d(1 - \frac{1}{2}d)}, \quad a_1 = \frac{EG_c}{\sigma_c^2} \frac{4}{\pi l_c}, \quad (5.13b)$$

where E stands for the Young's modulus of the material in the case of isotropic material, while σ_c represents the material's strength. Contrary to the degradation function used in Miehe's model, the formula for a_1 in Eq. (5.13)(b) includes σ_c . As a result, Wu's model has an elastic stage.

History variables

Damage models should reflect the physical properties of materials. A damage variable is irreversible and cannot be higher than 1. As a result, the boundedness $d \in [0, 1]$ and irreversibility condition $\dot{d} \geq 0$ should be respected. To ensure the irreversibility condition, the history field \mathcal{H} is introduced into Eq. (5.12). This field represents the maximum initial strain energy at $[0, t_n]$, where t_n is the current time. The two history fields for both Miehe's and Wu's models are defined as follows:

$$\mathcal{H}^M(\mathbf{x}, t_n) := \max_{0 \leq t \leq t_n} [\varphi_0^+(\mathbf{x}, t)], \quad (5.14a)$$

$$\mathcal{H}^W(\mathbf{x}, t_n) := \max_{0 \leq t \leq t_n} \left[\varphi_0^+(\mathbf{x}, t), \frac{1}{2} \frac{\sigma_c^2}{E} \right], \quad (5.14b)$$

where $\varphi_0^+(\mathbf{x}, t)$ represents the initial tensile strain energy at time t , as the compressive part does not contribute to damage in phase-field models. The $\varphi_0^+(\mathbf{x}, t)$ of Wu's model is calculated as:

$$\varphi_0^+ = \frac{1}{2} \frac{(\langle \bar{\sigma}_1 \rangle_+)^2}{E}, \quad (5.15)$$

where $\bar{\sigma}_1$ represents the major principal value of the effective stress $\bar{\sigma}$, which is determined by the elastic relation $\bar{\sigma} = \mathbb{C} : \varepsilon$. Here, \mathbb{C} refers to the material stiffness tensor without damage. The split operation, denoted by $\langle - \rangle_+$, is defined as $\langle x \rangle_+ = \{x, 0\}$. More details about the initial strain energy and split formula for Miehe's model can be found in [Miehe et al., 2010a, Chen et al., 2019b, Ma et al., 2023a].

As shown in [Mandal et al., 2019, Wu et al., 2020, Ma, 2022], the damage value in Miehe's model inherently satisfies the boundedness $d \in [0, 1]$. However, this is not the case for Wu's model due to its elastic stage. As a result, an additional condition, i.e., the Rankine energy ($\frac{1}{2} \frac{\sigma_c^2}{E}$), should be included in the history field \mathcal{H} for Wu's model to ensure $d = 0$ during the elastic stage.

Phase-field governing equations

According to Eqs. (5.12) to (5.15), the governing equations for Miehe's and Wu's model are written as

$$-2(1-d)\mathcal{H}^M + \frac{G_c}{l_c}d - \nabla \cdot (G_c l_c \nabla d) = 0, \quad (5.16a)$$

$$-\frac{4a_1(1-d)}{(2a_1d - 4d - a_1d^2 + 2d^2 + 2)^2}\mathcal{H}^W + \frac{2G_c}{\pi l_c}(1-d) - \nabla \cdot \left(\frac{2G_c l_c}{\pi} \nabla d \right) = 0, \quad (5.16b)$$

where Eq. (5.16)(a) is specific to Miehe's model while Eq. (5.16)(b) applies to Wu's model.

5.6 FFT-based solvers development

5.6.1 Miehe's phase-field damage model in FFT solver

A FFT solver of a variational phase-field model for brittle fracture has been proposed for the first time by [Chen et al. \[2019b\]](#). Relying on the staggered update scheme of [[Miehe et al., 2010a](#)], the phase-field and elastic problems have been separately solved both using the FFT method with fixed-point algorithm together with a convergence acceleration procedure. Benefiting from the FFT technique, the proposed method is easy to parallelize and convenient for image-based modeling.

Main assumptions that were made by [Chen et al. \[2019b\]](#) have led us to the following system of governing equations:

$$\frac{G_c}{l_c} (d - l_c^2 \Delta d) + \eta \dot{d} = 2(1-d)\mathcal{H}^M, \quad (5.17a)$$

$$\nabla \cdot \boldsymbol{\sigma}(\mathbf{u}, d) = \mathbf{0}, \quad (5.17b)$$

$$\boldsymbol{\varepsilon} = \frac{1}{2}(\nabla \mathbf{u} + (\nabla \mathbf{u})^T), \quad (5.17c)$$

$$\boldsymbol{\sigma} = g(d)^M [\lambda \langle \text{tr}(\boldsymbol{\varepsilon}) \rangle_+ \mathbf{I} + 2\mu \boldsymbol{\varepsilon}_+] + [\lambda \langle \text{tr}(\boldsymbol{\varepsilon}) \rangle_- \mathbf{I} + 2\mu \boldsymbol{\varepsilon}_-], \quad (5.17d)$$

where η is the viscous regularization parameter for convergence of the fixed-point algorithm, $\dot{\square}$ denotes the time derivative, λ and μ are the Lamé constants of a material, \mathbf{I} is the second-order unity tensor. In Eq. 5.17d we introduce the split of positive and negative strain tensors whose details can be found in [[Chen et al., 2019b](#)].

Besides the standard numerical test cases (such as Single Edge Notch Tensile, Double Edge Notch Tensile, etc. see [[Chen et al., 2019b](#)]) we also have applied them to continuous fiber reinforced composite unit cell with penny-shape defect (as shown in Fig. 5.8). In this test case we allowed only matrix material to be damaged and assumed that two phases materials have perfect interface.

This work has shown a great potential for the non-local damage modeling for composite materials. However, a main question has been raised (see Box 5.3.3): Is the assumption, made in Eq. 5.17a, could be still applicable to the heterogeneous materials with heterogeneous fracture properties?

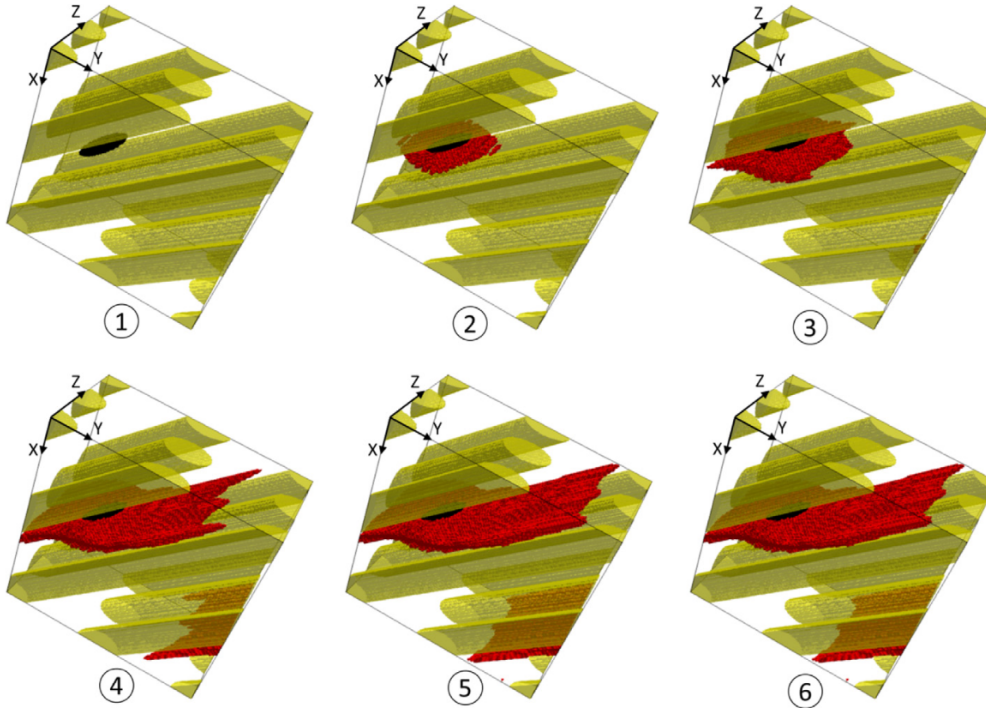


Figure 5.8: Crack patterns of the continuous fiber composite under tension in the x -axis at different loading levels. For the sake of clarity the matrix is hidden and only the voxels with damage variable greater than 0.9 are shown. [Chen et al., 2019b]

5.6.2 Complete formulation for heterogeneous phase-field damage in FFT-based solvers

As presented previously, the phase-field model has two important parameters: the critical energy release rate (G_c) and the regularization length (l_c). G_c is widely recognized as a material damage property, while l_c describes the crack bandwidth (see Fig. 5.6b). The smaller l_c , the narrower the crack band becomes (Fig. 5.9b). If $l_c = 0$, a sharp crack is fully recovered. Recently, there have been discussions in the literature about these parameters.

The implementation of the phase-field model, whether Miehe's or Wu's, requires special attention when dealing with Eq. 5.16a. To highlight the importance of the assumption, as shown in Eq. 5.17a, the complete formulation (as it is presented in Eq. 5.16a) has been implemented into the FFT-solver by Ma et al. [2023a]. It was shown that omitting certain terms in the phase-field equation, when dealing with heterogeneous materials, can result in an abnormal damage diffusion between the different material components.

$$\begin{aligned} &= G_c l_c \Delta d, \quad \text{in the case of homogeneous assumption} \\ \nabla \cdot (G_c l_c \nabla d) &= \nabla (G_c l_c) \cdot \nabla d + G_c l_c \Delta d, \quad \text{in the case of complete assumption} \end{aligned}$$

A selected summary of the results is shown in Fig. 5.9. For all aspects of the numerical implementation, the related article [Ma et al., 2023a] can be referred to. The simulations were

conducted on a two-half-fibers model (Fig. 5.9a) to ensure that the weakest point would be in the center of the unit cell. In this way, the influence of the boundary conditions would not interfere with the final results. There were four main groups of results: the results on the first line show damage profiles along the middle line of the unit cell; those on the second line show the damage field in the unit cell for the simplified formulation; those on the third line show the damage field for the complete formulation; and those on the fourth line show the averaged stress-strain response for both simplified and complete formulations.

It was observed that taking into account all the terms in the formulation preserves the diffusion of matrix damage field in the fiber material and significantly modifies the damage field, especially when l_c is sufficiently high compared to the distance between the fibers (refer to the images in the last row of Fig. 5.9). It was also shown that the influence of l_c on the mechanical response is more significant for heterogeneous materials. Furthermore, the choice of regularization length affects not only the macroscopic mechanical behavior but also the local crack propagation patterns.

5.6.3 Discussion on l_c sensitivity and implementation of the Wu's model

The primary focus of the current section is the relationship between l_c and the predicted mechanical behavior of a material. Initially, l_c was intended to be used as a numerical parameter to describe the crack bandwidth. However, some studies [Nguyen et al., 2016b, Zhang et al., 2017] have found that it can significantly affect the simulated mechanical behavior of materials in certain phase-field models, such as Miehe's phase-field model [Miehe et al., 2010b] which has also been confirmed in the previous section. As a result, this parameter is now commonly treated as a material parameter [Espadas-Escalante et al., 2019, Guillén-Hernández et al., 2019]. In the literature, there are two main approaches to determine the l_c value. One approach involves an analytical calculation of a 1D bar problem with a homogeneous crack phase-field [Nguyen et al., 2016b], while the other involves an inverse analysis of experimental results [Nguyen et al., 2016a]. Although these techniques can yield satisfactory results in some cases, they can also complicate the calculation. Additionally, Mandal et al. [2019] have found that these l_c estimates can sometimes be too large compared to the dimensions of the model, resulting in some unusual phenomena. ***As a result, it can be challenging to select an appropriate l_c that produces both accurate macroscopic responses and local crack patterns for certain phase-field models.***

One of the solutions is to decouple the connection between l_c and mechanical behavior and ensure that l_c only fulfills its original role of describing the degree of crack diffusion. This is one of the main advantages of Wu's phase-field model [Wu and Nguyen, 2018], which introduces traction-separation laws from the cohesive zone model into the phase-field theory to make l_c independent of mechanical response. Mandal et al. [2019] found that Wu's phase-field method exhibits l_c insensitivity when applied to homogeneous materials.

Ma et al. [2023b] has incorporated Wu's phase-field (as presented in Sec. 5.5) into the FFT-solver and investigated its sensitivity when applied to heterogeneous materials. Wu's model introduces a new degradation function to represent non-linearity. This brings about a

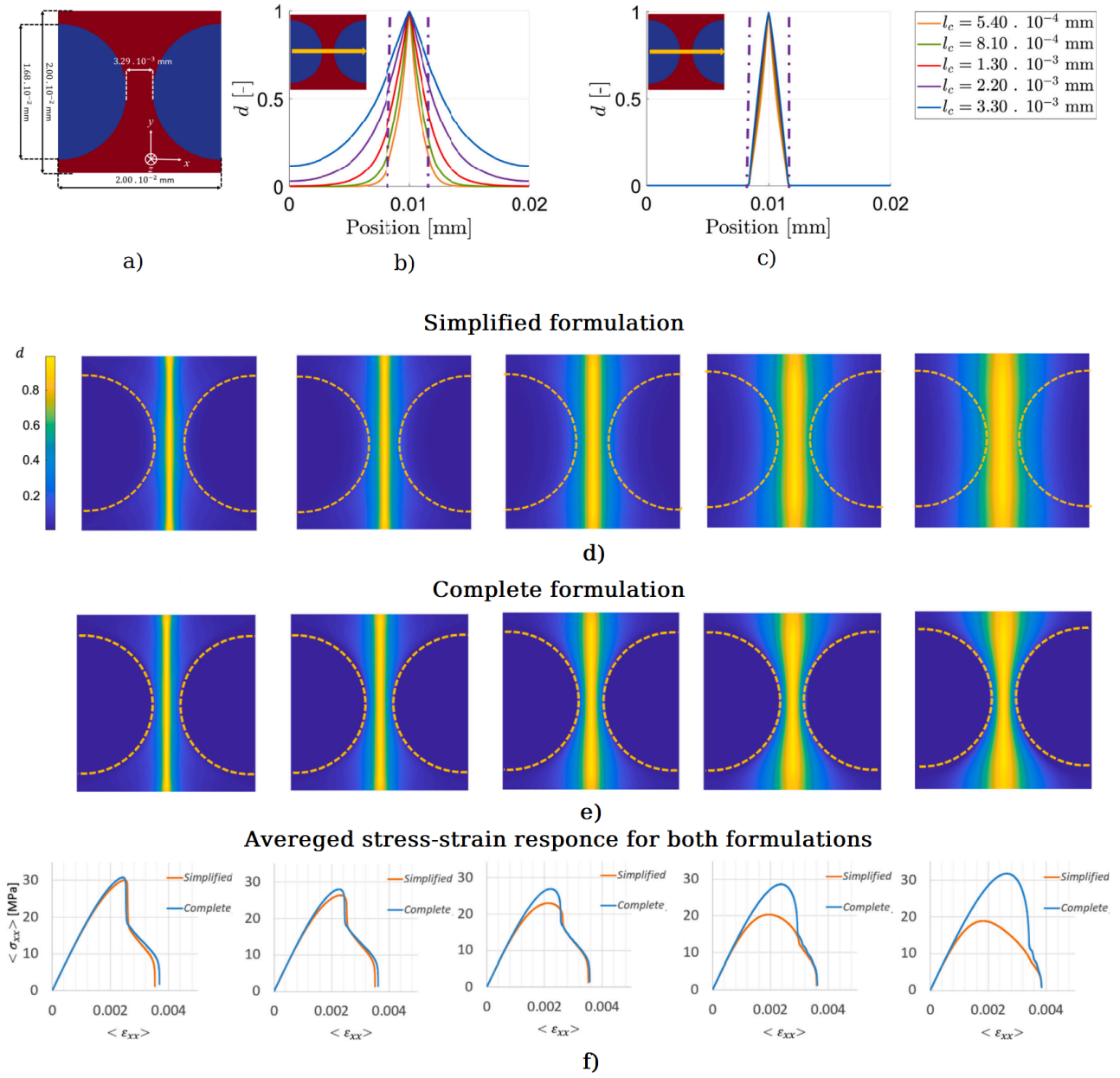


Figure 5.9: Summary of the results presented in [Ma et al., 2023b]: (a) model geometry description; (b) and (c) damage profiles in the middle of the model as function of the l_c ; (d) and (e) damage field for simplified and complete formulations respectively; and (f) comparison of the averaged stress-strain responses for. Remark: l_c values of matrix material were varied.

significant challenge when attempting to solve Wu's model using a fixed-point algorithm. Thus Newton–Raphson method has been updated to solve nonlinear equations. The linearization of the problem and its numerical solution with Conjugate Gradient (CG) solver can be found in the reference article [Ma et al., 2023b] which does not require to introduce a reference material or a polarization term. Ma et al. [2023b] solved the non-local term directly without any definition of the reference material and the polarization term. The main result is presented as follows.

$$\nabla \cdot \left(\frac{2G_c l_c}{\pi} \nabla d \right) = F^{-1} \left(Jk \cdot F \left(\frac{2G_c l_c}{\pi} F^{-1} \left(Jk \hat{d} \right) \right) \right)$$

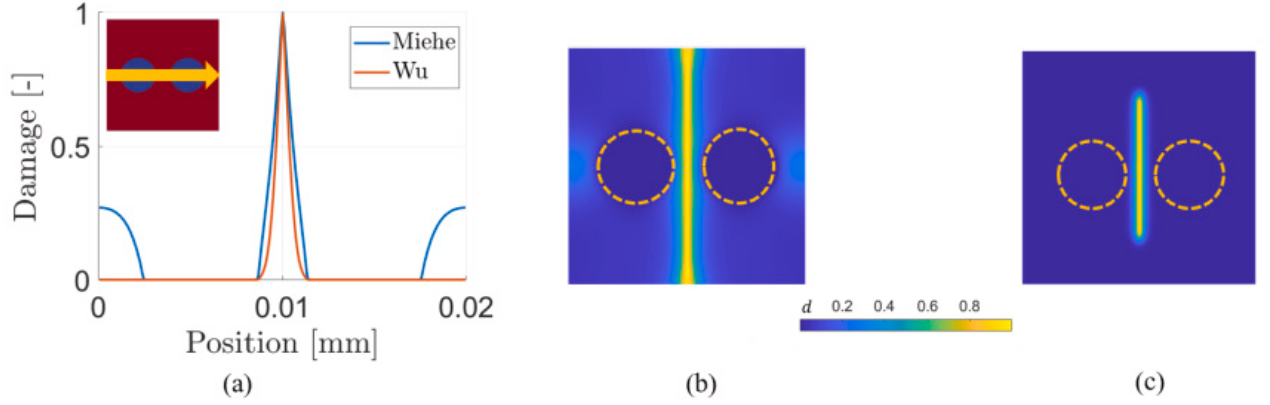


Figure 5.10: Summary of the results presented in [Ma et al., 2023b]: (c) damage profile along the central line for both Miehe's and Wu's models; (a) and (b) damage fields at the final loading increment.

Selected results are shown in Fig. 5.10. We can see that for Miehe's and Wu's models, the complete formulation, as presented in the previous section, is used. It is clearly seen that in Fig. 5.10a, no damage diffusion is observed in the fiber material. One of the main advantages of the Wu's model is that it introduces the threshold condition (term $\frac{1}{2} \frac{\sigma_c^2}{E}$, see Eq 5.14b) above which the damage is equal to zero as can be seen in Fig. 5.10b and c.

5.7 Conclusion

Below, the original contributions about FFT based solvers phase-field model for damage modeling in heterogeneous materials.

- **Implementation of FFT methods and phase-field model for large scale:** This approach uses an FFT solver for elastic and damage modeling based on a variational phase-field approximation for brittle fracture. The method is easily parallelizable, suitable for image-based modeling, and enhanced with a convergence acceleration procedure for improved computational performance. It offers an efficient alternative to standard FEM solvers for phase-field models of brittle fracture, particularly in image-based modeling with a large voxel count.
- **Analysis and optimization of spurious numerical oscillations:** The causes were investigated, and potential solutions were critically compared. The most severe cause, a zig-zag pattern at non-smooth interfaces, led to five times stronger oscillations. A solution was involved using a Discrete Green Operator (DGO). The second cause was a defect in the original FFT method, addressed by employing DGO. The third cause, the hourglass effect, was mitigated by a fully integrated formulation like SF. The Gibbs phenomenon did not affect the numerical oscillations. A combination of Willot's rotated scheme (W-S) and the proposed improved composite voxel technique appears optimal for FFT-based composites homogenization. Future studies could explore damage analysis based on this method.
- **Development of the complete formulation for heterogeneous materials:** The investigation of damage modeling based on non-local phase-field formulation led us to compare two possible formulations of a phase-field model: the simplified and complete formulations. The main difference lies in the omission of a term in the simplified formulation. While equivalent for homogeneous models, they diverge for heterogeneous ones due to varying values. The simplified formulation converges faster, but non-physical damage diffusion occurs in heterogeneous models, affecting local micro-level damage evaluation. Differences in macro-level relations are also observed, especially near interfaces with cracks.
- **Implementation of cohesive-type model:** Wu's phase-field model has been successfully implemented into the FFT-based solver. In Wu's phase-field model, the degradation function is nonlinear, making it challenging to solve Wu's phase-field evolution equation using the FFT solver with a fixed-point algorithm. To overcome this, a new phase-field solver based on the FFT method has been proposed. We took advantage of this new implementation to consider a strong coupling of the phase-field with the strain field to alleviate restrictions on the loading step.

6 .Perspectives

No sensible decision can be made any longer without taking into account not only the world as it is, but the world as it will be.

ISAAC ASIMOV

My research project is aligned with the three following research themes of Institut Mines-Télécom (IMT)¹: "*High-performance materials and eco-materials*" (Industrial transformations), "*Data analytics and Artificial Intelligence*" (Digital transformations), and "*Renewable energy and resources*" (Energy, ecological, and urban transformations). My project is logical continuation of my research activities shown in the previous chapters. Thus, I have gathered all my perspectives into the following two research themes:

1. **Multi-scale numerical modeling of heterogeneous materials** integrating *process-structure-property* paradigm.
2. **Durability of composite and hybrid structures** towards *digital twin*.

Each of these themes has several subjects to investigate. All presented research topics are organized by duration, starting from the short-term and ending with the long-term.

6.1 Multi-scale numerical modeling of heterogeneous materials integrating process-structure-property paradigm

6.1.1 Big picture

We have observed that the manufacturing process of composite structures can induce internal structural changes, such as misaligned reinforcements, thickness variation, and voids. In the previous sections, we have primarily focused on voids, as they are common composite defects, and their influence on mechanical properties depending on their location (intra- or inter-yarns), distribution (clustering or uniformly distributed), size (small or large), and shape (spherical or cigar-like), even with the same content. Some of these effects have been presented in the PhD theses under my co-supervision [Lui, 2017, Parvathaneni, 2020]. These defects are strongly correlated with the microstructure of material and appear at different material scales [Maes et al., 2022]. Hence, multi-scale variability plays a crucial role in non-linear static and fatigue behavior, triggering damage initiation and crack propagation [Cruanes et al., 2022]. Therefore, it is crucial to develop the most realistic material models with high fidelity and computational efficiency. However, there is still a gap between experimental measurements and numerical modeling when attempting to predict elastic, strength, and fatigue properties as well as their dependency on process-induced defects. Proposing a solution to quantify the margin for defect

¹Dilated description can be found on the official web-site of the research areas of the IMT. www.imt.fr/en/research-innovation/research/research-areas/

tolerance specific to loading and providing a process optimization guide are also of high interest to the industry.

Bringing all of these elements together allows us to present a *Big picture* (see Fig. 6.1). The key elements are structured based on material scales: 1) at the micro-scale, we observe variations in the geometries of each phase as well as clustering phenomena; 2) at the meso-scale, we notice different yarns and manufacturing defects such as inter-yarn voids, along with sensors to monitor performance even during the service; 3) at the macro and component-scale, we can discern a variety of geometric features, boundaries, and loading conditions.

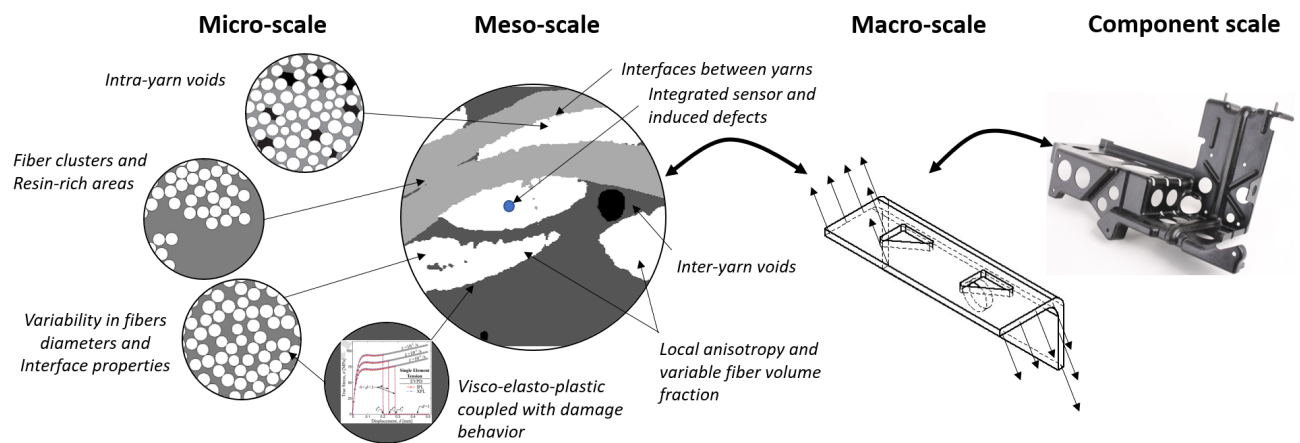


Figure 6.1: *Big picture: heterogeneous structures at different scales including the manufacturing defects and sensors integration.*

Moreover, the *Big Picture* (Fig. 6.1) reveals that we will have a plethora of data generated at different scales. There will be two main sources of data: 1) numerically generated data (results of different simulations, data about numerical micro-structure etc.); 2) experimentally collected data, encompassing static and fatigue mechanical tests, in-situ and ex-situ high-resolution micro-CT images etc. Thus, it is also important to store, share, and analyse such amount of data and leverage the advantages of **new numerical methods integrating artificial intelligence** to explore it to the maximum.

In this topic, the research will address multi-scale problems, focusing specifically on the statistical representation of manufacturing defects and their correlation with damage initiation and propagation across different scales.

6.1.2 Improvement of multi-scale observation techniques (short and mid-term)

The development of a multi-scale methodology should be grounded on a profound understanding of the complex phenomena that occur across different material scales. The quantification of geometrical variability (cross-section, form), distribution (location, clustering), and orientation of the phases of materials (i.e. fibers, matrix, voids, etc.) has a high impact on the prediction of the mechanical properties of new advanced heterogeneous materials. The most detailed and comprehensive information can be extracted from images (2D, 3D) and implemented into numerical material models. Within this research topic, the following subjects will be considered.

Segmentation enriched by the data

The heterogeneity and variability of material properties become crucial for predicting nonlinear behavior. Therefore, it is necessary to have a well-established tool or methodology to convert images into representative geometries for numerical models. As shown in Fig.6.1, we have several phases to identify during the image analysis. In general, we have fibers and matrix material. When we start to consider manufacturing defects, we introduce a third phase representing voids, which has a contrast close to the matrix phase (depending on the resolution of micro-tomography). When we assess the non-linear static and fatigue performance of composites, or attempt to follow the evolution of cracks in-situ or ex-situ, we would face additional issue in properly detecting all cracks.

In the literature, the following methods are considered for experimental data segmentation and analysis. [Sosa-Rey et al. \[2022\]](#) have proposed a smart segmentation of the three-phase materials using Machine Learning (ML) methods. Examples of such applications to textile composites can be found in [\[Mendoza et al., 2021\]](#) and [\[Pannier et al., 2023\]](#), where the authors have applied Convolutional Neural Network (CNN) for fast detection and reconstruction of the meso-scale structure of 3D textile-reinforced composite materials.

In the literature, the authors applied improvements either at the micro-scale, focusing on a detailed description of material phases and manufacturing defects, or directly at the meso-scale, focusing on textile meso-structure. It was also shown that the quality of segmentation may alter depending on the methodology and deep-learning based method will detect the actual form of defects [\[Upadhyay et al., 2024\]](#). However, the fact that the meso-scale and micro-scale voids are strongly correlated we would need enriched methodology to study coupling between the two scales. Thus, this is considered the main challenge in this research topic.

Realistic boundary conditions and embedded scans

For multi-scale modeling, various types of boundary conditions are utilized (such as stress uniform, displacement uniform, periodic, mixed). In the case of solving damage modeling for isotropic homogeneous materials [\[Chen et al., 2019b\]](#), the boundary conditions are not problematic. However, when focusing on realistic textile composites which are anisotropic heterogeneous materials [\[Chen et al., 2019c\]](#), it becomes evident that periodicity poses a significant limitation for numerical solutions.

The periodic boundary conditions may lead to artificial stress concentrations when applied to real images (as observed for 3D interlocks, as mentioned in [\[Chen et al., 2019c\]](#), or in [\[Garoz et al., 2019\]](#)). Thus, the main idea is to find a compromise between the size of the Region of Interest and its influence on the boundary effects. We have studied various potential solutions for the boundary layers (referred to as "margins"), including varying the size or rigidity of such artificially added materials. The most effective solution involved a technique to extend the boundary voxels to a certain distance (approximately a quarter of the RVE size). However, this technique is manual and highly dependent on the current textile meso-structure. Therefore, one of the solutions could be employing Machine Learning for the expansion of an RVE. The concept involves using such techniques to construct a boundary layer for better representation of realistic microstructures, considering smoothing and extension effects [\[Karamov et al., 2021\]](#).

A discussion about the quality of segmented images should also include the resolution and the capacity to determine the entire Representative Volume Element/Unit Cell (RVE/RUC) for textile composites. The main challenge is that focusing on local details may compromise the representativeness of scanned volume. One solution is to combine different levels of observation to construct a multi-level embedded model, enabling the study of local mechanisms and their interaction with the microstructure.

Research Environment and funding

The realization of micro-tomography observations can be conducted at the ISIS4D platform (IMT Nord Europe is a founding member of the platform). Collaboration with the Center for Numerical Systems (J. Mennesson) (on campus) will be prioritized for Deep Learning applications in segmentation and image processing. At the international level, discussions have been initiated with colleagues from the University of Bath (Y. Chen) and KU Leuven (S. Lomov, J. Ivens).

6.1.3 Harmfulness and tolerance of process induced defects during LCM (mid-term)

Completing the integrated chain from the manufacturing to the mechanical performance of a final part is a challenging task. In this chain, particular attention is paid to predicting the influence of defects on the final mechanical properties of composites manufactured by LCM. Moreover, recent trends indicate that composites (whether thermosets or thermoplastics) manufactured by LCM may still suffer from the presence of defects [Arwood et al., 2023].

The primary objective of this topic is to continue the research already presented in the summary and further improve the modeling under more realistic boundary conditions. In Chapter 4, only relatively simple uniaxial tension loading cases were considered under static and fatigue conditions. In contrast, the structure in service will be systematically subjected to complex loading (shear, bending, compression) and the corresponding complex local stress states, which in turn will lead to more complex nonlinear phenomena at the material level. This will require in-depth characterization studies of degradation mechanisms observed within the material. Another challenge will be to model materials or structures subjected to extreme conditions (high-pressure fatigue, cryogenic temperatures, etc.).

All these mentioned aspects require a synergy between **direct experimental observations** (utilizing various mechanical testing with in-situ image observations) and **advanced numerical techniques** for computational efficiency. This includes accelerated solvers that can be parallelized for heavy computations (e.g., Fast Fourier Transform-based solvers [Chen et al., 2019b]) and deep learning methods for strength prediction [Shinde et al., 2023] at the finer micro-scale. In this topic the three following subjects should be considered.

Geometry generation

The direction of the research in this section is continuation of the research presented in the Section 4 and mainly has been pursued in two PhD theses [Lui, 2017, Parvathaneni, 2020]. There are several directions to improve the generator of a numerical microstructure. The first

direction is linked to a mathematical algorithm improvement of the numerical microstructure generators.

For our multi-scale problem, we have distinguished two principal material scales that should be considered, namely micro- and meso-scales (as presented in the summary). For improvements at the micro-scale, extending to a 3D case should be formulated. While the statistical representation has been well presented, further investigation into their correlations is still needed. For instance, the appearance of voids in certain regions was treated only in terms of fiber volume fraction, and the shape of the yarns and the location of voids were not taken into account. The shape of the micro-voids are rather sharp due to the methodology used, which may introduce not-realistic stress concentrations in the modeling. Some new techniques are under development to address this issue (such as level-set smoothing functions or reduction of properties without physical modeling of defects). At the meso-scale, the structure tensor has been used for segmentation and numerical model definition. These techniques allow to generate numerical microstructures (both 2D and 3D). Generative adversarial neural networks have gained popularity [Henkes and Wessels, 2022]. The third direction explores the combination of physical based and deep learning methods focused on the segmentation of 3D interlock composites meso-scale model generation [Mendoza et al., 2021].

Regardless of the technique used for numerical model creation, the correlation between the meso-structure and inter-yarn voids has been established in the summary using random voxel selection or randomly placed voids of spherical shape. However, in reality, the locations and shapes of voids should be governed by the meso-structure. Therefore, this subject will be considered as the main current challenge in this research subject.

Non-linear modeling

For this part of the project, I will focus on an extension of the nonlinear modeling, including viscoelastic and viscoplastic material behaviors coupled with damage (as discussed in Chapter 4, Section 4.3.3, and Chapter 5). The main goal is to further model nonlinear phenomena such as the non-linear behavior of the polymer matrix coupled with debonding, decohesion, and matrix cracking in textile-reinforced composites. Damage mechanisms will be modeled using the theory of non-local damage based on phase-field theory. This theory is currently being adopted in many applications, particularly in predicting crack mechanisms with a complex behavior under static and dynamic loads. Based on the variational formulation of fracture mechanics, it can predict bifurcation, coalescence, and propagation of multiple cracks in heterogeneous and anisotropic media (PostDoc Y. Chen, Th. X. Ma 2020-2023). It represents a very promising approach for estimating the mechanical performance.

Acceleration techniques

Any multi-scale modeling technique requires solvers at a minimum of two material scales. In the summary, FEM and FFT solvers were utilized. Due to the intrinsic periodicity of the FFT method, it is more suitable for the smaller scale of material (micro-scale in the case of textiles), while FEM solvers are more appropriate for realistic macro-structure descriptions.

In the summary, an original approach based on FFT has been presented, particularly for mod-

eling damage using a phase field model. In this subject, one of the advancements has been the integration of a phase field model into the FFT-based approach, where the influence of regularization length is mitigated and the evolution equation of the phase field is nonlinear for heterogeneous materials (PostDoc Chen, 2019; Th. X. Ma, 2020-2023). We have seen that FFT methods can effectively predict the mechanical properties of composite materials at micro-scale, from real images obtained through tomography (Chapter 5.3.3) and have several substantial issues with macro-scale models due to intrinsic periodicity requirements. Thus, by combining both techniques – FFT at the micro-scale and FEM at the macro-scale – we can construct an effective multi-scale numerical strategy.

The second direction involves the total or partial replacement of conventional numerical methods (FEM, FFT) with approaches derived from artificial intelligence, particularly deep neural networks. Even with the most efficient numerical method, if we do not preserve the knowledge gained from simulations, we would need to rerun the simulation each time the loading conditions change. The primary challenge is to remove the partial redundancy of certain numerical calculations, such as multi-scale simulations, to reduce computation times. This strategy entails generating data using a conventional approach (FEM/FFT) and then learning from this data to construct a Reduced Order Model (ROM). The ROM developed at CERI MP (by M. SHAKOOR) consists of a specific type of neural network called an autoencoder for data compression, and a recurrent neural network for predictions. This model was successfully tested for crack growth prediction (PostDoc K. Shinde, 2021-2022) and published in [Shinde et al., 2023].

Research environment and funding

All manufacturing activities and process simulations of composites will be conducted in collaboration with researchers in our Center which has an excellent composites manufacturing facilities such as POPCOM platform. As for manufacturing textile fabrics with different architectures, we continue collaboration with the research team in GEMTEX (ENSAIT) (D. Soulat, A. Rached, F. Boussu). Regular calls for thesis projects in the Hauts-de-France region have also been identified and would be considered as potential funding opportunities to further explore and advance this research topic.

For future developments, ANR generic calls have been identified as the most suitable financial support program. Research teams from UML at Lille Technical University (T. Kanit) and the Department of Materials, Textiles, and Chemical Engineering at the Faculty of Engineering and Architecture of Ghent University (F.A. Gilabert) are involved.

FFT solvers were developed in collaboration with CEA Saclay (L. Gélébart) and the University of Bath (Y. Chen). The model based on autoencoder was developed during the DEEPMECH project (coordinated by M. Shakoor), funded by IMT Nord Europe.

6.2 Durability of composite and hybrid structures

To address the non-linear modeling of material behavior, including the in-service performance of the structure, I have investigated not only purely heterogeneous materials [Lui, 2017, Parvathaneni, 2020] but also metallic materials for numerical method validation [Vasseur, 2020]. For instance, in the case of new model development within the FFT solver [Chen et al., 2019b], several standard fracture mechanics tests were modeled to validate the numerical results. Another example is the PhD thesis of Vasseur [2020], in which the coupling between ultrasonic wave interaction with defects [Vasseur et al., 2023] in metallic parts and its correlation with fatigue crack propagation [Vasseur et al., 2020] have been studied. Additionally, I would like to highlight that the aforementioned works have provided significant motivation for both my current projects and those in the mid-term. It has been reported that even in isotropic materials with controlled defects in the form of hole clusters, the fatigue crack initiation and propagation process is highly complex. This complexity arises from several main factors, including multiple initiation sites of fatigue cracks, multi-mode crack propagation, as well as bifurcation and deviation of cracks.

6.2.1 Modeling of hybrid structures for hydrogen transport and storage (mid- and long-term)

Current trends in transport industry show the gradual shift away from fossil fuels. This necessitates the exploration of alternative clean energy sources, such as hydrogen emerging as a prominent one. Several main challenges are related to this shift. The first one is the storage and transport, and the second one is the distribution of hydrogen. The storage of hydrogen requires the development of high-pressure H₂ tanks made of composite materials possessing high specific strength. On the other hand, the distribution would be based on the utilization of the current stationary infrastructure (pipeline network and connections). Taking into account all these industrial challenges, the following two research topics will be investigated.

Modeling of composite materials for hydrogen storage tanks

Like textile-reinforced composites, filament-wound composites will have manufacturing defects. However, the nature and quantity of these defects differ. It is known that filament winding is a process that may result in relatively high void content in a final composite part. Thus, there are notable challenges to address: the heterogeneous structure and multi-scale behavior inherent in composites, as discussed in the previous chapters. These challenges become more pronounced when dealing with hybrid structures like polymer liner and composite skeleton, which introduce interface issues, variations in material behavior, and manufacturing defects, thereby compromising the accuracy of modeling efforts. Furthermore, the incorporation of sensors (such as optical sensors, piezoelectric devices, etc.) for structural health monitoring adds complexity to the manufacturing process and may induce microstructural modifications [Air et al., 2023].

In addition to common issues found in textile-reinforced composites, filament-wound structures have a specific meso-structure of the plies. The helical ply structure is very similar to braided composites. However, many standard approaches simplify this structure as a unidirectional ply.

Consequently, progressive damage modeling and burst pressure prediction remain challenging tasks. Moreover, the sensor integration is tricky and may modify the material structure and induce additional defects ("fish eye", voids etc.).

High-fidelity multi-scale modeling is crucial for developing effective numerical modeling strategies for static and cyclic loading. In conjunction with the manufacturing process and multi-scale characterization (microscopy and micro-tomography), this necessitates the establishment of well-defined experimental strategies. This includes investigating the representativeness of flat and/or cylindrical hybrid specimens, with possible integration of optical sensors using Fiber Bragg Gratings (FBG) and/or piezoelectric sensors (PZT), to replicate final curved cylindrical or spherical shapes of hydrogen tanks.

Modeling of hybrid strictures for stationary infrastructure for hydrogen distribution

A new research topic has recently been initiated at the Center for Materials and Processes at IMT Nord Europe in collaboration with CETIM (Senlis) and CETIM (Nantes). This topic focuses on the effects of hydrogen embrittlement (HE) on the mechanical performance of gas transport infrastructure in general for which hybrid heterogeneous materials may be used.

One of the main industrial challenges is that the effect of HE is poorly quantified by industrial norms of design for pressure vessels. Currently, there are only two norms (Article KD-10 of the American standard and a Japanese standard). Both norms treat the fatigue life prediction based on the Fracture Mechanics methods using simplified geometries. The lack of knowledge motivated industrial partners to find a solution for more complex geometries (welds, etc.).

Recent significant advancements in understanding HE mechanisms [Lynch, 2011] and numerical methods [Martínez-Pañeda et al., 2016] offer wide possibilities for optimal and safe design of hydrogen storage vessels. Studying hydrogen-induced degradation requires considering various influencing factors: the presence of defects and the environment (H concentration, static or dynamic mechanical loading)[Martin et al., 2019]. Thus, several modeling and numerical simulation studies have been conducted in recent years to better understand degradation mechanisms, particularly under static mechanical loadings: strain gradient plasticity model, cohesive zone model, phase-field modeling. Models have also been developed for fatigue loading, where hydrogen can influence the cyclic behavior [Hosseini et al., 2021], reduce the number of cycles required for crack initiation [Esaklul et al., 1983], and particularly accelerate the crack propagation [Shinko et al., 2021], thus significantly reducing the structure's lifetime. This influence depends, among other things, on the H concentration in the material, its susceptibility to HE, H diffusivity, and the amplitude and frequency of loading.

These models have often been experimentally validated by tests on standardized specimens. Their application to gas transport infrastructure is still very limited and would require implementing shell-type Finite Element (FE) models. Several studies have addressed this issue, particularly for the phase-field model [Proserpio et al., 2021]. However, coupling with the HE phenomenon has never been considered. Furthermore, the recent success of the phase-field-based method for predicting static rupture assisted by H₂ remains under-exploited in the literature [Golahmar et al., 2022].

Research environment and funding.

Further research will focus on investigating the influence of microstructural variations due to process-induced defects on the mechanical properties such as elasticity, strength, and fatigue. These are the main objectives of the new PhD thesis, which is co-supervised with KU Leuven as part of the Horizon Europe project ECOHYDRO (2023-2027, coordinated by prof. C.-H. Park).

These topics are currently being investigated in the research program of the PhD thesis (Th. Shaymaa MERHEB, under supervision of prof. S. Chaki), co-financed by the Hauts-de-France region and CETIM under an agreement for a joint laboratory for pressure equipment between IMT Nord Europe and CETIM in Senlis. The ANR program for industrial chairs has been identified for this topic. To conduct all experimental investigations necessary to validate the numerical models, the necessary experimental facilities are available via a joint laboratory with CETIM (Senlis) (LATEP) and CETIM (Nates) for testing gaseous hydrogen storage tanks and hybrid materials under hydrogen environment.

6.2.2 Digital twin for composite pressure vessels for hydrogen storage and transportation (long term)

The Structural Health Monitoring (SHM) of composite materials is one of the major industrial challenges for coming decades. Carbon fiber reinforced composites are widely used in automotive and transport industries. To monitor the state of the degradation of the materials, numerous non-destructive testing methods can be used. A particularly interesting way to monitor the evolution of material health is to capture the acoustic waves generated by the rupture of the composite's microscopic constituents. The number, intensity, and shape of the associated signals are indicative of the evolution of damage in the material [Harizi et al., 2022].

Digital twin for SHM

The research over the past 20 years on the structural health monitoring through acoustic emissions has focused on diagnosis, with some success but also significant limitations. In particular, the acoustic signature of a type of damage depends on the environment, and transitioning from laboratory specimens to real structures is challenging. Prognosis, on the other hand, requires the use of a model to simulate the effect of identified defects on mechanical strength. This field is much less developed than diagnosis, and the industry currently relies on empirical approaches associated with significant safety factors to fill this methodological gap, thereby increasing the weight of composite structures.

On the other hand, digital twin technologies and artificial intelligence have undergone a revolution in recent years. These approaches promise to compensate for the lack of understanding of the physical phenomena involved in mechanical systems by assimilating rich data during the service life of an industrial component. Typically, data from sensors are continuously used to enhance the predictive capabilities of a physical model by adjusting model parameters and/or correcting uncertain parts of the model using neural networks [Alvarez et al., 2021, Pulkathodi et al., 2023]. This is now achievable in real-time thanks to the existence of powerful model reduction methods and software environments facilitating access to artificial intelligence

technologies (libraries for calculations on differentiable graphs, e.g., PyTorch and TensorFlow). Two following subjects will be considered in this research topic.

This approach will model acoustic emission events for Structural Health Monitoring. The approach chosen is that of a real-time test-analysis dialogue (i.e., digital twin) using data assimilation and machine learning methods [Pulikkathodi et al., 2023]. The focus will be placed on both an experimental and a numerical component, with experiments being conducted to feed the models and demonstrate the capabilities of the digital twin strategy. A modeling approach will be established, that couples physical modeling with artificial intelligence to simulate the evolution of damage mechanisms in laminated composite structures and their associated acoustic emissions. This model will be fed by experimental data and validated for lab-scale prototypes (e.g. flat and/or cylindrical specimens with holes).

Digital twin for fatigue life prediction

The demand for digital twin for components and structures with complex geometrical shapes (such as pressure vessels, railway structures, wind turbine blades) subjected to various types of static and/or dynamic loads, including multi-physics conditions (stress, temperature), is high in the industry. This is because the primary purpose of digital twin is to provide numerical tools capable of assessing structural integrity and predicting their long-term, in-situ, and real-time behaviors.

The original digital twin for connected hydrogen storage tanks will integrate the complete mechanical fields (strains, temperatures, etc.) related to the conditions to which the tanks are subjected, and it should also provide the estimation of fatigue life based on these fields. Original hybrid technologies will be considered by combining conventional fatigue life prediction methods from the mechanics with new paradigms derived from artificial intelligence [Shinde et al., 2023].

A general architecture of the developed digital twin is presented in Figure 6.2 for monitoring the state of a pressure vessel. This approach combines a white-box model based on finite element (FE) simulation (adhering to international norms and design guides for pressure vessels) and a Machine Learning/ Deep Learning model. The developed digital twin hybridizes numerical models, providing an exact replica of the physical pressure vessel.

This combination ensures accuracy through the physical models, reactivity, and adaptability through the Machine Learning models, as well as the ability to generate a sufficiently large and reliable database for training. Firstly, we will elucidate the physical models used, which encompass stress and damage calculations by FE. Secondly, we will thoroughly apply Machine Learning/ Deep Learning algorithms for full field reconstruction (stress, deformation, etc.).

Research environment and funding

This part of the project is subscribed to the *"Computational Mechanics and Modeling of Materials and Processes"* research theme and the *"Digital Twin"* research theme of CERI MP. It also involves collaboration between different research teams.

The developed architecture of digital twin has been proposed within the JUNAP project fi-

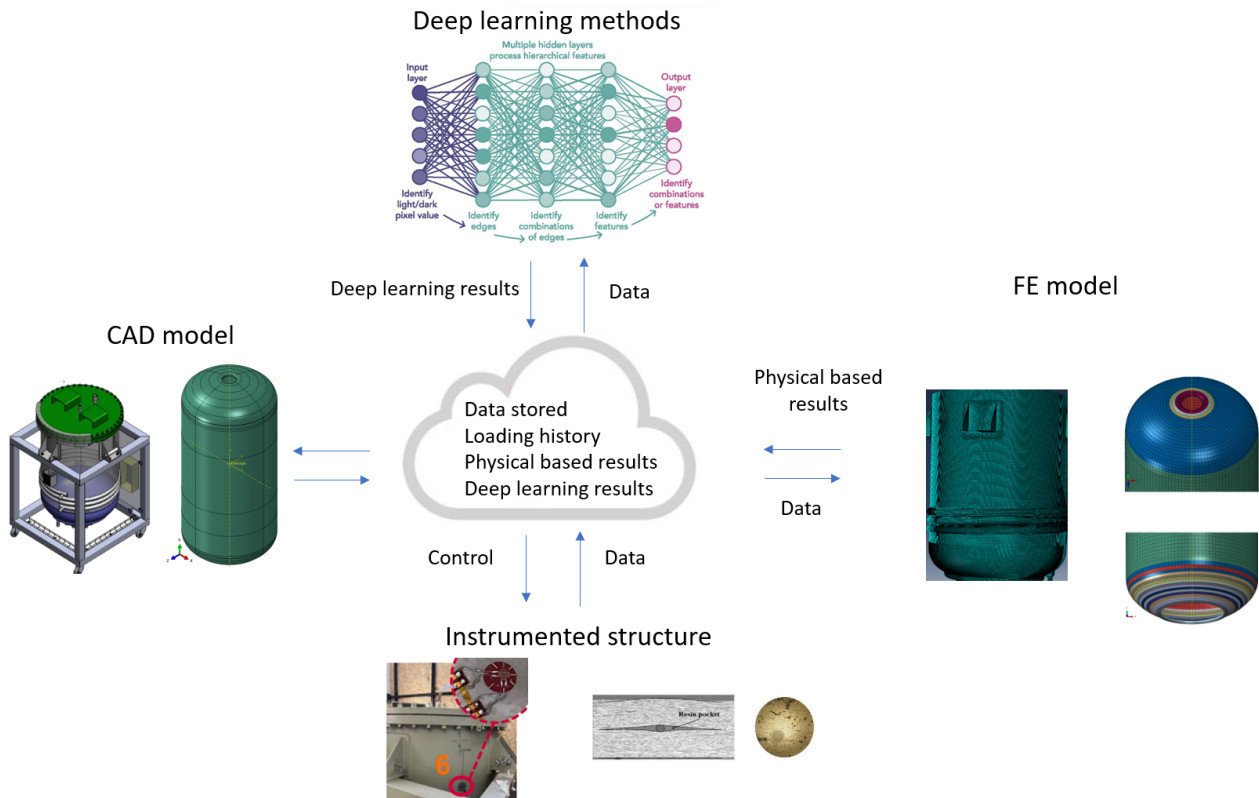


Figure 6.2: Architecture of the digital twin for the pressure vessel.

nanced by the Hauts-de-France region, supported in parallel by an industrial thesis project (Th. I. Khaled 2022-2025) financed by CETIM under an agreement for a joint laboratory for pressure equipment between IMT Nord Europe and CETIM (Senlis).

Coupling damage mechanics and acoustics emission will be studied ongoing PhD thesis (M. Chehazi, 2023-2026, financed by Carnot M.I.N.E.S) within collaboration with research team from MINES ParisTech (P. Kerfriden). Digital twin development for fatigue life prediction of the filament-wound composite hydrogen storage tank is the subject of a future PhD thesis financed by the ECOHYDRO Horizon Europe project (coordinated by C.H. Park). Additionally, within the CPER RITMEA project (coordinated by S. Chaki), a postdoctoral fellow will be financed to investigate the acoustic emission of the composite storage tanks to provide necessary data for model validation.

Bibliography

- AMITEX-FFTP. http://www.maisondelasimulation.fr/projects/amtex/general/_build/html/.
- FFTW. <http://www.fftw.org>.
- R.F. Agyei and M.D. Sangid. A supervised iterative approach to 3d microstructure reconstruction from acquired tomographic data of heterogeneous fibrous systems. *Composite Structures*, 206:234–246, 2018.
- A. Air, M. Shamsuddoha, and B. Gangadhara Prusty. A review of Type V composite pressure vessels and automated fibre placement based manufacturing. *Composites Part B: Engineering*, 253:110573, March 2023. ISSN 1359-8368. doi: 10.1016/j.compositesb.2023.110573.
- R.K. Abu Al-Rub and G.Z. Voyiadjis. On the coupling of anisotropic damage and plasticity models for ductile materials. *International Journal of Solids and Structures*, 40:2611–2643, 2003.
- P. Pereira Alvarez, P. Kerfriden, D. Ryckelynck, and V. Robin. Real-time data assimilation in welding operations using thermal imaging and accelerated high-fidelity digital twinning. *Mathematics*, 9(18):2263, 2021.
- Z. Arwood, D.S. Cousins, S. Young, A.P. Stebner, and D. Penumadu. Infusible thermoplastic composites for wind turbine blade manufacturing: Static characterization of thermoplastic laminates under ambient conditions. *Composites Part C: Open Access*, 11:100365, July 2023. ISSN 2666-6820. doi: 10.1016/j.jcomc.2023.100365.
- T. Baranowski, D. Dobrovolskij, K. Dremel, A. Hölzing, G. Lohfink, K. Schladitz, and S. Zabler. Local fiber orientation from x-ray region-of-interest computed tomography of large fiber reinforced composite components. *Composites Science and Technology*, 183:107786, 2019.
- E.J. Barbero, G.F. Abdelal, and A. Caceres. A micromechanics approach for damage modeling of polymer matrix composites. *Composite Structures*, 67:427–436, 2005.
- Bazant and Oh(1983). Crack band theory for fracture of concrete. *Mater Struct*, 16:155–177, 1983.
- A. Bensoussan, J.-L. Lions, and G. Papanicolaou. *Asymptotic analysis for periodic structures*, volume 374. American Mathematical Soc., 2011.
- S. Berbenni, V. Taupin, K.S. Djaka, and C. Fressengeas. A numerical spectral approach for solving elasto-static field dislocation and g-disclination mechanics. *International Journal of Solids and Structures*, 51(23-24): 4157–4175, 11 2014. ISSN 00207683. doi: 10.1016/j.ijsolstr.2014.08.009.
- B. Bourdin, G.A. Francfort, and J.-J. Marigo. Numerical experiments in revisited brittle fracture. *Journal of the Mechanics and Physics of Solids*, 48(4):797–826, 2000. ISSN 0022-5096. URL [https://doi.org/10.1016/S0022-5096\(99\)00028-9](https://doi.org/10.1016/S0022-5096(99)00028-9).
- B. Bourdin, G.A. Francfort, and J.-J. Marigo. The variational approach to fracture. *Journal of Elasticity 2008 91:1*, 91:5–148, 3 2008. ISSN 1573-2681. doi: 10.1007/S10659-007-9107-3.
- S. Brisard and L. Dormieux. FFT-based methods for the mechanics of composites: A general variational framework. *Computational Materials Science*, 49(3):663–671, 2010. ISSN 09270256. doi: 10.1016/j.commatsci.2010.06.009.
- C.M. Brown, W. Dreyer, and W.H. Müller. Discrete fourier transforms and their application to stress-strain problems in composite mechanics: A convergence study. *Proceedings of the Royal Society A: Mathematical, Physical and Engineering Sciences*, 458(2024):1967–1987, 8 2002. ISSN 13645021. doi: 10.1098/rspa.2001.0955.
- V.A. Buryachenko, N.J. Pagano, R.Y. Kim, and J.E. Spowart. Quantitative description and numerical simulation of random microstructures of composites and their effective elastic moduli. *International Journal of Solids and Structures*, 40(1):47–72, 2003. ISSN 0020-7683. doi: [https://doi.org/10.1016/S0020-7683\(02\)00462-6](https://doi.org/10.1016/S0020-7683(02)00462-6). URL <https://www.sciencedirect.com/science/article/pii/S0020768302004626>.
- K.J. Cain, G. Glinka, and A. Plumtree. Cyclic damage characterization of an off-axis unidirectional graphite bismaleimide composite. *Canadian Metallurgical Quarterly*, 45:433–440, 2006.
- C.C. Chamis. Mechanics of composite materials: past, present, and future. *J Compos Technol Res ASTM*, 11: 3–14, 1989.
- R. Charière, A. Marano, and L. Gélébart. Use of composite voxels in FFT based elastic simulations of hollow glass microspheres/polypropylene composites. *International Journal of Solids and Structures*, 182-183:1–14, 1 2020. ISSN 00207683. doi: 10.1016/j.ijsolstr.2019.08.002.
- D. Chen, K. Arakawa, and C. Xu. Reduction of void content of vacuum-assisted resin transfer molded composites by infusion pressure control. *Polymer Composites*, 36(9):1629–1637, 2015. ISSN 1548-0569. doi: 10.1002/pc.23071. URL <https://onlinelibrary.wiley.com/doi/abs/10.1002/pc.23071>. eprint: <https://onlinelibrary.wiley.com/doi/pdf/10.1002/pc.23071>.

- J.F. Chen, E.V. Morozov, and K. Shankar. A combined elastoplastic damage model for progressive failure analysis of composite materials and structures. *Composite Structures*, 94(12):3478–3489, 2012. ISSN 0263-8223. doi: <https://doi.org/10.1016/j.compstruct.2012.04.021>.
- Y. Chen, D. Vasiukov, L. Gélébart, and C.H. Park. Influence of voids presence on mechanical properties of 3d textile composites. In *13th International Conference on Textile Composites (TEXCOMP-13)*, volume 406 of *IOP Conf. Series: Materials Science and Engineering*. IOP Publishing, Nov 2018.
- Y. Chen, L. Gélébart, C. Chateau, M. Bornert, C. Sauder, and A. King. Analysis of the damage initiation in a SiC/SiC composite tube from a direct comparison between large-scale numerical simulation and synchrotron X-ray micro-computed tomography. *International Journal of Solids and Structures*, 161:111–126, 2019a. ISSN 00207683. doi: 10.1016/j.ijsolstr.2018.11.009.
- Y. Chen, D. Vasiukov, L. Gélébart, and C.H. Park. A FFT solver for variational phase-field modeling of brittle fracture. *Computer Methods in Applied Mechanics and Engineering*, 349, 2019b. ISSN 00457825. doi: 10.1016/j.cma.2019.02.017.
- Y. Chen, D. Vasiukov, L. Gélébart, and C.H. Park. Fast Fourier transform solver for damage modeling of composite materials. *JMST Advances*, 1(1):49–55, June 2019c. ISSN 2524-7913. doi: 10.1007/s42791-019-0004-2. URL <https://doi.org/10.1007/s42791-019-0004-2>.
- J. P. Chiverton, A. Kao, M. Roldo, and G. Tozzi. Automatic diameter and orientation distribution determination of fibrous materials in micro x-ray ct imaging data. *Journal of microscopy*, 272(3):180–195, 2018.
- C.L. Chow and T.J. Lu. On evolution laws of anisotropic damage. *Engineering Fracture Mechanics*, 34:679–701, 1989.
- C.L. Chow and T.J. Lu. An analytical and experimental study of mixed-mode ductile fracture under non-proportional loading. *International Journal of Damage Mechanics*, 1:191–236, 1992. doi: doi.org/10.1177/105678959200100203.
- Richard M Christensen. The World Wide Failure Exercise II Examination of Results. *Journal of Reinforced Plastics and Composites*, 32(21):1668–1672, November 2013. ISSN 0731-6844. doi: 10.1177/0731684413498634. URL <https://doi.org/10.1177/0731684413498634>. Publisher: SAGE Publications Ltd STM.
- C. Cruanes, K. K. Parvathaneni, D. Vasiukov, and C. H. Park. Investigation of fatigue behavior of three dimensional interlock composites by time-lapse micro-computed tomography. *Journal of Composites Science*, 6(1), 2022. ISSN 2504-477X. doi: 10.3390/jcs6010014. URL <https://www.mdpi.com/2504-477X/6/1/14>.
- R. de Borst and C. V. Verhoosel. Damage, Material Instabilities, and Failure. In *Encyclopedia of Computational Mechanics Second Edition*, pages 1–50. John Wiley & Sons, Ltd, 2017. ISBN 978-1-119-17681-7. doi: 10.1002/9781119176817.ecm2035.
- R. de Borst and C.V. Verhoosel. Gradient damage vs phase-field approaches for fracture: Similarities and differences. *Computer Methods in Applied Mechanics and Engineering*, 312:78–94, 2016. ISSN 0045-7825. doi: <https://doi.org/10.1016/j.cma.2016.05.015>. Phase Field Approaches to Fracture.
- R. de Borst, M.A. Crisfield, J.J.C. Remmers, and C.V. Verhoosel. *Non-Linear Finite Element Analysis of Solids and Structures*. John Wiley and Sons, 2012. ISBN 9780470666449. doi: 10.1002/9781118375938.
- K.S. Djaka, A. Villani, V. Taupin, L. Capolungo, and S. Berbenni. Field Dislocation Mechanics for heterogeneous elastic materials: A numerical spectral approach. *Computer Methods in Applied Mechanics and Engineering*, 315:921–942, 3 2017. ISSN 00457825. doi: 10.1016/j.cma.2016.11.036.
- A. Doitrand, C. Fagiano, F.X. Irisarri, and M. Hirsekorn. Comparison between voxel and consistent meso-scale models of woven composites. *Composites Part A: Applied Science and Manufacturing*, 73:143–154, 2015. ISSN 1359835X. doi: 10.1016/j.compositesa.2015.02.022.
- B. Drach, A. Drach, and I. Tsukrov. Characterization and statistical modeling of irregular porosity in carbon/carbon composites based on X-ray microtomography data. *ZAMM - Journal of Applied Mathematics and Mechanics / Zeitschrift für Angewandte Mathematik und Mechanik*, 93(5):346–366, 2013. ISSN 1521-4001. doi: 10.1002/zamm.201100190. eprint: <https://onlinelibrary.wiley.com/doi/pdf/10.1002/zamm.201100190>.
- W. Dreyer, W.H. Müller, and J. Olschewski. Approximate analytical 2D-solution for the stresses and strains in eigenstrained cubic materials. *Acta Mechanica*, 136(3):171–192, 1999. ISSN 00015970. doi: 10.1007/BF01179256.
- D. Durville. Modélisation par éléments finis du comportement mécanique de structures textiles: de la fibre au tissu. *Revue Européenne des Eléments*, 11(2-4):463–477, 2002.

- P. Eisenlohr, M. Diehl, R.A. Lebensohn, and F. Roters. A spectral method solution to crystal elastoviscoplasticity at finite strains. *International Journal of Plasticity*, 46:37–53, 2013. ISSN 0749-6419. doi: <https://doi.org/10.1016/j.ijplas.2012.09.012>. Microstructure-based Models of Plastic Deformation.
- E.N. Eliopoulos and T.P. Philippidis. A progressive damage simulation algorithm for gfrp composites under cyclic loading. part ii: Fe implementation and model validation. *Composites Science and Technology*, 71: 750–757, 2011.
- M.R. Erdata Nasution, N. Watanabe, A. Kondo, and A. Yudhanto. Thermomechanical properties and stress analysis of 3-d textile composites by asymptotic expansion homogenization method. *Composites Part B: Engineering*, 60:378–391, 2014. ISSN 1359-8368. doi: <https://doi.org/10.1016/j.compositesb.2013.12.038>. URL <https://www.sciencedirect.com/science/article/pii/S1359836813007683>.
- K.A. Esaklul, S. Jones, T. Brown, et al. Diffusion and stress relaxation during hydrogen embrittlement of titanium. *Scripta Metallurgica*, 17(1):75–78, 1983. doi: 10.1016/0036-9748(83)90457-X.
- J.D. Eshelby. The determination of the elastic field of an ellipsoidal inclusion, and related problems. *Proceedings of the Royal Society of London. Series A. Mathematical and Physical Sciences*, 241(1226):376–396, 1957. doi: 10.1098/rspa.1957.0133. URL <https://royalsocietypublishing.org/doi/10.1098/rspa.1957.0133>. Publisher: Royal Society.
- J.J. Espadas-Escalante, N.P. van Dijk, and P. Isaksson. A phase-field model for strength and fracture analyses of fiber-reinforced composites. *Composites Science and Technology*, 174:58–67, 2019. ISSN 0266-3538. doi: <https://doi.org/10.1016/j.compscitech.2018.10.031>.
- D.J. Eyre and G.W. Milton. A fast numerical scheme for computing the response of composites using grid refinement. *The European Physical Journal Applied Physics*, 6(1):41–47, 4 1999. ISSN 1286-0042. doi: 10.1051/epjap:1999150.
- J. Feder. Random sequential adsorption. *Journal of Theoretical Biology*, 87(2):237–254, 1980. ISSN 0022-5193. doi: [https://doi.org/10.1016/0022-5193\(80\)90358-6](https://doi.org/10.1016/0022-5193(80)90358-6). URL <https://www.sciencedirect.com/science/article/pii/0022519380903586>.
- Y.T. Feng, K. Han, and D.R.J. Owen. Filling domains with disks: an advancing front approach. *International Journal for Numerical Methods in Engineering*, 56(5):699–713, 2003. ISSN 1097-0207. doi: 10.1002/nme.583. URL <https://onlinelibrary.wiley.com/doi/abs/10.1002/nme.583>. eprint: <https://onlinelibrary.wiley.com/doi/pdf/10.1002/nme.583>.
- Th. Flatscher and H.E. Pettermann. A constitutive model for fiber-reinforced polymer plies accounting for plasticity and brittle damage including softening – implementation for implicit fem. *Composite Structures*, 93(9):2241–2249, 2011. ISSN 0263-8223. doi: <https://doi.org/10.1016/j.compstruct.2011.03.012>.
- G.A. Francfort and J.-J. Marigo. Revisiting brittle fracture as an energy minimization problem. *Journal of the Mechanics and Physics of Solids*, 46(8):1319–1342, 1998. ISSN 0022-5096. doi: [https://doi.org/10.1016/S0022-5096\(98\)00034-9](https://doi.org/10.1016/S0022-5096(98)00034-9).
- D. Garoz, F.A. Gilabert, R.D.B. Sevenois, S.W.F. Spronk, and W. Van Paepegem. Consistent application of periodic boundary conditions in implicit and explicit finite element simulations of damage in composites. *Composites Part B: Engineering*, 168:254–266, July 2019. ISSN 1359-8368. doi: 10.1016/j.compositesb.2018.12.023. URL <https://www.sciencedirect.com/science/article/pii/S1359836818337776>.
- M.G.D. Geers, V.G. Kouznetsova, and W.A.M. Brekelmans. Multi-scale computational homogenization: trends & challenges. *Journal of Computational and Applied Mathematics*, 234:2175–2182, 2010.
- L. Gélébart and R. Mondon-Cancel. Non-linear extension of FFT-based methods accelerated by conjugate gradients to evaluate the mechanical behavior of composite materials. *Computational Materials Science*, 77: 430–439, 9 2013. ISSN 09270256. doi: 10.1016/j.commatsci.2013.04.046.
- E. Ghossein and M. Lévesque. A fully automated numerical tool for a comprehensive validation of homogenization models and its application to spherical particles reinforced composites. *International Journal of Solids and Structures*, 49(11):1387–1398, 2012. ISSN 0020-7683. doi: <https://doi.org/10.1016/j.ijsolstr.2012.02.021>. URL <https://www.sciencedirect.com/science/article/pii/S0020768312000613>.
- A. Golahmar, H. Wang, Y. Zhang, et al. Hydrogen embrittlement and fatigue behavior of additively manufactured als10mg alloy. *International Journal of Fatigue*, 153:106521, 2022. doi: 10.1016/j.ijfatigue.2021.106521.
- A.A. Griffith. The phenomena of rupture and flow in solids. *Philosophical Transactions of the Royal Society of London*, 221:163–198, 1920.
- T. Guillén-Hernández, I. G. García, J. Reinoso, and M. Paggi. A micromechanical analysis of inter-fiber failure in long reinforced composites based on the phase field approach of fracture combined with the

- cohesive zone model. *International Journal of Fracture*, 220:181–203, 12 2019. ISSN 15732673. doi: 10.1007/S10704-019-00384-8/METRICS.
- W. Harizi, S. Chaki, G. Bourse, and M. Ourak. Damage mechanisms assessment of glass fiber-reinforced polymer (grfp) composites using multivariable analysis methods applied to acoustic emission data. *Composite Structures*, 289:115470, 2022.
- B. Harris. A historical review of the fatigue behavior of fibre-reinforced plastics. *Fatigue in Composites*, pages 1–35, 2003.
- Z. Hashin. The Elastic Moduli of Heterogeneous Materials. *Journal of Applied Mechanics*, 29(1):143–150, 03 1962. ISSN 0021-8936. doi: 10.1115/1.3636446. URL <https://doi.org/10.1115/1.3636446>.
- Z. Hashin. Failure criteria for unidirectional fiber composites. *J Appl Mech*, 47:329–334, 1980.
- Z. Hashin and S. Shtrikman. A variational approach to the theory of the elastic behaviour of multiphase materials. *Journal of the Mechanics and Physics of Solids*, 11(2):127–140, 1963. ISSN 0022-5096. doi: [https://doi.org/10.1016/0022-5096\(63\)90060-7](https://doi.org/10.1016/0022-5096(63)90060-7). URL <https://www.sciencedirect.com/science/article/pii/S0022509663900607>.
- N.M. Hassan and R.C. Batra. Modeling damage in polymeric composites. *Composites: Part B*, 39:66–82, 2008.
- A. Henkes and H. Wessels. Three-dimensional microstructure generation using generative adversarial neural networks in the context of continuum micromechanics. *Computer Methods in Applied Mechanics and Engineering*, 400:115497, October 2022. ISSN 0045-7825. doi: 10.1016/j.cma.2022.115497.
- R. Hill. A self-consistent mechanics of composite materials. *Journal of the Mechanics and Physics of Solids*, 13(4):213–222, 1965. ISSN 0022-5096. doi: [https://doi.org/10.1016/0022-5096\(65\)90010-4](https://doi.org/10.1016/0022-5096(65)90010-4). URL <https://www.sciencedirect.com/science/article/pii/S0022509665900104>.
- Z.S. Hosseini, W. Zhang, L. Wang, et al. Fatigue crack propagation in magnesium alloys: A phase-field approach. *Journal of Applied Mechanics*, 88(5):051010, 2021. doi: 10.1115/1.4049076.
- G. Huysmans, I. Verpoest, and P. Van Houtte. A poly-inclusion approach for the elastic modelling of knitted fabric composites. *Acta Materialia*, 46(9):3003–3013, 1998.
- T. Ishikawa and T.-W. Chou. Stiffness and strength behaviour of woven fabric composites. *Journal of Materials Science*, 17(11):3211–3220, Nov 1982. ISSN 1573-4803. doi: 10.1007/BF01203485. URL <https://doi.org/10.1007/BF01203485>.
- M. Jabbado and M.H. Maitournam. A high-cycle fatigue life model for variable amplitude multiaxial loading. *Fatigue Fracture Engineering Material Structures*, 31:67–75, 2007.
- M. Kabel, D. Merkert, and M. Schneider. Use of composite voxels in FFT-based homogenization. *Computer Methods in Applied Mechanics and Engineering*, 294:168–188, 2015. ISSN 00457825. doi: 10.1016/j.cma.2015.06.003.
- L.M. Kachanov. Time of rupture process under creep conditions. *Izy Akad Nank SSR Otd Tech Nauk*, 8:26–31, 1958.
- AS Kaddour and MJ Hinton. Maturity of 3D failure criteria for fibre-reinforced composites: Comparison between theories and experiments: Part B of WWFE-II. *Journal of Composite Materials*, 47(6-7):925–966, March 2013. ISSN 0021-9983. doi: 10.1177/0021998313478710. URL <https://doi.org/10.1177/0021998313478710>. Publisher: SAGE Publications Ltd STM.
- Radmir Karamov, Stepan V. Lomov, Ivan Sergeichev, Yentl Swolfs, and Iskander Akhatov. Inpainting micro-CT images of fibrous materials using deep learning. *Computational Materials Science*, 197:110551, September 2021. ISSN 0927-0256. doi: 10.1016/j.commatsci.2021.110551.
- B. Katalin. An algorithm to generate random dense arrangements for discrete element simulations of granular assemblies. *Granular Matter*, 7(1):31–43, Apr 2005. ISSN 1434-7636. doi: 10.1007/s10035-004-0187-5. URL <https://doi.org/10.1007/s10035-004-0187-5>.
- G. Kress. Examination of hashin’s failure criteria for the second world-wide failure exercise. *Journal of Composite Materials*, 46(19-20):2539–2561, 2012. doi: 10.1177/0021998312449892. URL <https://doi.org/10.1177/0021998312449892>.
- A. R. Labanieh, Y. Liu, D. Vasiukov, D. Soulat, and S. Panier. Influence of off-axis in-plane yarns on the mechanical properties of 3d composites. *Composites Part A: Applied Science and Manufacturing*, 98:45–57, 2017. ISSN 1359-835X. doi: <https://doi.org/10.1016/j.compositesa.2017.03.009>. URL <https://www.sciencedirect.com/science/article/pii/S1359835X17301045>.
- P. Ladeveze and E. Le Dantec. Damage modelling of the elementary ply for laminated composites. *Composite Science and Technology*, 43:257–267, 1992.

- P. Ladeveze and G. Lubineau. On damage mesomodel for laminates: micro-meso relationships, possibilities and limits. *Composites Science and Technology*, 61:2149–2158, 2001.
- P. Ladeveze and G. Lubineau. An enhanced mesomodel for laminates based on micromechanics. *Composites Science and Technology*, 62:533–541, 2002.
- P. Ladevéze and G. Lubineau. A computational mesodamage model for life prediction for laminates. In B. Harris, editor, *Fatigue in Composites*, pages 494–504. CRC Press, 2003.
- F. Laurin, N. Carrère, and J. F. Maire. A multiscale progressive failure approach for composite laminates based on thermodynamical viscoelastic and damage models. *Composites Part A: Applied Science and Manufacturing*, 38(1):198–209, January 2007. ISSN 1359-835X. doi: 10.1016/j.compositesa.2006.01.018. URL <https://www.sciencedirect.com/science/article/pii/S1359835X0600025X>.
- R.A. Lebensohn and A. Needleman. Numerical implementation of non-local polycrystal plasticity using fast Fourier transforms. *Journal of the Mechanics and Physics of Solids*, 97:333–351, 12 2016. ISSN 00225096. doi: 10.1016/j.jmps.2016.03.023.
- W. Leclerc, N. Ferguen, C. Pélegris, H. Haddad, E. Bellenger, and M. Guessasma. A numerical investigation of effective thermoelastic properties of interconnected alumina/al composites using fft and fe approaches. *Mechanics of Materials*, 92:42–57, 2016. ISSN 0167-6636. doi: <https://doi.org/10.1016/j.mechmat.2015.09.002>.
- J. Lemaître and R. Desmorat. *Engineering damage mechanics: ductile, creep, fatigue and brittle failures*. Springer, Berlin ; New York, 2005. ISBN 978-3-540-21503-5. OCLC: ocm56646827.
- Y. Liu, I. Straumit, D. Vasiukov, S.V. Lomov, and S. Panier. Prediction of linear and non-linear behavior of 3D woven composite using mesoscopic voxel models reconstructed from X-ray micro-tomography. *Composite Structures*, 179:568–579, 11 2017a. ISSN 02638223. doi: 10.1016/j.compstruct.2017.07.066.
- Y. Liu, D. Vasiukov, and S. Panier. A numerical approach to reconstruct mesoscopic yarn section of textile composites based upon x-ray micro-tomography. In *CFM 2017-23ème Congrès Français de Mécanique*, 2017b.
- S.V. Lomov, A.V. Gusakov, G. Huysmans, A. Prodromou, and I. Verpoest. Textile geometry preprocessor for meso-mechanical models of woven composites. *Composites Science and Technology*, 60(11):2083–2095, 2000.
- S.V. Lomov, D.S. Ivanov, I. Verpoest, M. Zako, T Kurashiki, H. Nakai, and S. Hiroswawa. Meso-fe modelling of textile composites: Road map, data flow and algorithms. *Composites Science and Technology*, 67:1870–1891, 2007.
- A.C. Long. *Design and Manufacture of Textile Composites - 1st Edition*. Series in Textiles. Woodhead Publishing, 1st edition edition, 2005. ISBN 978-1-85573-744-0. URL <https://shop.elsevier.com/books/design-and-manufacture-of-textile-composites/long/978-1-85573-744-0>.
- B.D. Lubachevsky and F.H. Stillinger. Geometric properties of random disk packings. *Journal of Statistical Physics*, 60(5):561–583, Sep 1990. ISSN 1572-9613. doi: 10.1007/BF01025983. URL <https://doi.org/10.1007/BF01025983>.
- G. Lubineau and P. Ladeveze. Construction of a micromechanics-based intralaminar mesomodel, and illustrations in abaqus/standard. *Computational Materials Science*, 43:137–145, 2008.
- S. Lucarini, L. Cobian, A. Voitus, and J. Segurado. Adaptation and validation of fft methods for homogenization of lattice based materials. *Computer Methods in Applied Mechanics and Engineering*, 388:114223, 2022. ISSN 0045-7825. doi: <https://doi.org/10.1016/j.cma.2021.114223>.
- Y. Lui. *Multi-scale simulation of interlock composite damage*. PhD thesis, IMT Lille Douai - University of Lille, 2017.
- S.P. Lynch. Hydrogen embrittlement (he) phenomena and mechanisms. In *Stress corrosion cracking: Theory and practice*. 2011.
- X. Ma. *The elastic and damage modeling of heterogeneous materials based on the Fast Fourier Transform*. PhD thesis, IMT Nord Europe - University of Lille, 2022.
- X. Ma, K.K. Parvathaneni, S.V. Lomov, D. Vasiukov, M. Shakoor, and C.H. Park. Quantitative comparison between fast fourier transform and finite element method for micromechanical modeling of composite. In *FiBreMOD conference 2019*, 12 2019.
- X. Ma, M. Shakoor, D. Vasiukov, S.V. Lomov, and C.H. Park. Numerical artifacts of fast fourier transform solvers for elastic problems of multi-phase materials: their causes and reduction methods. *Computational Mechanics 2021 67:6*, 67:1661–1683, 4 2021. ISSN 1432-0924. doi: 10.1007/S00466-021-02013-5.
- X. Ma, Y. Chen, M. Shakoor, D. Vasiukov, S.V. Lomov, and C.H. Park. Simplified and complete phase-field fracture formulations for heterogeneous materials and their solution using a fast fourier transform based

- numerical method. *Engineering Fracture Mechanics*, 279:109049, 2023a. ISSN 0013-7944. doi: <https://doi.org/10.1016/j.engfracmech.2023.109049>.
- X. Ma, D. Vasiukov, M. Shakoor, S. V. Lomov, and C. H. Park. Implementation of a phase field damage model with a nonlinear evolution equation in an fft-based solver. *Engineering Fracture Mechanics*, 290:109518, 2023b. ISSN 0013-7944. doi: <https://doi.org/10.1016/j.engfracmech.2023.109518>. URL <https://www.sciencedirect.com/science/article/pii/S0013794423004769>.
- V.K. Maes, K. Potter, and J. Kratz. Features and defects characterisation for virtual verification and certification of composites: A review. *Composites Part B: Engineering*, 246:110282, 2022. ISSN 1359-8368. doi: <https://doi.org/10.1016/j.compositesb.2022.110282>.
- P. Maimí, P.P. Camanho, J.A. Mayugo, and C.G. Dávila. A continuum damage model for composite laminates: Part i – constitutive model. *Mechanics of Materials*, 39(10):897–908, 2007. ISSN 0167-6636. doi: <https://doi.org/10.1016/j.mechmat.2007.03.005>.
- J.-F. Maire and J. Chaboche. A new formulation of continuum damage mechanics (cdm) for composite materials. *Aerospace Science and Technology*, 4:247–257, 1997.
- T.K. Mandal, V. P. Nguyen, and J.-Y. Wu. Length scale and mesh bias sensitivity of phase-field models for brittle and cohesive fracture. *Engineering Fracture Mechanics*, 217:106532, 2019. ISSN 0013-7944. doi: <https://doi.org/10.1016/j.engfracmech.2019.106532>.
- M.L. Martin, D.D. Johnson, R. Smith, et al. Nanoprecipitation strengthening in an ultrafine grained high-entropy alloy. *Acta Materialia*, 164:179–192, 2019. doi: 10.1016/j.actamat.2018.12.014.
- E. Martínez-Pañeda, A. Lopez, J. Marian, et al. Effect of hydrogen on dislocation nucleation in Al and Cu: A multiscale ab initio study. *arXiv preprint arXiv:1711.05616*, 2016.
- M. Mehdikhani, L. Gorbatikh, I. Verpoest, and S.V. Lomov. Voids in fiber-reinforced polymer composites: A review on their formation, characteristics, and effects on mechanical performance. *Journal of Composite Materials*, 53(12):1579–1669, May 2019. ISSN 0021-9983. doi: 10.1177/0021998318772152. URL <https://doi.org/10.1177/0021998318772152>. Publisher: SAGE Publications Ltd STM.
- A.R. Melro, P.P. Camanho, and S.T. Pinho. Generation of random distribution of fibres in long-fibre reinforced composites. *Composites Science and Technology*, 68(9):2092–2102, 2008.
- A. Mendoza, R. Trullo, and Y. Wielhorski. Descriptive modeling of textiles using FE simulations and deep learning. *Composites Science and Technology*, 213:108897, September 2021. ISSN 0266-3538. doi: 10.1016/j.compscitech.2021.108897.
- J.C. Michel, H. Moulinec, and P. Suquet. A computational method based on augmented lagrangians and fast fourier transforms for composites with high contrast. *Computer Modeling in Engineering and Sciences*, 1(2):79–88, 2000. ISSN 15261492. doi: 10.3970/cmesc.2000.001.239.
- C. Miehe, M. Hofacker, and F. Welschinger. A phase field model for rate-independent crack propagation: Robust algorithmic implementation based on operator splits. *Computer Methods in Applied Mechanics and Engineering*, 199(45):2765–2778, 2010a. ISSN 0045-7825. doi: <https://doi.org/10.1016/j.cma.2010.04.011>.
- C. Miehe, F. Welschinger, and M. Hofacker. Thermodynamically consistent phase-field models of fracture: Variational principles and multi-field fe implementations. *International Journal for Numerical Methods in Engineering*, 83(10):1273–1311, 2010b. doi: <https://doi.org/10.1002/nme.2861>.
- V. Monchiet and G. Bonnet. A polarization-based FFT iterative scheme for computing the effective properties of elastic composites with arbitrary contrast. *International Journal for Numerical Methods in Engineering*, 89(11):1419–1436, 3 2012. ISSN 00295981. doi: 10.1002/nme.3295.
- T. Mori and K. Tanaka. Average stress in matrix and average elastic energy of materials with misfitting inclusions. *Acta Metallurgica*, 21(5):571–574, 1973. ISSN 0001-6160. doi: [https://doi.org/10.1016/0001-6160\(73\)90064-3](https://doi.org/10.1016/0001-6160(73)90064-3). URL <https://www.sciencedirect.com/science/article/pii/0001616073900643>.
- H. Moulinec and P. Suquet. A fast numerical method for computing the linear and nonlinear mechanical properties of composites. *Comptes rendus de l'Académie des sciences. Série II, Mécanique, physique, chimie, astronomie*, 318(11):1417–1423, 1994. ISSN 1251-8069.
- H. Moulinec and P. Suquet. A FFT-Based Numerical Method for Computing the Mechanical Properties of Composites from Images of their Microstructures. In *IUTAM Symposium on Microstructure-Property Interactions in Composite Materials*, pages 235–246. Springer Netherlands, 1995. doi: 10.1007/978-94-011-0059-5_{\ }20.
- A.P. Mouritz, M.K. Bannister, P.J. Falzon, and K.H. Leong. Review of applications for advanced three-dimensional fibre textile composites. *Composites Part A: Applied Science and Manufacturing*, 30(12):

- 1445–1461, 1999. ISSN 1359-835X. doi: [https://doi.org/10.1016/S1359-835X\(99\)00034-2](https://doi.org/10.1016/S1359-835X(99)00034-2). URL <https://www.sciencedirect.com/science/article/pii/S1359835X99000342>.
- W. Müller. Mathematical vs. Experimental Stress Analysis of Inhomogeneities in Solids. In *International Seminar on Mechanics and Mechanisms of Solid-Solid Phase Transformations*, volume 06, pages 139–148. Springer, Berlin, Heidelberg, 1996. doi: 10.1051/jp4:1996114.
- M. Mühlstädt, W. Seifert, M.M.L. Arras, S. Maenz, K.D. Jandt, and J. Bossert. 3d model of intra-yarn fiber volume fraction gradients of woven fabrics. *Composite Structures*, 180:944–954, 2017. ISSN 0263-8223. doi: <https://doi.org/10.1016/j.compstruct.2017.08.049>. URL <https://www.sciencedirect.com/science/article/pii/S0263822317312734>.
- N. Naouar, D. Vasiukov, C. H. Park, S. V. Lomov, and P. Boisse. Meso-fe modelling of textile composites and x-ray tomography. *Journal of Materials Science*, 55(36):16969–16989, Dec 2020. ISSN 1573-4803. doi: 10.1007/s10853-020-05225-x. URL <https://doi.org/10.1007/s10853-020-05225-x>.
- S. Nemat-Nasser and M. Hori. *Micromechanics: overall properties of heterogeneous materials*. Elsevier, 2013.
- E.A.S. Neto, D. Peric, and D.R.J. Owen. *Computational methods for plasticity. Theory and applications*. Wiley, 2008.
- T.T. Nguyen, J. Yvonnet, M. Bornert, and C. Chateau. Initiation and propagation of complex 3d networks of cracks in heterogeneous quasi-brittle materials: Direct comparison between in situ testing-microct experiments and phase field simulations. *Journal of the Mechanics and Physics of Solids*, 95:320–350, 2016a. ISSN 0022-5096. doi: <https://doi.org/10.1016/j.jmps.2016.06.004>.
- T.T. Nguyen, J. Yvonnet, M. Bornert, C. Chateau, K. Sab, R. Romani, and R. Le Roy. On the choice of parameters in the phase field method for simulating crack initiation with experimental validation. *International Journal of Fracture*, 197:213–226, 2 2016b. ISSN 15732673. doi: 10.1007/S10704-016-0082-1/METRICS.
- T.T. Nguyen, J. Yvonnet, M. Bornert, C. Chateau, F. Bilteyst, and E. Steib. Large-scale simulations of quasi-brittle microcracking in realistic highly heterogeneous microstructures obtained from micro ct imaging. *Extreme Mechanics Letters*, 17:50–55, 2017. ISSN 2352-4316. doi: <https://doi.org/10.1016/j.eml.2017.09.013>.
- Y. Nikishkov, L. Airoldi, and A. Makeev. Measurement of voids in composites by x-ray computed tomography. *Composites Science and Technology*, 89:89–97, 2013. ISSN 0266-3538. doi: <https://doi.org/10.1016/j.compscitech.2013.09.019>. URL <https://www.sciencedirect.com/science/article/pii/S0266353813003813>.
- Y. Pannier, P. Coupé, T. Garrigues, M. Gueguen, and P. Carré. Automatic segmentation and fibre orientation estimation from low resolution X-ray computed tomography images of 3D woven composites. *Composite Structures*, 318:117087, August 2023. ISSN 0263-8223. doi: 10.1016/j.compstruct.2023.117087.
- K.-K. Parvathaneni. *Multi-scale simulation of interlock composite damage*. PhD thesis, IMT Nord Europe - University of Lille, 2020.
- R.H.J. Peerlings, R. de Borst, W.A.M. Brekelmans, and M.G.D. Geers. Localisation issues in local and nonlocal continuum approaches to fracture. *European Journal of Mechanics - A/Solids*, 21(2):175–189, 2002. ISSN 0997-7538. doi: [https://doi.org/10.1016/S0997-7538\(02\)01211-1](https://doi.org/10.1016/S0997-7538(02)01211-1). URL <https://www.sciencedirect.com/science/article/pii/S0997753802012111>.
- P. Perzyna. Fundamental problems in viscoplasticity. volume 9 of *Advances in Applied Mechanics*, pages 243–377. Elsevier, 1966. doi: [https://doi.org/10.1016/S0065-2156\(08\)70009-7](https://doi.org/10.1016/S0065-2156(08)70009-7). URL <https://www.sciencedirect.com/science/article/pii/S0065215608700097>.
- D. Proserpio, J. Lee, S. Park, et al. A phase-field study of hydrogen-induced cracking in polycrystalline aggregates. *Computer Methods in Applied Mechanics and Engineering*, 387:114019, 2021. doi: 10.1016/j.cma.2021.114019.
- A. Pulikkathodi, E. Lacazedieu, and L. Chamoin. Real-time inverse crack tracking in uncertain microstructures using pgd-based model reduction and extended kalman filtering. *Computational Mechanics*, 71(2):311–332, 2023.
- M. Quaresimin, P.A. Carraro, L.P. Mikkelsen, N. Lucato, L. Vivian, P. Brøndsted, B.F. Sørensen, J. Varna, and R. Talreja. Damage evolution under cyclic multiaxial stress state: A comparative analysis between glass/epoxy laminates and tubes. *Composites: Part B*, 61:282–290, 2014.
- K.L. Reifsnider. *Fatigue of Composite Materials*. Elsevier Amsterdam, 1991.
- B.W. Rosen. *Mechanics of composite strengthening*. 1965.

- M.N. Saleh and C. Soutis. Recent advancements in mechanical characterisation of 3d woven composites. *Mechanics of Advanced Materials and Modern Processes*, 3(1):12, Jul 2017. ISSN 2198-7874. doi: 10.1186/s40759-017-0027-z. URL <https://doi.org/10.1186/s40759-017-0027-z>.
- H. Sawadogo, S. Panier, and S. Hariri. Calorimetric analysis of dissipative effects associated with fatigue of gfrp composites. In W. Yao, J. Renard, and N.A. Himmel, editors, *Fatigue behavior of fiber reinforced polymers: experiments and simulations*, pages 161–171. DEStech Publications, 2012.
- R.A. Schapery. On the characterization of nonlinear viscoelastic materials. *Polymer Engineering & Science*, 9(4):295–310, 1969. ISSN 1548-2634. doi: 10.1002/pen.760090410.
- F. Schmidt and P. Horst. Damage mechanism and fatigue behaviour of uniaxially and sequentially loaded wound tube specimens. *Fifth International Conference on Fatigue of Composites*, pages 8–20, 2010.
- M. Schneider, D. Merkert, and M. Kabel. FFT-based homogenization for microstructures discretized by linear hexahedral elements. *International Journal for Numerical Methods in Engineering*, 109(10):1461–1489, 3 2017. ISSN 10970207. doi: 10.1002/nme.5336.
- M. Sherburn. *Geometric and mechanical modelling of textiles*. PhD thesis, University of Nottingham United Kingdom, 2007.
- A. Shigang, F. Daining, H. Rujie, and P. Yongmao. Effect of manufacturing defects on mechanical properties and failure features of 3D orthogonal woven C/C composites. *Composites Part B: Engineering*, 71:113–121, March 2015. ISSN 1359-8368. doi: 10.1016/j.compositesb.2014.11.003.
- K. Shinde, V. Itier, J. Mennesson, D. Vasiukov, and M. Shakoor. Dimensionality reduction through convolutional autoencoders for fracture patterns prediction. *Applied Mathematical Modelling*, 114:94–113, 2023. ISSN 0307-904X. doi: <https://doi.org/10.1016/j.apm.2022.09.034>. URL <https://www.sciencedirect.com/science/article/pii/S0307904X22004541>.
- T. Shinko, K. Suzuki, H. Tanaka, et al. Hydrogen embrittlement assessment of high-strength steels in sour environments. *Theoretical and Applied Fracture Mechanics*, 113:102885, 2021. doi: 10.1016/j.tafmec.2020.102885.
- J.C. Simo and T.J.R Hughes. *Computational Inelasticity*. Springer, 1997.
- S.M. Sisodia, S.C. Garcea, A.R. George, D.T. Fullwood, S.M. Spearing, and E.K. Gamstedt. High-resolution computed tomography in resin infused woven carbon fibre composites with voids. *Composites Science and Technology*, 131:12–21, 2016. ISSN 0266-3538. doi: <https://doi.org/10.1016/j.compscitech.2016.05.010>. URL <https://www.sciencedirect.com/science/article/pii/S0266353816303542>.
- B. Sonon, B. François, and T.J. Massart. A unified level set based methodology for fast generation of complex microstructural multi-phase rves. *Computer Methods in Applied Mechanics and Engineering*, 223-224:103–122, 2012. ISSN 0045-7825. doi: <https://doi.org/10.1016/j.cma.2012.02.018>. URL <https://www.sciencedirect.com/science/article/pii/S0045782512000606>.
- F. Sosa-Rey, Y. Abderrafai, A. Diouf Lewis, D. Therriault, N. Piccirelli, and M. Lévesque. Openfiberseg: Open-source segmentation of individual fibers and porosity in tomographic scans of additively manufactured short fiber reinforced composites. *Composites Science and Technology*, 226:109497, 2022. ISSN 0266-3538. doi: <https://doi.org/10.1016/j.compscitech.2022.109497>. URL <https://www.sciencedirect.com/science/article/pii/S0266353822002391>.
- D. Stefaniuk and M. Kachanov. Voigt-reuss and hashin-shtrikman bounds revisited. *International Journal of Engineering Science*, 191:103903, 2023. ISSN 0020-7225. doi: <https://doi.org/10.1016/j.ijengsci.2023.103903>. URL <https://www.sciencedirect.com/science/article/pii/S0020722523000940>.
- I. Straumit, S.V. Lomov, and M. Wevers. Quantification of the internal structure and automatic generation of voxel models of textile composites from x-ray computed tomography data. *Composites Part A: Applied Science and Manufacturing*, 69:150–158, 2015.
- I. Straumit, I. Baran, L. Gorbatikh, L. Farkas, C. Hahn, K. Ilin, J. Ivens, L. Lessard, Y. Liu, N. Nguyen, A. Matveeva, M. Mehdikhani, O. Shishkina, J. Soete, J. Takahashi, D. Vandepitte, D. Vasiukov, Y. Wan, E. Winterstein, M. Wevers, and S.V. Lomov. Micro-ct-based analysis of fibre-reinforced composites: Applications. In *In proceedings of European Conference for Composite Materials 18 (ECCM18)*, June 2018.
- P. Tan, L. Tong, and G.P. Steven. Micromechanics models for mechanical and thermomechanical properties of 3d through-the-thickness angle interlock woven composites. *Composites Part A: Applied Science and Manufacturing*, 30(5):637–648, 1999.

- M. Teßmann, S. Mohr, S. Gayetskyy, U. Haßler, R. Hanke, and G. Greiner. Automatic determination of fiber-length distribution in composite material using 3d ct data. *EURASIP journal on advances in signal processing*, 2010:1–9, 2010.
- I. Tretiak. *Effect of voids on the interlaminar failure of carbon/epoxy composites*. PhD thesis, University of Bristol, 2019.
- Shailee Upadhyay, Abraham George Smith, Dirk Vandepitte, Stepan V. Lomov, Yentl Swolfs, and Mahoor Mehdikhani. Deep-learning versus greyscale segmentation of voids in X-ray computed tomography images of filament-wound composites. *Composites Part A: Applied Science and Manufacturing*, 177:107937, February 2024. ISSN 1359-835X. doi: 10.1016/j.compositesa.2023.107937. URL <https://www.sciencedirect.com/science/article/pii/S1359835X23005134>.
- F.P. van der Meer. Mesolevel modeling of failure in composite laminates: constitutive, kinematic and algorithmic aspects. *Arch. Comput. Methods Eng*, 19:381 – 425, 2012.
- D. Vasiukov, A. Trameçon, and S. Mueller. Fatigue modeling in composite materials for industrial application. In *NAFEMS*, June 2014.
- D. Vasiukov, S. Panier, and A. Hachemi. Direct method for life prediction of fibre reinforced polymer composites based on kinematic of damage potential. *International Journal of Fatigue*, 70, 2015a. ISSN 01421123. doi: 10.1016/j.ijfatigue.2014.10.004.
- D. Vasiukov, S. Panier, and A. Hachemi. Non-linear material modeling of fiber-reinforced polymers based on coupled viscoelasticity-viscoplasticity with anisotropic continuous damage mechanics. *Composite Structures*, 132, 2015b. ISSN 02638223. doi: 10.1016/j.compstruct.2015.05.027.
- D. Vasiukov, A. Trameçon, S. Panier, and S. Mueller. Strategies and numerical implementation of fatigue life models for continuous fiber reinforced polymers. In *Proceedings of the American Society for Composites - 31st Technical Conference, ASC 2016*, 2016. ISBN 9781605953168.
- D. Vasiukov, K.-K. Parvathaneni, S.V. Lomov, and C.-H. Park. Multi-scale modelling of 3d textile composites with different orthogonal mesostructures including the influence of the composite manufacturing process. In *Proceedings of European Conference for Composite Materials 18 (ECCM18)*, June 2018.
- D. Vasiukov, Y. Chen, C.-H. Park, and L. Gelebart. Level set post-processing for automated meshing of woven composite ct scans with local fiber content control. In *7th ECCOMAS Thematic Conference on the Mechanical Response of Composites: COMPOSITES*, Septembre 2019.
- J. Vasseur. *Fiabilité prévisionnelle de la tenue en service de composants mécaniques en présence d'amas de porosités détectés et caractérisés par contrôle non destructif ultrasonore*. PhD thesis, IMT Lille Douai - University of Lille, 2020.
- J. Vasseur, F. Lefebvre, D. Vasiukov, S. Chaki, I. Huther, M. Marzin, B. Dupont, and N. Leymarie. Methodology of fatigue life assessment on components with porosity clusters. *Theoretical and Applied Fracture Mechanics*, 108:102619, 2020. ISSN 0167-8442. doi: <https://doi.org/10.1016/j.tafmec.2020.102619>. URL <https://www.sciencedirect.com/science/article/pii/S0167844220301956>.
- J. Vasseur, N. Leymarie, V. Dorval, B. Dupont, Vasiukov D., and S. Chaki. Simulation of ultrasonic tfm/fmc imaging for porosity clusters using multiple scattering modelling: Quantitative analyses and experimental comparisons. *NDT and E International*, 137:102827, 2023. ISSN 0963-8695. doi: <https://doi.org/10.1016/j.ndteint.2023.102827>. URL <https://www.sciencedirect.com/science/article/pii/S0963869523000427>.
- T.J. Vaughan and C.T. McCarthy. A combined experimental–numerical approach for generating statistically equivalent fibre distributions for high strength laminated composite materials. *Composites Science and Technology*, 70(2):291–297, 2010.
- A. Vidyasagar, W.L. Tan, and D.M. Kochmann. Predicting the effective response of bulk polycrystalline ferroelectric ceramics via improved spectral phase field methods. *Journal of the Mechanics and Physics of Solids*, 106:133–151, 9 2017. ISSN 00225096. doi: 10.1016/j.jmps.2017.05.017.
- M. Vogler, R. Rolfes, and P.P. Camanho. Modeling the inelastic deformation and fracture of polymer composites – part i: Plasticity model. *Mechanics of Materials*, 59:50–64, 2013. ISSN 0167-6636. doi: <https://doi.org/10.1016/j.mechmat.2012.12.002>.
- G.Z. Voyiadjis and T. Park. Anisotropic damage effect tensors for the symmetrization of the effective stress tensor. *Journal of Applied Mechanics*, 64:106–110, 1997.
- G.M. Vyas and S.T. Pinho. Computational implementation of a novel constitutive model for multidirectional composites. *Computational Materials Science*, 51(1):217–224, 2012. ISSN 0927-0256. doi: <https://doi.org/10.1016/j.commatsci.2011.07.038>.

- G.M. Vyas, S.T. Pinho, and P. Robinson. Constitutive modelling of fibre-reinforced composites with unidirectional plies using a plasticity-based approach. *Composites Science and Technology*, 71:1068–1074, 2011.
- Y. Wan, B. Sun, and B. Gu. Multi-scale structure modeling of damage behaviors of 3d orthogonal woven composite materials subject to quasi-static and high strain rate compressions. *Mechanics of Materials*, 94: 1–25, 2016. ISSN 0167-6636. doi: <https://doi.org/10.1016/j.mechmat.2015.11.012>. URL <https://www.sciencedirect.com/science/article/pii/S0167663615002549>.
- B. Wang, G. Fang, S. Liu, M. Fu, and J. Liang. Progressive damage analysis of 3d braided composites using fft-based method. *Composite Structures*, 192:255–263, 2018. ISSN 0263-8223. doi: <https://doi.org/10.1016/j.compstruct.2018.02.040>.
- Y. Wang and X. Sun. Digital-element simulation of textile processes. *Composites science and technology*, 61 (2):311–319, 2001.
- Y. Wang, Y. Zhou, and C. Jin. An analytical nonlinear model for plain-woven composites under off-axis loads. *Composite Structures*, 296:115905, 2022. ISSN 0263-8223. doi: <https://doi.org/10.1016/j.compstruct.2022.115905>. URL <https://www.sciencedirect.com/science/article/pii/S0263822322006699>.
- D. Weichert and G. Maier. *Inelastic analysis of structures under variable repeated loads: theory and engineering applications*. Kluwer Academic Press, 2000.
- Y. Wielhorski, A. Mendoza, M. Rubino, and S. Roux. Numerical modeling of 3D woven composite reinforcements: A review. *Composites Part A: Applied Science and Manufacturing*, 154:106729, March 2022. ISSN 1359-835X. doi: 10.1016/j.compositesa.2021.106729. URL <https://www.sciencedirect.com/science/article/pii/S1359835X21004437>.
- F. Willot. Fourier-based schemes for computing the mechanical response of composites with accurate local fields. *Comptes Rendus - Mécanique*, 343(3):232–245, 2015. ISSN 16310721. doi: 10.1016/j.crme.2014.12.005.
- F. Willot and Y.-P. Pellegrini. Fast Fourier Transform computations and build-up of plastic deformation in 2D, elastic-perfectly plastic, pixelwise disordered porous media. In *11th International Symposium on Continuum Models and Discrete Systems*, pages 443–449. Presses des mines, 7 2008.
- F. Willot, B. Abdallah, and Y.-P. Pellegrini. Fourier-based schemes with modified Green operator for computing the electrical response of heterogeneous media with accurate local fields. *International Journal for Numerical Methods in Engineering*, 98(7):518–533, 5 2014. ISSN 00295981. doi: 10.1002/nme.4641.
- B. Wintiba, B. Sonon, K.E.M. Kamel, and T.J. Massart. An automated procedure for the generation and conformal discretization of 3D woven composites RVEs. *Composite Structures*, 180:955–971, 11 2017. ISSN 02638223. doi: 10.1016/j.compstruct.2017.08.010.
- B. Wintiba, D. Vasiukov, S. Panier, S. V. Lomov, K.E.M. Kamel, and T.J. Massart. Automated reconstruction and conformal discretization of 3d woven composite ct scans with local fiber volume fraction control. *Composite Structures*, 248:112438, Sep 2020. ISSN 0263-8223. URL <https://www.sciencedirect.com/science/article/pii/S0263822319326030>.
- J.-Y. Wu. A unified phase-field theory for the mechanics of damage and quasi-brittle failure. *Journal of the Mechanics and Physics of Solids*, 103:72–99, 2017. ISSN 0022-5096. doi: <https://doi.org/10.1016/j.jmps.2017.03.015>.
- J.-Y. Wu and V.P. Nguyen. A length scale insensitive phase-field damage model for brittle fracture. *Journal of the Mechanics and Physics of Solids*, 119:20–42, 2018. ISSN 0022-5096. doi: <https://doi.org/10.1016/j.jmps.2018.06.006>.
- J.-Y. Wu, V.P. Nguyen, C.T. Nguyen, D. Sutula, S. Sinaie, and S.P.A. Bordas. Phase-field modeling of fracture. In Stéphane P.A. Bordas and Daniel S. Balint, editors, *Advances in Applied Mechanics*, volume 53, pages 1–183. Elsevier, 2020. doi: <https://doi.org/10.1016/bs.aams.2019.08.001>.
- Y. Wu, M. Jia, X. Gou, and W. Xu. Average eshelby tensor of an arbitrarily shaped inclusion from convexity to non-convexity: Effective elastic properties of composites. *International Journal of Solids and Structures*, 269:112183, 2023. ISSN 0020-7683. doi: <https://doi.org/10.1016/j.ijsolstr.2023.112183>. URL <https://www.sciencedirect.com/science/article/pii/S002076832300080X>.
- J. Zarka, J. Frelat, G. Inglebert, and P. Kasmai-Navidi. *A new approach in inelastic analysis of structures*. Martinus Nijhoff Publisher, 1990.
- J. Zeman, J. Vondřejc, J. Novák, and I. Marek. Accelerating a FFT-based solver for numerical homogenization of periodic media by conjugate gradients. *Journal of Computational Physics*, 229(21):8065–8071, 10 2010. ISSN 0021-9991. doi: 10.1016/J.JCP.2010.07.010.

- Xue Zhang, Chet Vignes, Scott W. Sloan, and Daichao Sheng. Numerical evaluation of the phase-field model for brittle fracture with emphasis on the length scale. *Computational Mechanics* 2017 59:5, 59:737–752, 1 2017. ISSN 1432-0924. doi: 10.1007/S00466-017-1373-8.
- T. Zheng, J. Wei, Z. Shi, T. Li, Z. Wu, et al. An overview of modeling yarn’s 3d geometric configuration. *Journal of Textile Science and Technology*, 1(01):12, 2015.
- S. Zhou and X. Zhuang. Adaptive phase field simulation of quasi-static crack propagation in rocks. *Underground Space*, 3(3):190–205, 2018. ISSN 2467-9674. doi: <https://doi.org/10.1016/j.undsp.2018.04.006>. Computational Modeling of Fracture in Geotechnical Engineering Part I.